Technische Universität München
TUM School of Engineering and Design

Syngas Fermentation Studies for Enhanced Alcohol Production with *Clostridium ragsdalei*

Luis Guilherme Sampaio de Oliveira

Vollständiger Abdruck der von der TUM School of Engineering and Design der Technischen Universität München zur Erlangung eines

Doktors der Ingenieurwissenschaften (Dr. -Ing.)

genehmigten Dissertation.

Vorsitz: Prof. Dr. rer. nat. Thomas Hamacher

Prüfer*innen der Dissertation:

1. Prof. Dr.-Ing. Dirk Weuster-Botz
2. Prof. Dr. Bastian Blombach

Die Dissertation wurde am 23.05.2023 bei der Technischen Universität München eingereicht und durch die TUM School of Engineering and Design am 04.09.2023 angenommen.

Acknowledgments

This dissertation was produced during my work as a research assistant at the Chair of Bioprocess Engineering, Technical University of Munich, under the guidance of Prof. Dr.-Ing. Dirk Weuster-Botz. I would like to express my heartfelt gratitude to all those who contributed to the development of this work in various ways.

Firstly, I wish to acknowledge the invaluable support and guidance of Prof. Dr.-Ing. Dirk Weuster-Botz, without which this dissertation would not have been possible. I am grateful for his constant encouragement, helpful insights, and critical evaluation of my scientific work. I particularly appreciate the freedom he afforded me to conduct my research.

I extend my thanks to Prof. Dr. Bastian Blombach for serving as the second examiner and Prof. Dr. Thomas Hamacher for acting as the exam chairman.

I am also grateful to Prof. Dr.-Ing. Hartmut Spliethoff, Dr.-Ing. Sebastian Fendt, Philipp Johne and Philipp Leuter of the Chair of Energy Systems for their excellent collaboration on the ReGasFerm project and insightful discussions.

My appreciation goes to my students Bruno Takeshi Hediger, Elina Marie Hutter, Patric Schlumprecht, Verena Holzmüller and Simon Röhrenbach for their productive work and engaging deliberations.

Thank you, Markus Amann, for your impromptu assistance and support with technological issues. Thank you to Patrick Meins and Markus Amann for your support with the paperwork and organizational needs.

I would like to acknowledge the excellent cooperation and the wonderful working environment provided by my colleagues at the Chair of Biochemical Engineering and the Professorship of Systems Biotechnology.

Acima de tudo sou grato aos meus pais, Ro e Tonio, que infelizmente nunca lerão minha dissertação, mas que no fundo permitiram que tudo isso acontecesse. E à minha família, Sophie e Alba, que me dão propósito.

Contents

1 Introduction

Human induced global warming has caused an increase in the global mean temperature of 0.87 °C relative to pre-industrial levels and is expected to increase to 1.5 °C between 2030 and 2052 (Allen M. R., et al., 2018). An increase of 1.5 °C in the global mean temperature would have severe consequences for natural systems, as well as for human systems and well-being (Hoegh-Guldberg, O. et al., 2018). Reversing this trend requires an integrated approached of reducing emissions on a broad scale.

The transport sector corresponds to 15% of greenhouse gas emissions and contributed with a temperature increase of 0.24 °C (Dhakal, S. et al., 2022). Thus, decarbonizing the transport sector, which is fossil fuel driven, is key to achieve lower emissions. The invasion of Ukraine by Russia threw another layer into the use of fossil fuel, requiring policy makers and market participants to prepare for supply disruptions (IEA, 2022b). One of the ways to decarbonize and foment the use of local energy sources is the production of biofuels, amongst which bioethanol has the highest global demand, demand which is expected to grow by 10 billion litres per year until 2027 (IEA, 2022b).

Bioethanol is produced globally mainly from corn starch and sugar cane (Sharma et al. 2020) through the fermentation with yeasts (Tse et al. 2021). However, the use of these edible feedstocks for fuel production puts pressure on food security (IEA, 2022a). Furthermore, the carbon in biomass is only partially accessible for ethanol production, since the lignin fraction, which can amount to 40% of the non-carbohydrate mass in plants (Yoo et al., 2020), is not used. In this regard, the production of synthesis gas (syngas) from non-edible biomass and its fermentation with syngas fermenting microorganism is a promising alternative to produce ethanol and other fuels, with the potential of using all the available carbon in the feedstock.

Acetogenic bacteria are a relevant group of bacteria, capable of producing acetyl-CoA from two molecules of CO_2 using the Wood-Ljungdahl pathway. They show a wide spectrum of organic substrates, but some acetogens gained attention for their capacity to produce alcohols from CO or H_2 as electron donors. The first bacterial isolate capable of converting CO and H_2 and CO_2 to ethanol was identified by Barik et al. (1988), and this strain was later named *Clostridium ljungdahlii*. Ever since, *C. ljungdahlii* has been established as a model microorganism, being extensively studied both from a process perspective, as well as through genetic modifications. Other clostridial strains have also been isolated, which show a different product spectrum or higher alcohol productivity. Amongst these, *Clostridium ragsdalei* has

been shown to be a promising strain to increase alcohol productions (Bengelsdorf et al., 2016; Saxena and Tanner, 2011). One of the key challenges in the syngas fermentation is shifting carbon to alcohol production from acetate formation, the main product of acetogenic bacteria.

2 Motivation and Scope

The broad use of fossil fuels in energy generation, transportation and industrial activity led to high emissions of greenhouse gases, which resulted in an increase in the global mean temperature of 0.87 °C since the pre-industrial era and a further increasing trend (Allen M. R., et al., 2018). Such temperature increases are having and will have a great impact in natural and human systems (Hoegh-Guldberg, O. et al., 2018). The transport sector alone was responsible for an increase in temperature of 0.24 °C (Dhakal, S. et al., 2022), and thus alternative fuels from renewable sources are key to reducing the net greenhouse gas emissions from this sector.

Ethanol is a well stablished biofuel, with a global consumption of 106.4 billion litres in 2019 and an increasing trend in use (IEA, 2022b; IEA, 2022a). Its production is, however, in conflict with the food supply chain, as most of the ethanol produced comes from corn starch or sugar cane. Even though several industrial units are technologically equipped to convert the cellulosic and hemi-cellulosic fractions of the feedstock into ethanol, these units still use edible feedstock for ethanol production. Here, the synthesis gas (syngas) fermentation is a promising alternative for ethanol production. Syngas from the exhaust in industrial processes or obtained from the gasification of biogenic residues can be used by acetogens, which are able to convert the main syngas components CO, H_2 and CO_2 into organic acids and alcohols. This way, through syngas fermentation it is possible to produce a renewable fuel, which substantially reduces the emissions footprint in the transport sector. Furthermore, in the case of syngas from industrial exhaust gases, it avoids new emissions by fixating exhaust carbon into usable fuels. In the case of the fermentation of syngas from the gasification of biogenic residues, it avoids a conflict with food security by not using edible crops and improves the carbon footprint by enabling the conversion of the whole carbon in the feedstock to ethanol. Syngas fermentation has in fact reached commercial scale, with the company LanzaTech operating three commercial plants attached to manufacturing sites in China and achieving an ethanol production of 20 million gallons in 2020 (Lanzatech, 2023).

Clostridium ragsdalei is an acetogenic bacterial strain able to grow autotrophically with CO or H_2 with CO_2 (Huhnke et al., 2008). As an acetogen, it uses the Wood-Ljungdahl pathway (WLP) to convert two molecules of CO_2 into acetyl-CoA, which then serves as a starting point for biomass or product formation. It converts acetyl-CoA into acetate, which can be further reduced to ethanol, or into 2,3-butanediol. *C. ragsdalei* has a high similarity to the model acetogen *Clostridium ljungdahlii*, with a 16S rDNA gene sequence similarity of 99.9% (Huhnke et al., 2008) and an average nucleotide identity of 95.9% (Lee et al., 2019), putting both strains

in the same clade, but a DNA-DNA hybridization of 57% (Huhnke et al., 2008), showing that it is clearly a different strain from *C. ljungdhalii*. Despite this similarity, the only published comparison of both strains, conducted in anaerobic flasks under autotrophic conditions, showed very different process performances: the final cell dry weight of *C. ragsdalei* was 57% lower than that with *C. ljungdahlii*, but the ethanol concentration increased by 110% and the ethanol to acetate ratio increased 4.33-fold (Bengelsdorf et al., 2016). This favoured alcohol formation conveys *C. ragsdalei* research interest. Nevertheless, this strain has been substantially less studied than *C. ljungdahlii;* a search in the platform Google Scholar® showed 18 publications with the term "*Clostridium ragsdalei"* in the title since 1988 and 123 with the term "*Clostridium ljungdahlii"* in the same period. Therefore, one aim of this work is to assess the performance of the syngas fermentation with *C. ragsdalei* regarding biomass and alcohol formation under the optimal conditions of pH 6.0 and temperature of 37 °C, as reported by the describing patents (Tanner et al., 1993; Huhnke et al., 2008), in comparison to the model acetogen *C. ljungdahlii* and in a more relevant reactor setup of a continuously gassed stirred-tank reactor.

Besides the main constituents of syngas, other impurities might be present depending on the fuel employed and the gasification conditions. These impurities might, in turn, change the outcomes of the syngas fermentation. Thus, when considering an integrated process of biomass gasification to produce syngas and subsequent fermentation, assessing the effects of various impurities on the process is crucial to design the proper gas cleanup and conditioning steps. Considering syngas derived from biogenic residues, fuel bound nitrogen might be converted to N_2, char and tar bound nitrogen, hydrogen cyanide and ammonia (Broer and Brown, 2016), while sulfur is mostly converted to hydrogen sulfide (H_2S) and to a lesser extent to carbonyl sulfide (COS) (Broer et al., 2015). Therefore, quantifying to which extent different concentrations of impurities influence the syngas fermentation with *C. ragsdalei* and comparing its tolerance to impurities with that of the model acetogen *C. ljungdahlii* will lead to a better selection of strains for the syngas fermentation, as well as enable a more precise gas cleanup focused only on the inhibiting impurities.

Syngas fermentation is considered a promising alternative to produce several compounds, with ethanol being the most prominent, given its large and well stablished market (Kennes et al., 2016; IEA, 2022b). However, fomenting alcohol production from syngas is challenging, since the formation of acetate yields more ATP per mol CO or H_2 than the formation of ethanol or 2,3-butanediol (Richter et al., 2016; Schuchmann and Müller, 2014). Therefore, investigating which conditions favour alcohol production is key to improve the economic feasibility of the ethanol formation from syngas. This can be done through very different approaches, such as manipulating the medium composition, changing the pH, increasing the

CO content in the syngas and through the genetic engineering of strains (Ramió-Pujol et al., 2015). Such studies are mostly conducted in anaerobic flasks (Abubackar et al., 2012; Bengelsdorf et al., 2016; Jack et a., 2019; Saxena and Tanner, 2010; Saxena and Tanner, 2012), which fail to represent a more relevant reactor setup with a better control of process parameters. Therefore, a thorough and systematic comparison of the effects of key process parameters on the alcohol, and more specifically, ethanol production is of utmost importance to the further development of the syngas fermentation as a viable technology. This should be conducted in the more relevant reactor setup of the continuously gassed stirred-tank reactor, with an ensured continuous gas supply with higher volumetric power inputs and control of the parameters of the process.

To achieve these aims, the following approach is planned:

- The performance of the syngas fermentation with *C. ragsdalei* should be compared to that of the model acetogen *C. ljungdahlii* under the optimal conditions of pH 6.0 and 37 °C in a continuously gassed stirred-tank reactor in batch mode. Key process indicators to compare are *e.g.* specific growth rate, gas uptake rates, and final concentrations of cell dry weight (CDW) and the naturally produced products acetate, ethanol and 2,3-butanediol.
- Using biogenic residues as feedstock for syngas has the potential to increase the economic feasibility of the syngas fermentation, given its low or even absent cost (Kennes et al., 2016). This syngas, however, might contain several impurities, which can impact the outcomes of the syngas fermentation. Therefore, a comparative analysis of the tolerance of the strains *C. ljungdahlii* and *C. ragsdalei* to several syngas impurities should be conducted. The impurities chosen are ammonium, nitrate, and hydrogen sulfide.
- To improve the alcohol productivity in the syngas fermentation with *C. ragsdalei*, a thorough study on the influence of different process parameters should be conducted. The chosen parameters are pH, temperature, and CO partial pressure. Furthermore, besides the individual effect of each change in the parameters, their combination should be assessed as well. This will lead to identifying broad and ideal conditions to increase the alcohol production in the syngas fermentation.

3 Theoretical Background

This chapter describes some characteristics of synthesis gas (syngas) fermenting acetogens, which give them research and industrial interest. A more detailed description of the autotrophic metabolism of these microorganisms is described, with focus on the strains used in this work *Clostridium ljungdahlii* and *Clostridium ragsdalei.* The relevance of the synthesis gas fermentation is presented, as well as the key aspects that influence its conversion to alcohols. Lastly, key fundamentals of bioprocess engineering relevant to this work are laid out.

3.1 Synthesis Gas Fermenting Acetogens

Acetogens are obligate anaerobic bacteria that use the reductive acetyl-CoA pathway to produce acetyl-CoA from two molecules of CO_2 and couple it to energy conservation (Ragsdale and Pierce, 2008; Schuchmann and Müller, 2016). They are able to grow with several substrates, both organic and inorganic. This flexibility conveys the acetogens an ecological advantage, placing them in several anaerobic food webs (Grethlein and Jain, 1992; Schuchmann and Müller, 2016).

3.1.1 Autotrophic Metabolism of Acetogens

The elucidation of the Wood-Ljungdahl pathway (WLP) came with studies with *Moorella thermoacetica*, with the observation of the stoichiometric conversion of glucose to acetate, which would imply the use of reducing equivalents from glucose oxidation in the fixation of the generated CO_2 (Ragsdale and Pierce 2008). Later, Kerby and Zeikus (1983) would show that *M. thermoacetica* could also grow with H_2/CO_2 and adapt to grow with 100% CO.

Through the WLP, acetyl-CoA is produced by reducing two CO_2 molecules in two complementary branches, the methyl and the carbonyl branch. A schematic representation of the WLP is shown in Figure 1, and the following description of the pathway will be based on knowledge from *C. ljungdahlii* or similar strains.

The methyl branch reduces CO_2 in a series of reactions to a protein bound methyl group. The first reaction step is the reduction of CO_2 to formate, which is carried out by a formate dehydrogenase (FDH) complex with an electron bifurcating hydrogenase, using ferredoxin and nicotinamide adenine dinucleotide phosphate (NADPH). This enzyme complex was identified by Wang et al. (2013) with *C. autoethanogenum*, and the genome of *C. ljungdahlii* also contains such an enzyme complex (Schuchmann and Müller 2014). Most recent works

confirm that the CO_2 reduction into the methyl branch is conducted by this enzyme complex in *C. ljungdahlii* (Aklujkar et al. 2017; Hermann et al. 2020). Formate undergoes condensation with tetrahydrofolate (THF) forming formyl-tetrahydrofolate (HCO-THF) with adenosine triphosphate (ATP) consumption by a formyl-tetrahydrofolate synthetase. HCO-THF undergoes cyclization and further reduction to methylene-tetrahydrofolate (CH_2-THF) with NADPH by a bifunctional formyl-tetrahydrofolate cyclohydrolase/methylene- tetrahydrofolate dehydrogenase. CH_2-THF is finally reduced to methyl-tetrahydrofolate (CH_3-THF) with an electron bifurcating methylene tetrahydrofolate reductase, which couples the reduction of CH_2-THF with nicotinamide adenine dinucleotide (NADH) to the endergonic electron transfer from NADH to ferredoxin (Richter et al., 2016). A methyltransferase transfers the methyl group of the CH_3-THF to the corrinoid iron-sulfur protein (CFeSP). The methyl group is transferred to the cobalt center of the corrinoid, which is highly reactive. The CFeSP also possesses an iron-sulfur cluster, which is responsible for the reactivation of the cobalt in case it suffers oxidative inactivation (Ragsdale and Pierce 2008). The CFeSP bound methyl group corresponds to the methyl group in the acetyl group of the acetyl-CoA.

The carbonyl branch supplies the acetyl-CoA with the carbonyl group. It reduces CO_2 to CO or directly uses CO and incorporates it to acetyl-CoA. This is conducted by a carbon monoxide dehydrogenase/acetyl-CoA synthase complex (CODH/ACS). *C. ljungdahlii* also produces an orphan CODH, which is only involved in the reduction of CO_2 to CO in growth with H_2/CO_2 (Richter et al. 2016). The CODH/ACS complex is key in the WLP and works through the formation of several organometallic intermediates from CO, methyl, and acetyl with nickel atoms. The active centers of the subunits of the CODH/ACS contain nickel and iron-sulfur clusters (Ragsdale 2007, 2008; Ragsdale and Pierce 2008).

The overall formation of acetyl-CoA from the two CO_2 molecules can be described in a simplified form by:

$$2CO_2 + 8[H] + ATP \xrightarrow{CoAHS} Acetyl - CoA + ADP + P_i + 3H_2O \quad (3.1)$$

, where [H] represent the reducing agents.

The WLP consumes ATP and requires the input of a variety of reducing agents to fixate carbon into acetyl-CoA, which serves as the starting point for anabolism through the production of pyruvate by the pyruvate:ferredoxin oxidoreductase (PFOR). Therefore, it needs to be coupled to an autotrophic form of energy conservation.

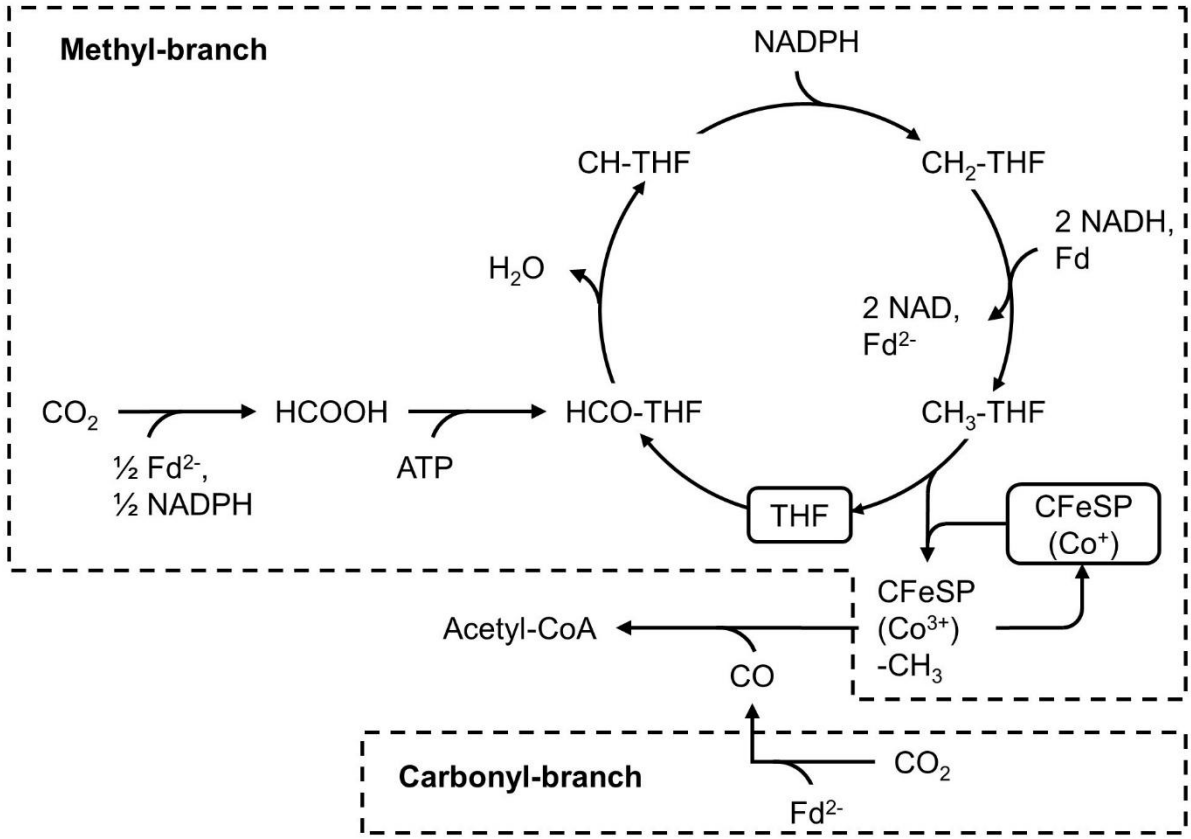

Figure 1 – Simplified version of the reductive acetyl-CoA pathway, or Wood-Ljungdahl pathway (WLP), for the fixation of two CO_2 molecules into one acetyl group bound to the coenzyme A (Acetyl-CoA), with the required reducing agents and cofactors. The enzymes responsible for the individual reactions were excluded from the figure. For a description of the WLP, see text in subsection 3.1.1.

3.1.2 Energy Conservation of Acetogens

The WLP fixates inorganic carbon with the net use of ATP and reducing agents. These are provided by the production of acetate, the generation of a membrane gradient, directly from the electron donors (CO, H_2) and through redox rebalancing. Each of these aspects will be described in this subsection, with the description below considering only energy conservation with the major syngas components CO, H_2 and CO_2. A schematic representation of these energy conserving processes is shown in Figure 2.

The first two items, acetate production and the membrane gradient, are independent of electron donor (CO, H_2) and supply ATP. A phosphotransacetylase converts acetyl-CoA to acetyl phosphate, which is further converted to acetate by an acetate kinase with the release of ATP. Considering equation 3.1, since 1 mole of acetate can be produced from 1 mole acetyl-CoA, the production of acetate from two moles CO_2 is ATP neutral disregarding further mechanisms. The stoichiometry of acetate formation from CO or H_2/CO_2 follows (Sun et al. 2019):

$$4CO + 2H_2O \rightarrow CH_3COOH + 2CO_2 \qquad \Delta G^0 = -154.6\ kJ\ mol^{-1} \qquad (3.2)$$

$$4H_2 + 2CO_2 \rightarrow CH_3COOH + 2H_2O \qquad \Delta G^0 = -74.3\ kJ\ mol^{-1} \qquad (3.3)$$

ATP is also produced by the generation of a chemiosmotic gradient, and the coupling of the WLP and chemiosmosis is the key element in the autotrophic energy conservation of acetogens. In fact, as late as in 2008 this coupling had not been identified, even though there were already evidences for it (Ragsdale, 2008b). The mechanisms and enzyme complexes involved in the generation of this gradient vary for different acetogens: for *C. ljungdahlii* and *C. ragsdalei*, this gradient is generated by the Rnf complex with a proton gradient. The Rnf is a membrane integral ferredoxin-NAD oxidoreductase enzyme complex, which transfers electrons from 1 mole of reduced ferredoxin to NAD, whereby translocating 2 protons through the cell membrane. This gradient, or proton motive force (PMF), is used by a membrane-bound ATP synthase to generate ATP with a yield of 1 ATP per 3.66 mol protons (Richter et al. 2016). The equation that governs the Rnf complex coupled with the ATP synthase is:

$$0.546(ADP + P_i) + NAD^+ + Fd^{-2} + H^+ \rightarrow 0.546ATP + NADH + Fd \qquad (3.4)$$

Reducing agents required for the WLP and chemiosmosis are supplied by the electron donors and rebalanced by electron bifurcation. Starting with H_2 as electron donor, *C. ljungdahlii* has the genetic potential to encode several hydrogenases (Schuchmann and Müller, 2014), but mainly two enzymes play a role in the supply of electrons. A bifurcating hydrogenase complex HydABC transfers electrons from H_2 to ferredoxin and NAD and a bifurcating iron only hydrogenase HytA-E/FDH complex which couples the CO_2 reduction to formate and the electron transfer from H_2 to ferredoxin and NADP. The HytA-E is the most abundant hydrogenase in the proteome of syngas/CO growing cells, and is therefore the most relevant enzyme in the use of H_2 (Wang et al. 2013; Richter et al. 2016). Carbon monoxide donates electrons to ferredoxin by the carbon monoxide dehydrogenase (CODH), as described in section 3.1.1. The equations that govern the electron transfer from CO and H_2 (by the HytA-E) are:

$$CO + H_2O + Fd \rightarrow CO_2 + 2H^+ + Fd^{-2} \qquad (3.5)$$

$$2H_2 + NADP^+ + Fd \rightarrow 3H^+ + NADPH + Fd^{-2} \qquad (3.6)$$

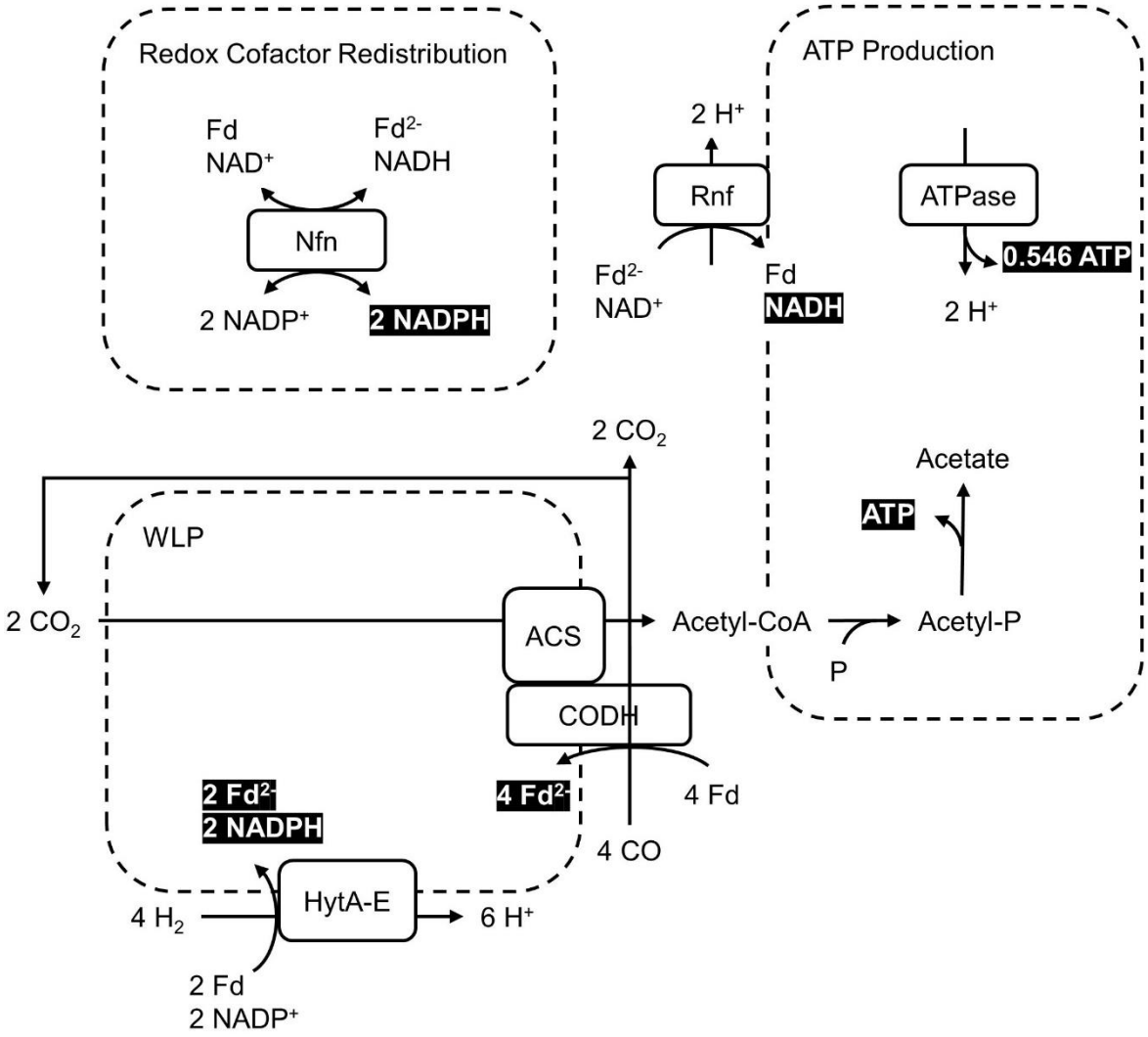

Figure 2 – Schematic representation of the energy conserving mechanisms and the Wood-Ljungdahl pathway (WLP) in *C. ljungdahlii*. The hydrogenase HytA-E produces reduced ferredoxin (Fd^{2-}) and NADPH from H_2 and the carbon monoxide dehydrogenase (CODH), which is in complex with the acetyl-CoA synthase (ACS), produces Fd^{2-} from CO. Acetate is produced from acetyl-CoA, whereby ATP is produced. Reduced ferredoxin drives the translocation of proton by the Rnf, a membrane bound ferredoxin-NAD oxidoreductase enzyme complex, whereby NADH is also generated. The chemiosmotic potential generated by the proton translocation drives the ATP formation by a membrane bound ATP synthase (ATPase). The electron-bifurcating transhydrogenase Nfn reversibly rebalances NADH, NADPH and ferredoxin.

The last aspect of energy conservation in acetogens is the rebalancing of reducing agents. The WLP requires per mol acetyl-CoA 0.5 mol reduced ferredoxin, 2 mol NADH and 1.5 mol NADPH, whereas CO as electron donor supplies only reduced ferredoxin and H_2 supplies mainly ferredoxin and NADPH in equal quantities with the most abundant HytA-E. Thus, a rebalancing of the redox cofactors is required depending on electron donor. The Rnf complex transfers electrons from reduced ferredoxin to NAD, being the main source of NADH in the cell. The conclusive rebalancing is achieved through an electron-bifurcating transhydrogenase

Nfn, which reversibly couples the electron transfer from reduced ferredoxin to NADP and the transfer from NADH to NADP. The key in the Nfn lies in its reversibility, producing net NADPH with CO as electron donor and producing net NADH with H_2 as electron donor (Hermann et al., 2021; Richter et al., 2016). The reaction that governs the Nfn is:

$$2NADP^+ + Fd^{-2} + NADH + H^+ \leftrightarrow 2NADPH + Fd + NAD^+ \quad (3.7)$$

Combining these energy conserving mechanisms, the production of acetate with H_2 and CO_2 yields 0.903 mol ATP, whereas acetate production with CO yields 1.503 mol ATP (Richter et al., 2016, Wiechmann and Müller, 2019)

3.1.3 *Clostridium ljungdahlii* and *Clostridium ragsdalei*

Clostridium ljungdahlii was first identified by Barik et al. (1988) as an unknown bacterial isolate from chicken yard waste capable of converting CO and H_2/CO_2 to ethanol. The strain was later described by Tanner et al. (1993) as strictly anaerobic, spore forming, rod shaped, gram-positive and motile. It shows a broad substrate spectrum including CO, H_2/CO_2, ethanol, pyruvate, fumarate, threose, arabinose, ribose, xylose, glucose and fructose; growth on formate is poor and malate is metabolized without cell growth. Optimal pH and temperature for growth are pH 6.0 and 37 °C, with growth possible at an initial pH within the range of pH 4.0 and pH 7.0. It naturally produces acetate, ethanol and 2,3-butanediol.

Clostridium ragsdalei was isolated from sediments of the Duck Pond at the University of Oklahoma and published by Huhnke et al., (2008). It is rarely motile, rod-shaped, gram-positive and spore-forming. It is strictly anaerobic, and can grow on CO, CO_2/H_2, pyruvate, threose, xylose, mannose, fructose, glucose, sucrose, ethanol, 1-propanol, casamino acids, glutamate, serine, choline and alanine. Optimal pH for growth is between pH 6.0 and pH 6.3 and the optimal temperature is between 30 °C and 37 °C. Optimal pH for CO metabolism lies between pH 5.5 and pH 6.0.

Both strains belong to the same clade, with an average nucleotide identity (ANI) of 95.9% (Lee et al. 2019). Despite the high level of similarities, both strains show some key differences, which were highlighted by a comparative study presented by Bengelsdorf et al. (2016). *C. ljungdahlii* contains twenty genes encoding alcohol dehydrogenases, whereas *C. ragsdalei* contains sixteen; *C. ragsdalei* possesses four gene copies coding for an aldehyde:ferredoxin oxidoreductase, whereas *C. ljungdahlii* possesses two. These differences were also demonstrated in the same publication through the performance of each strain in a batch cultivation in anaerobic flasks with 50% (v/v) CO, 5% (v/v) CO_2, 45% (v/v) H_2. The final optical density of the *C. ljungdahlii* culture was roughly twofold that of *C. ragsdalei*, while the acetate

concentration was almost threefold higher. Interestingly, the ethanol concentration in the culture of *C. ragsdalei* was the highest presented in the study.

3.2 Synthesis Gas Fermentation and Alcohol Production

Synthesis gas (syngas) is a term originally used in the petrochemical industry and describes a gas mixture of CO and H_2, with lower quantities of CH_4 and N_2. It was produced mainly from the steam reforming of methane, and the resulting gas was used for methanol synthesis, or the resulting hydrogen was used for ammonia production (Fowles and Carlsson 2021). The meaning of the term syngas has been broadened, comprising gas mixtures composed mainly of CO, H_2 and CO_2, and the sources for syngas production broadened as well, including the gasification of coal, coke, and biomass.

Interest in syngas fermentation was initially based on the concept of coal gasification, with the resulting syngas being fermented by acetogens. These microorganisms were known to produce organic acids or methane from syngas, until the first publication with a bacterial isolate showed the production of ethanol from syngas (Barik et al. 1988). Since then, focus shifted to the more valuable alcohol production with syngas fermentation, and the possible sources of syngas were widened to include industrial exhaust gasses or syngas derived from the gasification of biomass.

Ethanol is a globally relevant chemical, with the global consumption of 106.4 billion litres in 2019, increasing from 61.7 billion litres in 2010. The biggest consumers and producers of ethanol are the United States of America (USA) and Brazil, both countries which have policies to blend ethanol with gasoline (IEA, 2022b). More than 94% of the USA's production of bioethanol comes from corn starch, whereas in Brazil, the main feed stock is sugar cane (Sharma et al. 2020). The general process scheme involves a pre-treatment of the feedstock, hydrolysis, and fermentation of the sugars, with *Saccharomyces cerevisiae* being the most used yeast for industrial ethanol production (Tse et al. 2021).

Depending on the feedstock, the ethanol production is divided into generations. First generation ethanol refers to the production of ethanol from starch or sugar rich feedstocks, such as corn, and sugarcane, respectively. Second generation ethanol utilizes non-edible feedstocks, such as lignocellulosic materials; in this case, the feedstock needs to be pretreated and the available cellulose/hemicellulose hydrolysed into usable sugars. The third generation refers to the use of algal biomass for ethanol production, which requires a different sort of pretreatment to provide usable sugars for the fermentation step (Tse et al. 2021). With

this in consideration, ethanol from syngas fermentation lies within the term second generation ethanol (Kennes et al. 2016).

In this section, key aspects of the alcohol production from syngas are described. Firstly, the uptake of the different main gas components CO, H_2 and CO_2 are discussed and, within the framework of using syngas from the gasification of biomass, the effect of syngas impurities in the syngas fermentation are outlined. Secondly, the metabolic pathways involved in alcohol production and the key factors influencing the production of the alcohols ethanol and 2,3-butanediol from syngas are described.

3.2.1 CO, CO_2 and H_2 in the Syngas Fermentation

The main components of syngas are CO, CO_2 and H_2. For the autotrophic growth with CO and H_2/CO_2, the acetogens use the WLP for carbon fixation linked to chemiosmosis and acetate formation for energy conservation (see subsections 3.1.1 and 3.1.2), whereby CO or H_2 serve as electron donors to drive these processes. In the context of a coupled gasification/syngas fermentation process, the concentration of CO, CO_2 and H_2 are determined by the gasification process. Here, not only the gasification conditions, but also the composition of the feedstock and the reversible conversion of CO to H_2 and CO_2 are limits to the final composition of the syngas (Broer et al. 2015).

The different redox potentials of -558 mV for CO (Hurst and Lewis 2010) and -414 mV for H_2 (Wang et al. 2013), under standard conditions, imply that each electron donor supplies the cells differently with electrons. Given this difference, the uptake of either CO or H_2 by the cells is strongly regulated by thermodynamic considerations. Hu et al. (2011) conducted a theoretical thermodynamic analysis of the electron transfer from CO and H_2 to NAD and ferredoxin based on the Gibbs free energy of the electron transfer reactions under common process conditions (pH, ionic strength, temperature). It was concluded that in none of the studied conditions the electron transfer from H_2 to these redox cofactors was more thermodynamically favourable than that from CO. Moreover, it was also concluded that if the ratio of reduced redox cofactors to the oxidized redox factor is high, the electron transfer from H_2 can be thermodynamically unfeasible, whereas this scenario was not foreseen for CO in any of the analysed conditions. These conclusions by Hu et al. (2011) are in accordance with the results presented by Younesi et al. (2005), which showed that with *C. ljungdahlii* in serum bottles with a closed atmosphere, the consumption of H_2 resumed only after CO was completely depleted from the atmosphere. Additionally, H_2 consumption was only observed at the highest studied partial pressures (0,32 atm and 0,36 atm) despite CO depletion, indicating possibly a thermodynamic unfeasibility under lower hydrogen partial pressures.

Besides thermodynamic considerations, the inhibitory effects of CO on the activity of hydrogenases also play a role in the preference of CO over H_2. More specifically, it has been shown that CO inhibits the CO_2 reduction to formate with ferredoxin and NADPH by inhibiting the hydrogenase in the HytA-E/FDH complex (Wang et al. 2013), which is the main hydrogenase for the electron transfer from H_2 to ferredoxin and NADP and the most abundant protein in the proteome in *C. ljungdahlii* (Richter et al., 2016). Wang et al. (2013) concluded that the inhibition occurred in the HytA subunit and argued that growth is nevertheless possible with CO since intracellular CO concentrations were assumed to be very low, the HytA-E is present at very high concentrations and possesses a very high activity.

3.2.2 Synthesis Gas Fermentation: Effect of Impurities

Syngas is not only composed of its main components but, depending on the feedstock used and the production method, it can contain impurities. In the context of syngas from the gasification of biomass, a broad spectrum of minor components might be present, such as aromatics, smaller alkanes, alkenes and alkynes, hydrogen sulfide (H_2S) and carbonyl sulfide (COS), hydrogen cyanide (HCN), ammonia (NH_3) and nitrogen oxides (NO_x) (Datar et al. 2004; Oswald et al. 2018; Liakakou et al. 2021). Table 1 contains the concentration for some of these impurities reported in different references, for different feedstocks.

Table 1 – Concentration of impurities in the syngas obtained from the gasification of different biogenic feedstocks.

Component	Concentration, ppm	Feedstock (Reference)
$C_2H_2 + C_2H_4 + C_2H_6$	40800	Lignin (Liakakou et al. 2021)
Aromatics	7883	
H_2S	1165	
COS	31	
$C_2H_2 + C_2H_4 + C_2H_6$	10000 – 58000*	Switchgrass (Broer et al. 2015)
H_2S	170 – 320	
COS	20 – 49	
NH_3	1270 - 2270	
HCN	254 – 454*	
NO_x	140 – 150 (NO)	Switchgrass (Datar et al., 2004; Ahmed and Lewis, 2007)

*interpreted/calculated from graphical representations in the original publication

How each of these components affects the fermentation performance is important when coupling biomass gasification and subsequent fermentation, since they might impact the

fermentation negatively. Therefore, it is not surprising that several publications in which biomass gasification and fermentation were coupled, the syngas went through a gas cleanup step prior to being supplied to the fermentation, thus avoiding possible negative effects (Datar et al., 2004; Liakakou et al., 2021; Ramachandriya et al., 2013; Rückel et al., 2022).

Fuel bound nitrogen (FBN) is mainly converted to N_2, char and tar bound nitrogen, hydrogen cyanide and ammonia (Broer and Brown, 2016). Ammonia and HCN combined can mount up to more than 50% of FBN in the steam gasification of switchgrass (Broer et al., 2015), and thus could influence the performance of the syngas fermentation, since both components are soluble in water and would accumulate in a continuously gasified process. At a pH range of pH 4.0 – pH 6.0, relevant for the syngas fermentation with *C. ljungdahlii* and *C. ragsdalei*, ammonia is present in aqueous solutions fully as ammonium; given its high solubility, a continuously gassed process would accumulate ammonia in form of ammonium, and thus possible effects of ammonium in such processes are of interest. Ammonium is present in most of the cultivation media for syngas fermentation, and concentrations up to 155.2 mM NH_4^+ had a beneficial effect on the continuously gassed syngas fermentation with *C. carboxidivorans* (Rückel et al., 2021), whereas the increase from 46.75 mM to 116.88 mM NH_4^+ had no negative effect in the batch syngas fermentation with *C. ragsdalei* (Saxena and Tanner, 2012). HCN is in the same pH range as dissolved HCN, and thereby the continuous gassing with a HCN containing gas would lead to an equilibrium between the gaseous and the liquid phase, putting a limit in how much HCN can accumulate in the reactor. Oswald et al. (2018) demonstrated that HCN had an inhibitory effect in batch processes with *C. ljungdahlii.* This inhibition was expressed as a prolonged lag-phase for HCN concentrations up to 0.1 mM, after which cells adapted. No adaption was observed with 1.0 mM HCN.

Sulfur present in the fuel is mostly converted to H_2S after gasification (Broer et al. 2015). Rückel et al. (2021) investigated the influence of sulfide in the continuously gassed syngas fermentation with *C. carboxidivorans* through the addition of thioacetamide and observed that the equivalent addition of up to 29.4 mM sulfide had a positive effect in biomass growth and alcohol production. In batch processes with *C. ragsdalei*, Hu et al. (2010) observed a slightly negative effect of up to 1.9 mM sulfide on the biomass growth and a slight improvement in the ethanol production. Negative effects from sulfide are associated with its dissolved undissociated form, which permeates through the cell membrane and can cause DNA damage or protein denaturation (O'Flaherty et al., 1998; Ntagia et al., 2020).

Nitrogen oxide (NO) has been shown to have a strong reversible effect on the hydrogenase of *C. carboxidivorans*, with complete inhibition occurring with 160 ppm NO (Ahmed and Lewis, 2007). Interestingly, it was also shown that the cells were able to produce ethanol in a batch

process in which 130 ppm NO was added to the gaseous phase after the fourth day, despite the almost full inhibition of the hydrogenase. Dissolved NO is in equilibrium with nitrite and nitrate, and the latter two could also influence the syngas fermentation. Emerson et al. (2019) investigated the effect of added nitrate in the growth of *C. ljungdahlii* with H_2/CO_2. Nitrate could function as an electron acceptor, bypassing the WLP and receiving electrons from H_2, thus enabling a further functioning of the Rnf/ATP synthase system for ATP generation. 15 mM nitrate increased the maximal cell dry weight concentration achieved, whereby no ethanol was built while nitrate was still available, and formate was produced in the exponential growth phase. With CO/CO_2 as substrate, the nitrate supplementation had a negative effect.

3.2.3 Pathways for Ethanol and 2,3-Butanediol Formation

Ethanol Production

C. ljungdahlii and *C. ragsdalei* have the genetic potential to produce ethanol from acetyl-CoA through two pathways: through the direct reduction of acetyl-CoA to acetaldehyde and further reduction to ethanol, or through the production of acetate, which is reduced to acetaldehyde and further to ethanol. The first route involves a NADH using aldehyde dehydrogenase (ALDH) to produce acetaldehyde. The second route involves acetate production, as previously described in subsection 3.1.2, and the ferredoxin dependent reduction of acetate to acetaldehyde by an aldehyde:ferredoxin oxidoreductase (AOR). Once aldehyde was produced, it is further reduced to ethanol by an alcohol dehydrogenase with NADH as redox cofactor (Köpke et al., 2010). The production of ethanol through acetate offers the benefit of the ATP production related to the acetate formation, and thus is the primary route for ethanol formation in *C. ljungdahlii* (Richter et al., 2016).

Ethanol formation from CO or H_2/CO_2 follows the stoichiometry (Sun et al. 2019)

$$6CO + 3H_2O \rightarrow C_2H_5OH + 4CO_2 \qquad \Delta G^0 = -97.0\ kJ\ mol^{-1} \tag{3.8}$$

$$6H_2 + 2CO_2 \rightarrow C_2H_5OH + 3H_2O \qquad \Delta G^0 = -217.4\ kJ\ mol^{-1} \tag{3.9}$$

Acetogens such as *C. ljungdahlii* and *C. ragsdalei* produce ethanol as a form to dissipate energy as the flow of electrons increases (Allaart et al., 2023), whereby further ATP can be generated with the Rnf complex. The production of acetate from acetyl-CoA and the reduction of acetate to ethanol with the corresponding ATP yield follows:

$$Acetyl - CoA + ADP + P_i \rightarrow CH_3COOH + ATP \tag{3.10}$$

$$CH_3COOH + 2\ CO/2\ H_2 + 1/0\ H_2O\ + 0.546/0.273\ (ADP + P_i) \rightarrow C_2H_5OH + 2\ CO_2/1\ H_2O + 0.546/0.273\ ATP \tag{3.11}$$

2,3-Butanediol Production

2,3-butanediol is derived from pyruvate in acetogens, which is formed by the reductive carboxylation of acetyl-CoA by a pyruvate:ferredoxin oxidoreductase (PFOR). This step is reversible and it represents the link between the heterotrophic metabolism and the WLP by the assimilation of CO_2 from the formation of acetyl-CoA from pyruvate (Ragsdale, 2008b). Two pyruvate molecules form acetolactate with the release of CO_2, a reaction catalysed by an acetolactate synthase. Acetolactate undergoes decarboxylation, releasing CO_2 by an acetolactate decarboxylase forming R-acetoin. Acetoin is finally reduced to 2,3-butanediol with a NADH dependent 2,3-butanediol dehydrogenase (BDH) or a NADPH dependent primary-secondary alcohol dehydrogenase (CaADH). 2,3-butanediol formation is thought to serve as a form of deacidification from the accumulation of pyruvic acid and as an overflow mechanism if the intracellular environment is overly reduced (Köpke et al., 2011).

2,3-butanediol formation from CO or H_2/CO_2 follows the stoichiometries (Rückel et al. 2022) and ATP yields of:

$$11CO + 5H_2O \rightarrow C_4H_{10}O_2 + 7CO_2 \qquad \Delta G^0 = -361.8\ kJ\ mol^{-1} \tag{3.12}$$

$$11H_2 + 4CO_2 \rightarrow C_4H_{10}O_2 + 6H_2O \qquad \Delta G^0 = -140.7\ kJ\ mol^{-1} \tag{3.13}$$

$$4Acetyl - CoA + 3\ CO/3\ H_2 + 1/0\ H_2O\ + 1.055/-0.995\ (ADP + P_i) \rightarrow C_4H_{10}O_2 + 3\ CO_2/2\ H_2O + 1.055/-0.995\ ATP \tag{3.14}$$

The pathways to the formation of ethanol and 2,3-butanediol in acetogens are schematically shown in Figure 3.

3.2.4 Key Influences of Alcohol Formation with Acetogens

Several factors influence the production of ethanol and 2,3 butanediol by *C. ljungdahlii* and *C. ragsdalei*. In this subsection, some of these factors will be described.

Medium Composition

The medium composition for syngas fermenting acetogens contains inorganic nitrogen and phosphate sources, minerals (mainly sodium, calcium, magnesium, and potassium), commonly yeast extract, trace metals, vitamins and a reducing agent. Detailed studies to the effect of each individual component in the alcohol formation with syngas fermentation are scarcely available and hardly comparable since the overall medium composition and the

experimental setup might differ. Nevertheless, some aspects can be gathered from the published literature.

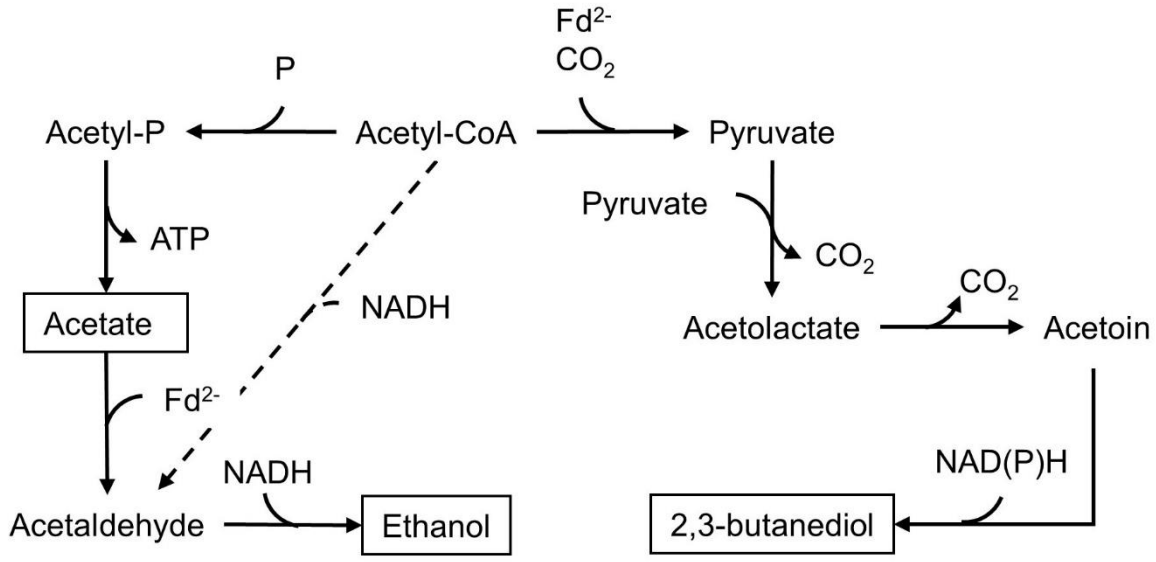

Figure 3 – Pathways to the formation of acetate, ethanol and 2,3-butanediol from acetyl-CoA. A phosphotransacetylase converts acetyl-CoA to acetyl phosphate (Acetyl-P), which is further converted to acetate by an acetate kinase with the release of ATP. Acetate is reduced to acetaldehyde with ferredoxin by an aldehyde:ferredoxin oxidoreductase (AOR). Acetaldehyde is reduced with NADH to ethanol by an alcohol dehydrogenase. Alternatively, acetaldehyde can be directly formed from Acetyl-CoA using an aldehyde dehydrogenase and NADH. 2,3-butanediol formation starts with the formation of pyruvate from acetyl-CoA using ferredoxin through a pyruvate:ferredoxin oxidoreductase. Acetolactate is formed from pyruvate and further converted to acetoin, which is finally reduced to 2,3-butanediol by either a NADH dependent 2,3-butanediol dehydrogenase (BDH) or a NADPH dependent primary-secondary alcohol dehydrogenase (CaADH)

Saxena and Tanner (2012) investigated the effect of the ions of sodium, calcium, magnesium and potassium, as well as the ions of ammonium and phosphate, and vitamins in the syngas fermentation with *C. ragsdalei*. The processes were conducted in anaerobic tubes with a gas mixture of $CO:N_2:CO_2$ (70:24:6). For Na^+, Ca^{2+}, Mg^{2+} and K^+, the changes studied were their complete removal or a fivefold increase in the concentration. It was observed that the absence of magnesium ions and the fivefold increase in sodium ions hemmed growth and ethanol formation, fomenting acetate production; in all other cases with these minerals, no difference was observed. The complete removal of ammonium and phosphate also hemmed growth and alcohol formation and fomented acetate production, while their increase to 2.5-fold of the standard concentration had no influence in the process performance. The removal of the vitamin solution from the medium also had no influence on growth, ethanol, and acetate formation.

The effect of trace metals ions in the syngas fermentation with *C. ragsdalei* was studied by Saxena and Tanner (2011). They observed that the ethanol formation and final cell dry weight concentration were strongly influenced by an individual tenfold increase in the concentrations of nickel ions (394% and 44.1% increases for ethanol and the specific growth rate, respectively) and zinc ions (425% and 41.2% increases for ethanol and the specific growth rate, respectively) and to a lesser extent by the tenfold increase of the tungsten content. The removal of copper from the medium also had a positive effect in the ethanol formation. Despite the similar results generated by the increase in the ions of nickel and zinc, their effect on the activities of the FDH, CODH, hydrogenase and alcohol dehydrogenase were very distinct, with negligible changes observed with the zinc ion supplementation and strong increases in the activities of the CODH and hydrogenase with the nickel ion supplementation.

Ricci et al. (2021) studied the influence of medium composition in the formation of 2,3-butanediol with *C. ljungdahlii* and *C. autoethanogenum.* They observed that the 2,3-butanediol production increased almost twofold with a medium with higher vitamins and iron concentration. Analysing the publication in more detail, the only component which can be individually assessed is iron, and its 3.6-fold increase in the medium led to an increase of roughly 10% in the final 2,3-butanediol concentration.

Cysteine is the most common reducing agent in the syngas fermentation with acetogens. The effect of cysteine in the syngas fermentation with *C. autoethanogenum* and *C. ljungdahlii* was studied by Abubackar et al. (2012) in serum vials, and Infantes et al. (2020) in continuously gassed stirred-tank reactors, respectively. Both studies observed little effect of increasing the initial cysteine concentration in biomass growth and alcohol formation.

pH, Temperature and Acid Crash

The acetate reduction to ethanol can function as a mechanism to avoid intracellular acidification. As acetate is produced and released into the medium, the external pH decreases if not controlled. Acetic acid is partially dissociated in aqueous solutions, and the fraction of dissociated/undissociated acid is governed by the thermodynamic conditions. Assuming that equilibrium conditions for the dissociation applies, each fraction is determined by:

$$pK_a = pH + log[HA] - log[A^-] \quad (3.15)$$

pK_a Dissociation constant for the monoacid

$[HA], [A^-]$ Concentration of undissociated (HA) and dissociated acid (A^-), M

pK_a of acetic acid at 25 °C is 4.756 (Lide, 2008). Using this relation, as the external pH decreases due to acetate production, not only the overall concentration of the acetic acid pair increases, but also the fraction of undissociated acid, as can be seen in Figure 4 by the molar fractions of undissociated acetic acid and acetate as a function of pH.

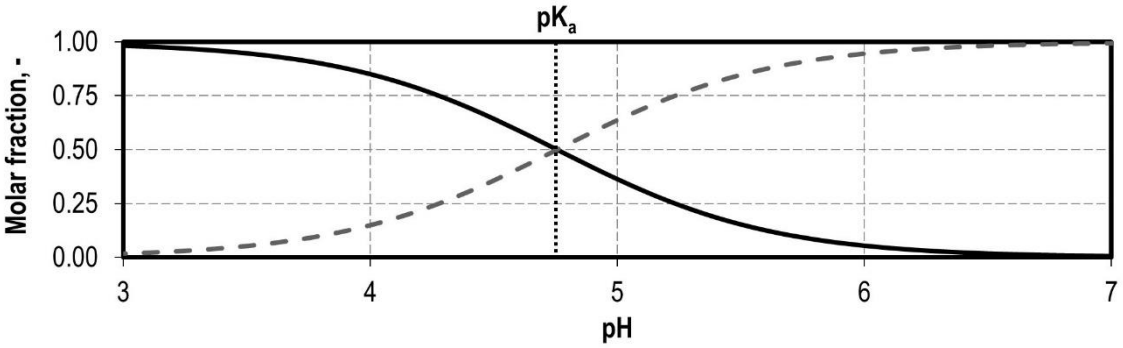

Figure 4 – Molar fractions of undissociated acetic acid (black line) and acetate (dashed line) as a function of pH, based on a pK_a for acetic acid at 25 °C of 4.756 (Lide, 2008)

External undissociated acetic acid can freely diffuse through the cell membrane into the cell. Internal cell conditions, assumed to be pH 6.0 (Richter et al. 2016), force a dissociation of the undissociated acetic acid, which lowers internal cell pH. The cells counter this acidic load by reducing acetate to ethanol. This beneficial effect of a lower pH on ethanol production has been shown in several publications (Abubackar et al., 2016; Abubackar et al., 2012; Arslan et al., 2019; Cotter et al., 2009b; Infantes et al., 2020; Richter et al., 2016; Richter et al., 2013). The effects of pH on the 2,3-butanediol production from syngas fermentation are less well studied. It has been however hypothesized, that the 2,3-butanediol production could also be fomented by lower pH as a deacidification mechanism (Köpke et al., 2011).

Inversely, higher pH foments acid production. Maddox et al. (2000) enlisted three common reasons for failing to trigger solvent production in acetone-butanol-ethanol (ABE) fermentations with *Clostridia*: (1) High pH, which is a metabolic regulation of the cells and is instant; (2) culture degeneration, which occurs over continuous processes with a genetic change in the population and is very slow; and (3) the acid crash, which occurs fast and is particular to a fermentation run. Maddox et al. (2000) argued that the reason for the acid crash is the overly fast accumulation of undissociated acids, and that the strategies for overcoming it involve slowing acid formation or the overall process. These could be achieved by lowering the pH, the process temperature, or the yeast extract concentration. Ramió-Pujol et al. (2015) used these recommendations and compared processes in test tubes with *C. carboxidivorans* at 37 °C and 25 °C. The ethanol concentration increased from 1.56 mM to 32.1 mM with the decrease in process temperature, whereas the formation of the chain-elongated alcohols

butanol and hexanol were only observed at 25 °C. Shen et al. (2017) pursued a similar approach as Ramió-Pujol et al. (2015) with *C. carboxidivorans*, more than doubling the alcohol production in anaerobic flasks with daily replenishing of the gaseous phase with a temperature profile of 37 °C for 24 h and 25 °C for another 120 h.

Wang et al. (2011) argued that the reason for the acid crash in ABE fermentation is the accumulation of intracellular formic acid. This was tested by constructing a recombinant strain of *Clostridium acetobutylicum* with formate dehydrogenase activity (FDH) and successfully countering the acid crash. However, *C. carboxidivorans,* studied by Ramió-Pujol et al. (2015), has FDH activity, and thus acid crash does not directly explain the improvement in the alcohol production. Shen et al. (2020) conducted a comparative transcriptome analysis of processes with *C. carboxidivorans* at 37 °C and 25 °C and observed that genes of the WLP were upregulated at 37 °C, while the lower temperature of 25 °C was more advantageous for the genes linked to chain elongation. Surprisingly, the expression of genes linked to the aldehyde:ferredoxin oxidoreductase were equally high at both temperatures, despite the beneficial effect of the lower temperature on the alcohol formation. Thus, lowering the process temperature might be beneficial for solvent production more through a metabolic readjustment than for avoiding an acid crash.

Carbon Source and Redox Balancing

Syngas has variable concentrations of CO, H_2 and CO_2, which are dependent on its source and production method, and ideally all three components should be converted to the desired products. However, whether CO or H_2 is used as an electron donor in the gas fermentation plays a key role in the production of alcohols.

CO and H_2 transfer electrons differently, as previously discussed in subsection 3.1.2. CO transfers electrons solely to the more reduced redox cofactor ferredoxin and H_2 transfers electrons to ferredoxin and NADP by the HytA-E. Considering the production of 1 mol of acetyl-CoA from 2 mol of CO_2, 4 mol of CO are oxidized, producing 4 mol of ferredoxin; with H_2 as electron donor, 4 mol of H_2 are oxidized producing 2 mol of ferredoxin and 2 mol of NADPH. Thus, CO offers a more negative redox potential from the same acetyl-CoA production in comparison to H_2. This has deep implications for the performance of the syngas fermentation, both for the biomass growth as well as for the alcohol production.

The cells derive ATP from the chemiosmosis generated by the Rnf complex, which drives the membrane bound ATP synthase, and from the production of acetate, as previously discussed in subsection 3.1.2. The Rnf complex uses for this purpose reduced ferredoxin to translocate

the protons through the membrane, whereby also reducing NAD. A higher availability of ferredoxin from CO as electron donor would thus enable more ATP production and thus biomass growth. With H_2, less redox potential is available, and the cell compensates the lower ATP production from the Rnf complex/ATP synthase by producing more acetate, which in turn deviates carbon from biomass production. Richter et al. (2016) calculated that the ATP generation per mol acetate with CO is 1.503 mol ATP and with H_2 is 0.956 mol ATP.

Furthermore, a lower redox potential from CO would also favor the reduction of acetate to ethanol, and the reduction of acetoin to 2,3-butanediol. This has been well demonstrated with *C. ljungdahlii* by Phillips et al. (1994), which showed in continuously gassed processes in stirred-tank reactors a 2.5-fold higher final cell dry weight concentration with CO than with H_2, and a roughly twice higher specific growth rate. Additionally, the biomass related product yield increased with H_2 by 4.7 fold, with the acetate to ethanol ratio more than doubling with H_2, corroborating the previously discussed necessity to produce more acetate for ATP generation. Ricci et al. (2021) showed with *C. ljungdahlii* and *C. autoethanogenum* that the 2,3-butanediol production is also deeply impacted by the gas composition. With both strains, no 2,3-butanediol was produced with H_2 and CO_2 as substrates, and the highest 2,3-butanediol final concetration was obtained with a gas composition of 80% CO and 20% CO_2.

3.3 Bioprocess Engineering Fundamentals

In this section, some bioprocess engineering fundamentals are described, which contribute to the understanding of the processes conducted in this study. When applicable, the connection to the syngas fermentation will be highlighted. Unless indicated otherwise, the fundamentals presented here were taken from Weuster-Botz and Takors (2018) and Takors and Weuster-Botz (2018).

Kinetic for Microbial Growth

Given a cell culture, microbial growth is the increase in the cell mass of the culture. This growth in cell mass is often correlated to the increase in the cell number, whereby several cases differ from this assumption, such as hypha-building fungi or microalgae in the lipid accumulation phase. To support this growth, all nutrients should be available in the cell broth, as well as the thermodynamic conditions (pH, ionic strength, temperature, pressure) should be supportive.

Given a medium with an initial nutrient concentration ideal for growth and ideal thermodynamic conditions, upon inoculation, the cell mass undergoes different growth phases in an ideally

mixed environment. Initially, they adapt to the new conditions without growth; once adaption occurred, cell growth resumes, increasing until reaching the exponential phase, a phase in which growth occurs unhindered. As the cell mass growth and the substrates are depleted, growth slows and subsequently stops. This can occur due to a complete substrate depletion, the accumulation of toxic (by)products, or growth correlated changes in some thermodynamic conditions or other reasons. Lastly, in continued exposure to these conditions, the cell mass decreases. These phases of an ideal batch process are depicted in Figure 5.

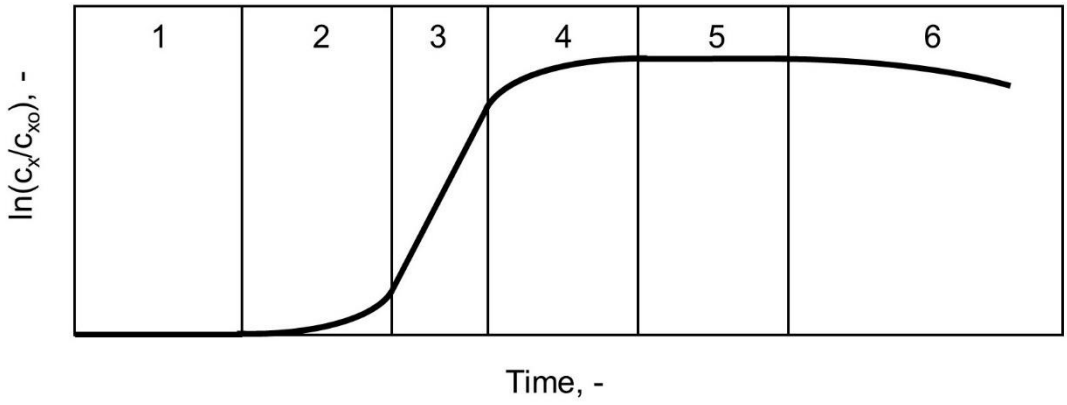

Figure 5 – Growth phases of a cell culture inoculated with a cell dry weight concentration c_{X0}. 1 – lag phase; 2 – first transition phase; 3 – exponential growth phase; 4 – second transition phase; 5 – stationary phase; 6 – death phase.

Assuming that the cell culture can be described as a homogeneous culture (unstructured), and neglecting the individual metabolic reactions (unsegregated), the cell growth can be described by the specific growth rate, defined as

$$\mu \equiv \frac{1}{c_X} \cdot \frac{dc_X}{dt} \tag{3.16}$$

μ Specific growth rate, h^{-1}

c_X Cell concentration, g L^{-1}

t Time, h

The specific growth rate is dependent on the thermodynamic conditions, as well as substrate concentration, product inhibition and other possible inhibiting factors. It reaches its maximum in the exponential growth phase, in which it is also constant with time.

To account for substrate limitation, a common description of the specific growth rate is

$$\mu = \mu_{max} \cdot \prod \frac{c_{s,i}}{K_{s,i} + c_{s,i}} \tag{3.17}$$

μ_{max} Maximal specific growth rate, h^{-1}

$c_{s,i}$ Substrate *i* concentration, g L^{-1}

$K_{s,i}$ Saturation constant of substrate *i*, g L^{-1}

Whereby equation 3.17 is often simplified to account for the effect of one limiting substrate.

Some substrates can inhibit growth, as is the case with *Clostridium aceticum* using CO as substrate (Mayer et al. 2018). A common mathematical description for substrate inhibition is

$$\mu = \mu_{max} \cdot \frac{c_s}{K_s + c_s + c_s \cdot \left(\frac{c_s}{K_I}\right)^n} \tag{3.18}$$

n Sensitivity factor, -

K_I Inhibition constant, g L^{-1}

The formation of products which are growth coupled can be associated to the specific growth rate by

$$r_p \equiv \frac{dc_p}{dt} = q_p \cdot c_X = \frac{\mu}{Y_{Xp,\mu}} \cdot c_X \tag{3.19}$$

r_p Product formation rate, g L^{-1} h^{-1}

c_p Product concentration, g L^{-1}

q_p Specific product formation rate, h^{-1}

$Y_{Xp,\mu}$ (Biomass related) product yield, g g^{-1}

The specific product formation rate can also be expanded to include the product formation independent of growth by

$$q_p = \frac{\mu}{Y_{Xp,\mu}} + k_p \tag{3.20}$$

k_p Growth independent product formation rate, g L^{-1} h^{-1}

Ideally Stirred-Tank Reactor

Bioreactors are equipment in which materials are converted through the action of enzymes, cells, or microorganisms. The standard bioreactor employed is the stirred-tank reactor, in which impellers provide the power for homogenizing, suspending, and dispersing. Assuming

that the reactor is perfectly homogeneous, and thus all conditions are the same within the whole liquid volume of the reactor, a batch process can be described by

$$\frac{dm_i}{dt} = \frac{d(V \cdot c_i)}{dt} = V \cdot r_i \tag{3.21}$$

m_i Mass of component *i* in the reactor volume, g

c_i Concentration of component *i*, g L^{-1}

V Reactor volume, L

r_i Component *i* production rate, g L^{-1} h^{-1}

Applying this mass balance in a reactor with constant volume for the biomass concentration during the exponential growth phase, in which all nutrients are available, and the cells grow with a constant maximal specific growth rate, it renders

$$\frac{dc_x}{dt} = \mu_{max} \cdot c_X \tag{3.22}$$

Which upon integration results in the biomass concentration over time

$$c_X = c_{x0} \cdot e^{\mu_{max} \cdot t} \tag{3.23}$$

A batch process requires that all nutrients are present at the process start. However, a more common operation mode is the fed-batch process, in which a certain nutrient is fed to the reactor as desired. This modus is suitable for several specific cases, for instance to reduce the formation of byproducts, mitigate substrate inhibition, supply gaseous substrates or specifically direct the metabolism through the substrate availability. In this case, the mass balance of the fed-batch stirred-tank reactor is described by

$$\frac{dm_i}{dt} = \frac{d(V \cdot c_i)}{dt} = F_{in} \cdot c_{in,i} + V \cdot r_i \tag{3.24}$$

F_{in} Volume flow of feed, L h^{-1}

$c_{in,i}$ Concentration of component *i* in feed, g L^{-1}

Gas-Liquid Mass Transport

With gaseous substrates, as is the case in the syngas fermentation, supplying the cells with sufficient substrate is necessary to avoid a substrate limitation. When considering a gassed stirred-tank reactor, the molecules in the gaseous phase are transferred from the bulk gas through the gas-liquid interface to the bulk liquid, and from the bulk liquid through the cell membrane inside the cell.

To describe this transport of a gas molecule, some assumptions can be taken. Firstly, assuming that the reactor is ideally mixed, the dissolved gas in the liquid bulk and the gas bubbles are homogeneously distributed. Secondly, the transport resistance from the liquid bulk to the cells can be neglected, since the surface area of the cells can be up to three orders of magnitude higher than the surface area of the gas-liquid transport (Phillips et al., 2017). Therefore, the main transport resistance lies in the mass transfer from the gas bulk to the liquid bulk, which is commonly described by the two-film theory. This theory assumes that a boundary layer exists on each side of the gas-liquid interface, in which mass transport occurs diffusively. A schematic representation of the two-film theory is shown in Figure 6.

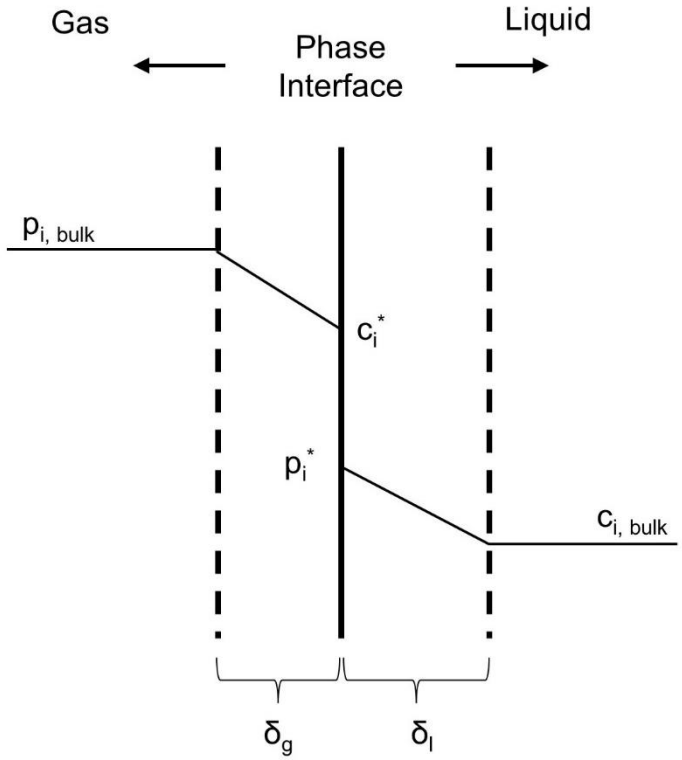

Figure 6 – Schematic representation of the mass transport phenomenon of component *i* from the gas bulk, with a partial pressure p_i, to the liquid bulk, with a concentration c_i, according to the two-film theory. Adjacent to the interface are boundary layers on each side with length of δ_g and δ_l for the gaseous and the liquid phase, respectively, in which component *i* is transferred through diffusion. On the interface, thermodynamical equilibrium between phases prevails, with the concentration and partial pressure identified by *.

On the phase interface, the concentrations in the gaseous and liquid phases are in equilibrium, and thus can be described by the Henry's law.

$$p_{i,s} = H_i \cdot c_i^* \tag{3.25}$$

$p_{i,s}$ Partial pressure of *i* on the interface, kPa

H_i Henry constant of *i*, kPa L mol^{-1}

c_i^* Equilibrium concentration of *i* on the interface, mol L^1

The molar flow density of a component on each film can be described as

$$q_i' = k_{g,i} \cdot \left(c_g - c_{g,s}\right)_i \quad (3.26)$$

$$q_i' = k_{l,i} \cdot \left(c_{l,s} - c_l\right)_i \quad (3.27)$$

$$q_i' = K_{l,i} \cdot (c_l^* - c_l)_i \quad (3.28)$$

q_i' Molar flow density of *i*, mol m^2 s^-

k_g, k_l Transport coefficient of the gas (*g*) and liquid (*l*) phases, m s^{-1}

$K_{l,i}$ Overall transport coefficient, m s^{-1}

Combining equations 3.25 – 3.28, the overall transport coefficient can be defined as

$$\frac{1}{K_{l,i}} = \frac{1}{k_{l,i}} + \frac{1}{H_i \cdot k_{g,i}} \quad (3.29)$$

Given that the diffusion coefficient of a component is substantially higher in the gaseous phase, the transport resistance in the gas phase is substantially lower than in the liquid phase. Thus, the second term of equation 3.29 is negligible and the overall transfer coefficient equals the transfer coefficient of the liquid phase ($K_{l,i} = k_{l,i}$).

The relationship described in equations 3.28 and 3.29 for an interface can be extrapolated to the reactor volume with the introduction of the volumetric surface area, which considers the surface area for mass transport per reactor volume. Thus, the transfer rate can be described by

$$q_i = k_l \cdot a \cdot (c_l^* - c_l)_i \quad (3.30)$$

a Volumetric surface area, m^2 m^{-3}

Equation 3.30 enables the interpretation of the transfer rate as composed of three factors: the concentration gradient $(c_l^* - c_l)_i$, the available surface area a and the transfer coefficient k_l. Thus, to improve the transfer rate

- the gradient can be increased by *e.g.* increasing the operating pressure, which increases the gas solubility;
- the volumetric surface area can be increased by *e.g.* decreasing the diameter of bubbles with an appropriate sparger;
- the mass transfer coefficient can be increased by increasing the stirrer speed.

4 Materials and Methods

In this chapter, the materials, process setup and analytical methods used in this work will be presented. These include the *clostridial* strains used, handling and cultivation conditions and the reactor system implemented, as well as the analytical methods required to assess and evaluate the processes. A list of the chemicals and equipment used is presented in the Appendix.

4.1 Bacterial Strains *Clostridium ljungdahlii* and *Clostridium ragsdalei*

The bacterial strains *Clostridium ljungdahlii* (DSM 13528) and *Clostridium ragsdalei* (DSM 15248) were used in all processes conducted in this work and were obtained from the German Collection of Microorganisms and Cell Cultures (DSMZ, Braunschweig, Germany). Acquired *C. ljungdahlii* was delivered freeze-dried, whereas *C. ragsdalei* was initially delivered as an active culture and later in the duration of this work also as a freeze-dried culture.

4.2 Anaerobic Work and Anaerobic Medium Preparation

Handling of both strains and anaerobic medium preparation was conducted entirely under anaerobic conditions. Working steps, which required an open atmosphere, were conducted in a flexible polyvinylchloride anaerobic chamber with internal gas recirculation (Coy Laboratory Products Inc., Grass Lake, USA) and accessed with integrated gloves. The chamber was filled with forming gas (5% (v/v) H_2 and 95% (v/v) N_2). Invasive oxygen was converted with the present hydrogen to water on palladium catalysts, and desiccants removed the formed water from the atmosphere. The catalyst and the desiccants were contained within wire meshes, which were stacked on the fan box that recirculates the gas phase. The humidity and contents of oxygen and hydrogen in the atmosphere were monitored, and accordingly the desiccants were regenerated, or the atmosphere refilled with forming gas. Desiccants were regenerated in a drying oven overnight at 170 °C. A HEPA-Filter unit was integrated in the chamber to sterilize its atmosphere.

The chamber contained two adjacent airlocks to transfer objects into the chamber. For this transfer, the objects were placed inside the airlocks and its atmosphere was emptied using a vacuum pump (Coy Laboratory Products Inc., Grass Lake, USA) and refilled with forming gas.

This process was repeated three times and conducted manually. A schematic representation of the anaerobic chamber is shown in Figure 7.

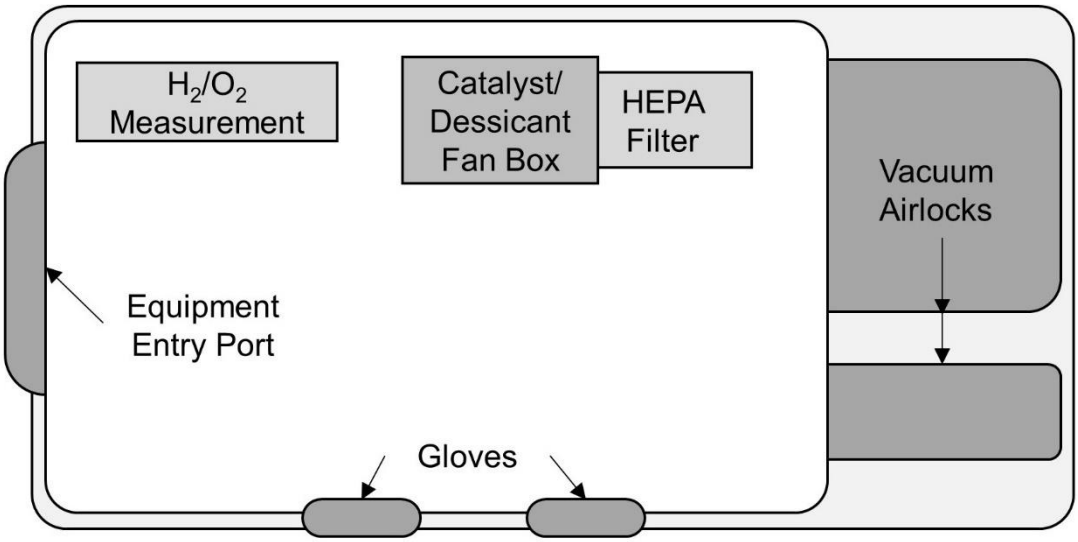

Figure 7 – Schematic representation of the anaerobic chamber described in subsection 4.2.

Anaerobic media were prepared either by mixing dried chemicals with anaerobic water inside the anaerobic chamber, or by previously removing the oxygen from the medium and subsequently filling up to the end volume with anaerobic water inside the anaerobic chamber. Anaerobic water/media were produced by boiling it in a heating mantle (Wise Therm WHM 12015, Witeg, Wertheim, Germany) for 20 minutes and subsequently gassing it with N_2 for 20 minutes in an ice bath.

4.3 Cultivation Medium

The cultivation medium for the processes with *C. ljungdahlii* and *C. ragsdalei* was constituted according to Doll et al. (2018), with its composition based on stocks solutions presented in Table 2, and the composition of the individual stock solutions in Table 21 in the Appendix.

The magnesium and calcium solutions were stored at room temperature. The mineral and trace elements solutions were stored at 4 °C. The vitamin solution was stored at -20 °C. The cysteine solution was anaerobic, placed in flasks with a butyl rubber septum, sterilized and stored at room temperature. Sterilization was conducted with vertical floor standing autoclaves at 121 °C for 20 minutes.

Table 2 – Composition of the cultivation medium according to Doll et al. (2018), based on stock solutions. The compositions of the stock solutions are presented in Table 21 in the Appendix.

Component	Concentration	Unit
Mineral Solution	30	mL L^{-1}
Magnesium Solution	60	mL L^{-1}
Calcium Solution	60	mL L^{-1}
Trace Elements Solution	10	mL L^{-1}
Vitamin Solution	10	mL L^{-1}
Yeast Extract	1	g L^{-1}
2-(N-morpholino)ethanesulfonic acid (MES)*	15	g L^{-1}
Cysteine-HCl Solution	8	mL L^{-1}

* MES (buffer) was only used in anaerobic flasks.

The mineral, magnesium, calcium, trace elements and vitamin solutions, the yeast extract and, if applicable, 2-(N-morpholino)ethanesulfonic acid were combined and the volume was adjusted with deionized water. The pH of the solution was adjusted to pH 6.0 with the addition of 10 M NaOH. In the case of anaerobic flasks, the solution was anaerobised and transferred into the anaerobic chamber. There, its volume was completed with anaerobic water and the final solution was divided in coated flasks to a volume of 100 mL. These flasks were sealed with butyl rubber septa and sterilized at 121 °C for 20 minutes. For media for continuously gassed processes in stirred-tank reactors, no buffer was added and the pH was not adjusted prior to sterilization. In this case, pH control and oxygen removal were conducted in the reactor.

The cysteine solution was added accordingly prior to inoculation with the use of single-use syringes and sterile cannulas.

4.4 Culture Handling

Acquired freeze-dried cells from the DSMZ were reactivated and used to produce frozen cell stocks. These came in glass ampules, which were opened in the anaerobic chamber and the dry content was resuspended initially in 1 mL growth medium with fructose. This inoculum was transferred to 8 Hungate-tubes with 5 mL growth medium. The Hungate-tubes were placed in a shaking incubator at 37 °C with 100 rpm.

Once growth was observed, the cell culture was transferred to anaerobic flasks with 100 mL medium with 5 g L^{-1} fructose. These were also placed in the shaking incubator at 37 °C with

100 rpm. In the end of the exponential growth phase, one flask was transferred into the anaerobic chamber. There, sterilized glycerine was added as anti-freeze protection up to 10% (v/v) of the cell suspension and subsequently transferred to Hungate-tubes in 5 mL aliquots. These cell stocks were stored at -80 °C.

Active cultures of *C. ragsdalei* were received from the DSMZ in Hungate-tubes. The cell suspension was transferred to 500 mL anaerobic flasks with 100 mL cultivation medium and gassed with 1.2 bar CO, 0.4 bar H_2 and 0.4 bar CO_2. The flasks were kept at 37 °C with 100 rpm in a shaking incubator. The cell suspension was transferred twice a week with an inoculum volume of 1% v/v. This active cell maintenance was kept for 12 weeks, after which a new active culture would be acquired.

4.5 Preculture Preparation

Precultures of *C. ljungdahlii* were produced from the frozen cell stocks. Those of *C. ragsdalei* were produced from the active culture maintenance, and for the results in section 5 (A Closer Look into CO and H_2 as Electron Donors) and for two replicates of the reference process (pH 6.0 and 37 °C), the precultures were produced from frozen stocks as well.

For frozen stocks, a two-step cultivation was conducted. The frozen stocks were thawed at room temperature and used to inoculate 500 mL anaerobic flasks with 100 mL sterile cultivation medium and gassed with 1.2 bar CO, 0.4 bar H_2 and 0.4 bar CO_2. Inoculum volume was 2.5 mL and the flasks were kept at 37 °C with 100 rpm. After 48 h to 72 h, 2 mL of cell broth were transferred to another equally prepared anaerobe flask. The cells were harvested after 44 – 48 h.

For harvesting, the flasks with cells in the end of the exponential growth phase were purged with N_2. This was done by three sequential cycles alternating the gassing of the flasks with N_2 to 2 bar and the release of the gas to the exhaust, normalizing the pressure. The pressure was measured with a manual manometer. The gas phase was accessed with sterile cannulas attached to the gassing pipe, the manometer, and the pipe to the exhaust. Afterwards, the flasks were transferred to the anaerobic chamber, where the cell suspension was transferred to 50 mL polypropylene tubes with screw cap. The tubes were transferred out of the anaerobic chamber and centrifuged in a floor-standing centrifuge for 10 minutes at room temperature and 4500 rpm. The centrifuged cells with supernatant were re-transferred into the anaerobic chamber, where the supernatant was discarded and the cell pellet resuspended with an anaerobic phosphate saline buffer (PBS, pH 7,4, composition in Table 22). The volume of PBS

used was such, that a 10 mL resuspended inoculum would achieve an initial optical density (wavelength of 600 nm) of 0.1 in the reactor.

4.6 Autotrophic Batch Processes in Continuously Gassed Stirred-Tank Reactors

A 2-L stirred glass tank reactor (Infors HT, Bottmingen, Switzerland) was used for the continuously gassed batch processes. The double jacketed reactor was equipped with two Rushton impellers for stirring and 3 baffles. Gassing was conducted through a gassing frit, placed under the Rushton impellers. The inlet gas was previously sterile filtered through a filter integrated in the inlet gas pipe. A temperature sensor monitored the temperature in the reactor, and the temperature was controlled with a recirculating pump using water as cooling/heating agent. The pH was monitored with a pH probe and controlled with the addition of 3 M NaOH or 2 M H_2SO_4, conducted with integrated peristaltic pumps. Redox of the culture was monitored with a redox probe. The software (Iris V5.3, Infors HT, Bottmingen, Switzerland) carried out the control of the pH and temperature based on the desired set point. A flowchart of the reaction system is shown in Figure 8.

Independent mass flow controllers (WMR 4000, Westphal Mess-und Regeltechnik GmbH, Ottobrunn, Germany) modulated the gassing of the reactor with CO, H_2, N_2 and CO_2 individually. The exhaust gas was cooled to 2 °C with a reflux condenser and analysed for CO, CO_2, H_2, and H_2S, combining a mass flow meter (Wagner Mess- und Regeltechnik GmbH, Offenbach, Germany) and a micro-gas chromatograph (490 Micro GC System, Agilent Technologies, Santa Clara, USA). The micro GC was equipped with three channels with individual separation columns (channel 1: molecular sieve, carrier gas argon, 80 °C, 250 kPa, for the separation of H_2, N_2, and CO; channel 2: PlotPQ, carrier gas helium, 80° C, 150 kPa, for the separation of CO_2, NH_3, and NO_x; channel 3: CP-Sil 5, carrier gas helium, 45 °C, 100 kPa, for the separation of CO_2, and H_2S). Every channel used an individual thermal conductivity detector.

Prior to a process, the reactor was cleaned, filled with 1 L water and the calibrated pH and redox probes were attached to the reactor. The pH and redox probes were calibrated prior to every process with a two-point calibration. The reactor and medium without cysteine and vitamins were sterilized in a floor-standing autoclave (121 °C, 20 minutes). After sterilisation, the reactor was emptied, and medium transferred to the reactor with a peristaltic pump (Watson Marlow, Cornwall, United Kingdom) through a sterilized hose. The pH and temperature were adjusted with the reactor system, and the vitamin solution was sterile filtered and added through a septum on the reactor top. The reactor was gassed overnight with the

desired gas mixture, to ensure anaerobic conditions and a steady state on the moment of inoculation. On the day of inoculation, cysteine was added to the reactor from the anaerobic stock solution with a sterile syringe and cannula through the septum on the reactor top, the cells were harvested, and the reactor inoculated with a sterile single-use syringe and cannula equally through the septum on the reactor top. Inoculation was so, that the initial optical density at 600 nm was 0.1. Processes were conducted with a temperature of 37 °C, pH 6.0, stirrer speed of 800 rpm (volumetric power input of 3.5 W L^{-1}), no overpressure and a gas flow of 1.0 NL h^{-1} H_2, 1.0 NL h^{-1} CO_2 and 3.0 NL h^{-1} CO, unless otherwise mentioned.

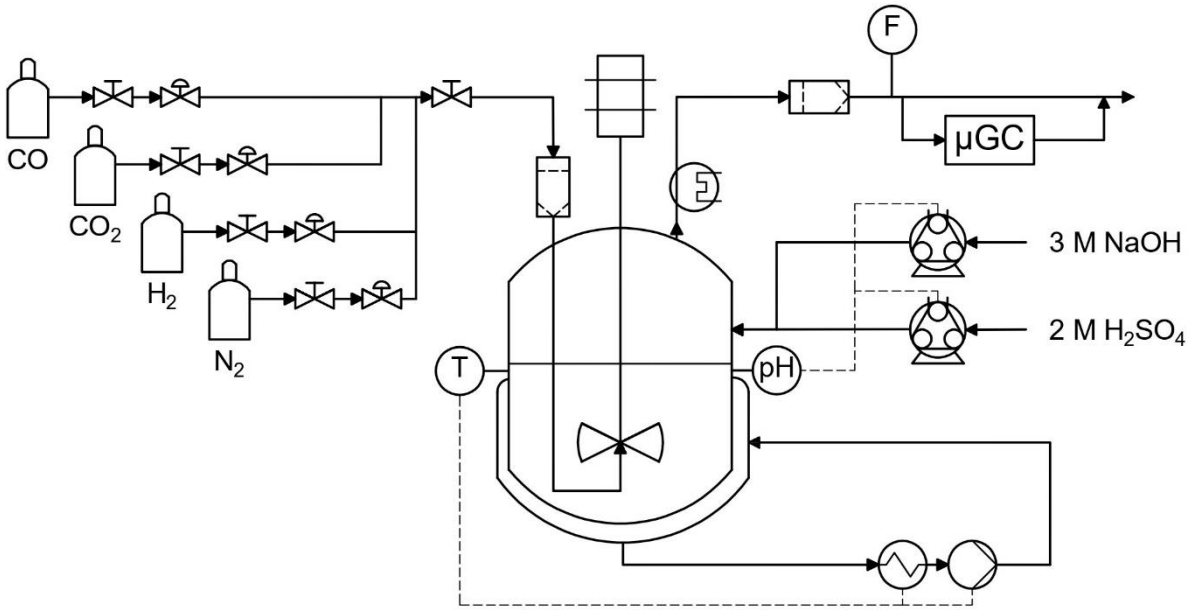

Figure 8 – Flowchart of the reaction system described in subsection 4.6. The double-jacketed reactor was gassed with sterile filtered and individually adjustable volume flows of CO, CO_2, H_2 and N_2. The exhaust gas was cooled, and the volume flow was measured with a mass flow meter, as well as the gas composition quantified with a gas chromatograph (μGC). The temperature of the reactor was controlled with a loop with water in the double jacket, and the pH was controlled with the addition of 3 M NaOH or 2 M H_2SO_4 through peristaltic pumps.

4.7 Analytical Methods

To evaluate the conducted processes, several analytical methods were employed, which will be described in this subsection. For the analysis of the liquid phase, samples were taken from the reactor with a single-use sterile syringe and a sterile cannula through the septum of the reactor top.

Cell Dry Weight Concentration and Optical Density

The optical density (OD_{600}) at a wavelength of 600 nm was used to assess the biomass growth in the processes. The OD_{600} was correlated to the cell dry weight concentration (CDW) for both *C. ljungdahlii* and *C. ragsdalei*. The optical density was quantified with a spectrophotometer (Genesys 10S UV-Vis, Thermo Scientific)

To attain this correlation, cells were cultivated as a preculture (see section 4.5). Once achieving the end of the exponential growth phase, the cells were concentrated to an OD_{600} of 10 with the same process as the cell harvesting, described in section 4.5. A dilution series was performed with this concentrated cell suspension, and the corresponding OD_{600}s were measured. Each dilution was also placed 1.5 mL polypropylene (PP) microtubes and centrifuged (13000 rpm, 10 min) in a table-top centrifuge. The PP microtubes were previously dried (80 °C, 24 h) and weighed. The supernatant was discarded and the microtubes with the cell pellets were dried in the drying oven at 80 °C until the weight stabilized. The difference between the weight of the empty microtubes and the weight of these tubes with the dried cell pellet, with the known volume of the cell suspension, quantifies the CDW concentration, which can be correlated to the OD as follows:

$$c_X = \alpha \cdot OD_{600} \tag{4.1}$$

α OD-CDW concentration factor, g L^{-1}

c_X Cell dry weight concentration, g L^{-1}

OD_{600} Optical density at 600 nm

The quantified correlation factors used in this work were 0.41 ± 0.01 g L^{-1} for *C. ljungdahlii* and 0.42 ± 0.03 g L^{-1} for *C. ragsdalei.*

Product Concentration with HPLC

The quantification of acetate, ethanol and 2,3-butanediol in the cell broth was conducted with high-performance liquid chromatography (HPLC), using a chromatograph (Finnigan Surveyor, Thermo Fisher Scientific) with an ion exchange column (Aminex-HPX-87H, Biorad) and a refractive index detector (Finnigan Surveyor RI Plus Detector, Thermo Fisher Scientific). Prior to the measurement, samples were sterile filtered (0.2 µm) and stored in crimp vials at 4 °C. 5 mM H_2SO_4 was used as an eluent at 0.5 mL min^{-1} in isocratic mode and a column temperature of 60 °C was employed.

Measurements were conducted with external standards, in which the concentration of the desired component were known. The areas under the peaks obtained in the chromatogram were used to determine the concentration of components, based on the calibration curve obtained with the external standards. The software Agilent EZChrom Elite was used to determine these areas. Aside from the main products, sugars and other organic acids could also be quantified with this method.

Exhaust Gas Analysis and Gas Uptake Rates

The exhaust gas was analysed combining the gas composition obtained from the micro-GC and the volume flows from the mass flow meter. Analogously to the quantification of products in the liquid phase, the quantification of the molar fraction of each gas in the exhaust was performed with a calibration curve derived from standards, which correlated the area under each peak in the chromatogram and the known gas composition. For this purpose, the micro-GC was periodically calibrated with different gas compositions for CO, CO_2 and H_2, set with the mass flow controller. For H_2S, calibration was conducted with acquired gas bottles with 100 ppm, 250 ppm and 500 ppm of H_2S.

The exhaust volume flow was adjusted for its composition with an empirical correlation derived from the individual gasses with

$$F_{exhaust} = \frac{1}{\sum \frac{\upsilon_i}{G_i}} \cdot F_{measured} \tag{4.2}$$

F Gas volume flow, NL h^{-1}

υ_i Component i molar fraction

G_i Component i conversion factor

The component conversion factor was empirically determined correlating the set volume flow of a component and the measured volume flow with the mass flow meter.

With the known exhaust volume flow of each component and the input volume flow, the volume uptake was quantified. This was converted to a molar uptake rate considering the ideal gas law and the reactor volume.

Dissolved Nitrite

Nitrite was measured on sterile filtered samples with the spectrophotometric method from García-Robledo et al. (2014). The reagent employed was the Griess reagent, which consists

of equal volumes of a sulphanilamide solution and a N-(1-naphthyl)-ethylenediamine dihydrochloride (NED) solution. The sulphanilamide solution was prepared by dissolving 5.0 g of sulphanilamide in 50 mL of a solution of 12 N HCl, and after dilution completing the total volume to 500 mL with deionized water. The NED solution consisted of 0.5 g of NED in 500 mL deionized water.

Samples were diluted with deionized water to render 1 mL of diluted sample. 50 µL of Griess reagent was added to the diluted sample and let react at room temperature for 20 min. After the reaction time, reacted samples were measured with a spectrophotometer at a wavelength of 540 nm. Quantification of nitrite was conducted with the measurement of standards with known nitrite concentrations.

Dissolved Sulfide

Dissolved sulfide was quantified using the method based on Cline (1969) using sterile filtered samples immediately after sampling. 500 µL of appropriately dissolved sample was mixed with 20 µL of a 4 g L^{-1} N-N-dimethyl-p-phenylene diamine sulfate (DMPD) solution and 20 µL of a 6 g L^{-1} $FeCl_3$ solution. Both solutions were prepared in 50% (v/v) hydrochloric acid and stored at 4 °C. Samples with reagents were incubated for 20 min at room temperature and the absorbance was measured at 670 nm with a spectrophotometer. Final quantification was conducted with a calibration curve derived from a series of standards with Na_2S dissolved in deionized water.

Quantification of Cysteine

The cysteine concentration was measured with sterile filtered samples through the quantification of free thiols by a modified method based on Aitken and Learmonth (2009). Samples from the reactor were immediately analysed after sampling. 300 µL of phosphate buffer, 300 µL of diluted sample, and 12.5 µL of Ellman's solution were mixed and left to incubate for 5 min at room temperature before the measurement of the absorbance at 412 nm with a spectrophotometer. The phosphate buffer consisted of 33.79 g L^{-1} K_2HPO_4, 0.79 g L^{-1} KH_2PO_4, and 3.59 g L^{-1} EDTA dissolved in demineralized water. The Ellman's solution consisted of 4.0 g L^{-1} 5,5′-dithiobis-(2-nitrobenzoic acid) dissolved in phosphate buffer and was stored at 8 °C to avoid degradation. Anaerobe growth medium without cysteine hydrochloride was used for dilutions and as a reference. A new set of standards, which consisted of growth medium with varying cysteine hydrochloride concentrations, was produced and measured for every process. Measurements were conducted in duplicates.

The method was proven adequate for the cysteine measurement, given its high sensitivity, non-responsiveness to yeast extract (data not shown) and lower sensitivity to sulfide. This can be seen in Figure 9, which shows measurements of the cysteine and Na_2S concentrations in growth medium, showing that the method is more sensitive to cysteine than sulfide, given the higher slope for Na_2S, and works within a broad absorption range, shown by the high coefficients of correlation.

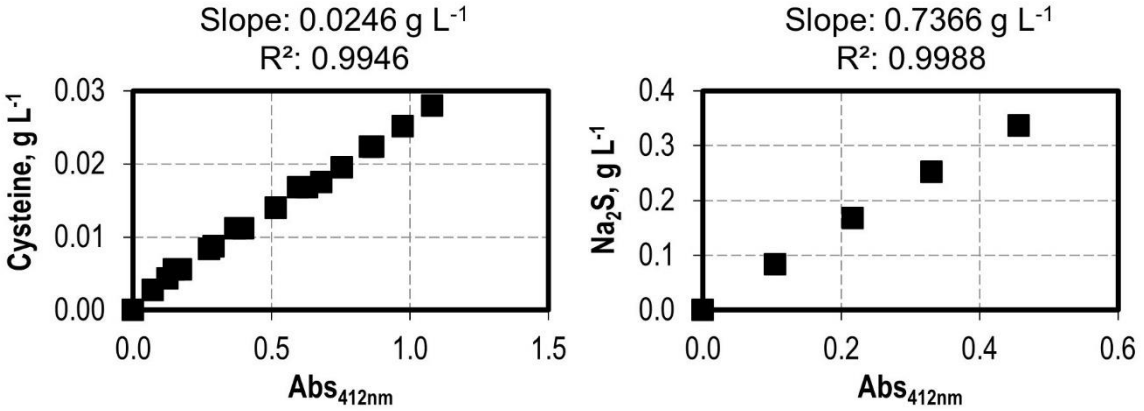

Figure 9 – Cysteine and sodium sulfide (Na_2S) measurement, as well as the slope and coefficient of correlation of the linear regression of the concentration and the absorption at the wavelength of 412 nm. Measurements were conducted in growth medium (subsection 4.3) with varying cysteine and Na_2S concentrations.

Specific Growth Rates and Production Rates

The specific growth rates were calculated in the exponential growth phase using equation 3.23. This was done by the linear interpolation of the natural logarithm of the measured OD divided by the initial OD and the time. The specific growth rate was the slope of the line in the interval identified as the exponential growth phase. The errors reported in this dissertation with the values of the specific growth rates correspond to the standard errors from the linearization, which was conducted with Microsoft Excel 2016 (Microsoft, Redmond, Washington, USA).

To determine the consumption/production rates of CDW, products and cysteine, the measured concentrations were estimated based on a nonlinear regression of the form:

$$c(t) = a_1 + \frac{a_2}{a_3 \cdot e^{-a_4 \cdot (t - a_5)} + a_6} \tag{4.3}$$

c Concentration, g L^{-1}

a_i Empirical coefficients

This equation leads to a S-shaped curved with a horizontal asymptote and has no biological background. In cases that the concentration profile was S-shaped with a linear asymptote, the describing equation was expanded to:

$$c(t) = a_7 + t \cdot \left[a_1 + \frac{a_2}{a_3 \cdot e^{-a_4 \cdot (t - a_5)} + a_6} \right] \tag{4.4}$$

The empirical coefficients were identified for each process by minimizing the residual sum of squares (RSS) changing the empirical coefficients a_i (Microsoft Excel 2016, Microsoft, Redmond, Washington, USA). With the nonlinear regression, it is possible to calculate the consumption/production rates by taking the derivative of equations 4.3 and 4.4 with respect to time. The results are:

$$r_i(t) = \frac{dc_i}{dt} = -\frac{a_2 \cdot a_3 \cdot a_4 \cdot e^{-a_4 \cdot (t - a_5)}}{(a_3 \cdot e^{-a_4 \cdot (t - a_5)} + a_6)^2} \tag{4.5}$$

$$r_i(t) = \frac{dc_i}{dt} = a_1 + \frac{a_2 \cdot \left[a_6 + a_3 \cdot e^{-a_4 \cdot (t - a_5)} \cdot (a_4 \cdot t + 1) \right]}{(a_3 \cdot e^{-a_4 \cdot (t - a_5)} + a_6)^2} \tag{4.6}$$

Figure 10 shows two examples of this nonlinear regression on the ethanol concentration of two different process: one using the S-shaped curve with the horizontal asymptote following equation 4.3 and one using the S-shaped curved with upwards linear asymptote following equation 4.4. The production rates are also shown, following equations 4.5 and 4.6.

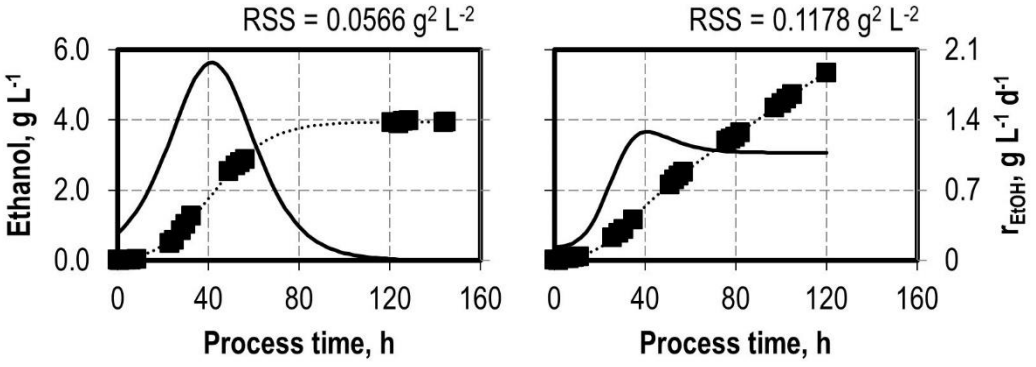

Figure 10 – Exemplary nonlinear regression of the ethanol concentration of two different processes with the S-shaped curve with the horizontal asymptote from equation 4.3 (left chart) and the S-shaped curved with upwards linear asymptote from equation 4.4 (right chart). Ethanol concentration (black squares, primary axis); nonlinear regression of the concentration (dotted line); ethanol production rates r_{EtOH} (black line, secondary axis) based on equation 4.5 (left) and 4.6 (right). The residual sum of squares (RSS) from each regression is given on top of each chart.

5 Fermentation of Artificial Syngas

This chapter reports and discusses the performance of the continuously gassed batch syngas fermentation with *C. ragsdalei* in comparison to the model acetogen *C. ljungdahlii.* To assess the different process performances, batch processes were conducted with a syngas composition of 60% (v/v) CO, 20% (v/v) CO_2 and 20% (v/v) H_2, gas flow of 5.0 NL h^{-1}, working volume of 1 L, temperature of 37 °C and a constant pH 6.0 in a continuously gassed stirred-tanked reactor. The processes with *C. ljungdahlii* were conducted in duplicate and those with *C. ragsdalei* were conducted in triplicate. The cell dry weight (CDW) concentration, acetate, ethanol and 2,3-butanediol concentrations, as well as the CO uptake rates, and the inline measured redox potentials (RP) of the cell culture are graphically shown in Figure 11.

The batch process profiles of each strain are strongly distinct. *C. ljungdahlii* CDW concentration increased throughout the whole process, with a specific growth rate of 0.02 ± 0.0004 h^{-1} and a late adaption phase between the 16th and 33rd process hours. *C. ragsdalei* CDW concentration increased with a specific growth rate of 0.10 ± 0.006 h^{-1} until the 33rd process hour, after which it decreased until the end of the process. This led to final CDW concentrations of 0.65 g L^{-1} and 0.45 g L^{-1} for *C. ljungdahlii* and *C. ragsdalei*, respectively.

This CDW concentration profile is reflected in the CO uptake rates, which reached a maximum at the 32nd process hour of 15.37 ± 1.35 mmol CO L^{-1} h^{-1} (centred moving average with five values) with *C. ragsdalei*, after which it sharply decreased. In contrast, the CO uptake rate increased steadily with *C. ljungdahlii* to 12.4 mmol CO L^{-1} h^{-1} at the end of the process. No hydrogen was consumed in any of the processes. The RP of the culture showed an inverse relationship to the CDW concentration for both strains, in the process interval in which the CDW concentration was increasing. The RP decreased steadily reaching its minimum of -500 mV at process end with *C. ljungdahlii*, whereas the minimum with *C. ragsdalei* was -504 mV, achieved at the 37th process hour, at a phase at which the CDW concentration was at its highest.

Acetate, ethanol and 2,3-butanediol were produced in all batch processes, with *C. ragsdalei* forming more acetate (7.48 g L^{-1}) and ethanol (2.33 g L^{-1}), while *C. ljungdahlii* formed more 2,3-butanediol (1.75 g L^{-1}). A summary of these key process parameters is shown in Table 3.

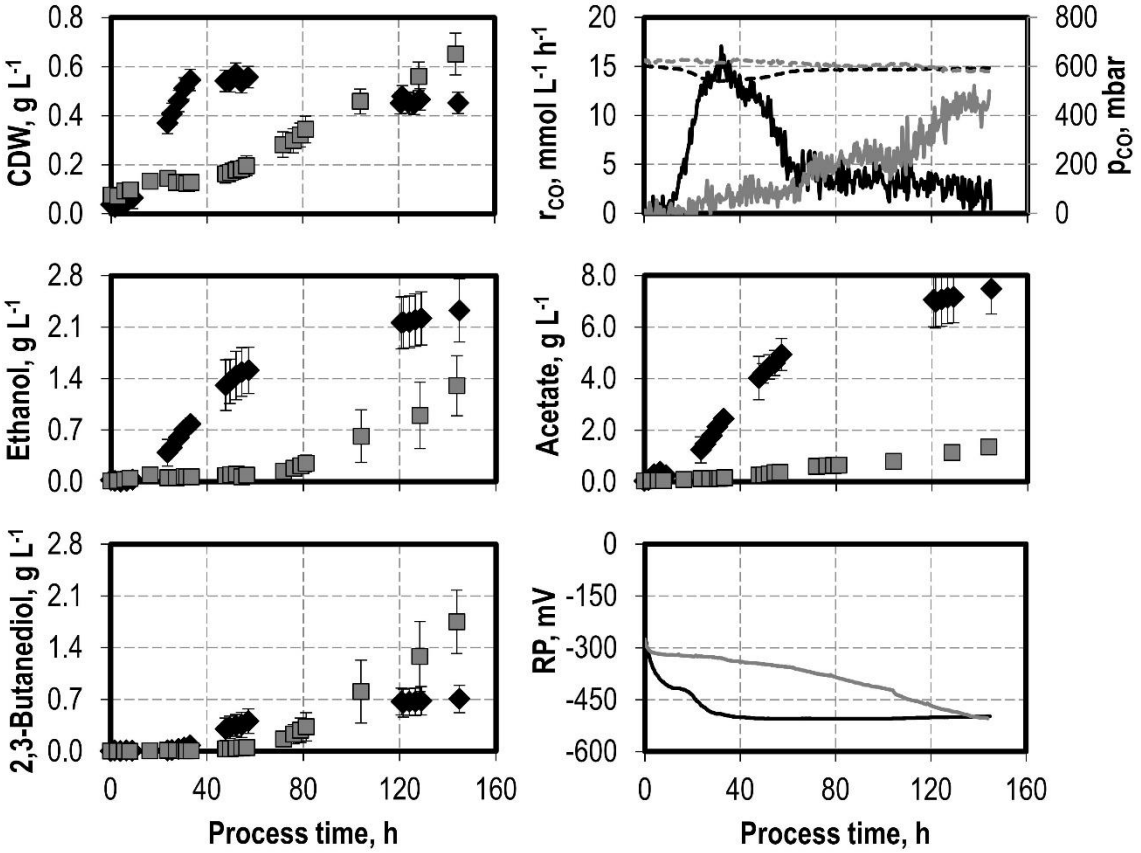

Figure 11 – Cell dry weight (CDW) concentration, CO uptake rate (r_{CO}), CO partial pressure in the exhaust (p_{CO}, dashed lines, right axis), ethanol, acetate and 2,3-butanediol concentrations and redox potential (RP) of autotrophic batch processes with *C. ljungdahlii* (grey squares, grey lines) and *C. ragsdalei* (black diamonds, black lines). Processes were conducted with pH 6.0, 37 °C, working volume of 1 L, volumetric power input of 3.5 W L^{-1} (800 rpm), gas flow of 5.0 NL h^{-1} with a gas composition of 3:1:1 ($CO:H_2:CO_2$). *C. ragsdalei* processes were conducted in triplicate and error bars represent the standard deviations. *C. ljungdahlii* processes were conducted in duplicate. For the r_{CO} and RP, values represent the mean without standard deviation.

To investigate how to counter the low specific growth rate of *C. ljungdahlii*, batch processes were conducted with lower CO partial pressures of 200 mbar and 100 mbar. The aim was to assess if carbon monoxide might have an inhibitory influence in *C. ljungdahlii*, as has been previously observed with other *clostridial* strains. Carbon monoxide partial pressure was chosen as the variable to change, since the patent describing *C. ljungdahlii* already stablished ideal pH and temperatures, and the medium composition used has been also extensively used in published studies. The courses of the CDW and product concentrations of these processes, as well as the CO and H_2 uptake rates are shown in Figure 12. To account for the effect of CO on growth, data will be shown to the 50th process hour.

Table 3 – Final cell dry weight (CDW), specific growth rate at the exponential growth phase, acetate, ethanol and 2,3-butanediol concentrations, and maximal CO uptake rate (centered moving average with five values) in the batch processes with *C. ljungdahlii* and *C. ragsdalei* depicted in Figure 11. Errors in the concentrations correspond to the standard deviation of replicates.

	C. ljungdahlii	*C. ragsdalei*
CDW, g L^{-1}	0.65 ± 0.09	0.45 ± 0.03
Specific growth rate, h^{-1}	0.02 ± 0.0004[1]	0.10 ± 0.006[1]
Acetate, g L^{-1}	1.34 ± 0.02	7.48 ± 0.98
Ethanol, g L^{-1}	1.3 ± 0.41	2.33 ± 0.43
2,3-butanediol, g L^{-1}	1.75 ± 0.43	0.71 ± 0.18
CO max. uptake rate, mmol L^{-1} h^{-1}	12.47	15.3 ± 1.35[2]

[1]Errors represent the standard error of the linear regression to obtain the specific growth rate.
[2]Values represent the mean of the five uptake rates around the maximum value, and error represent their standard deviation.

The biomass formation was strongly favoured with the lower CO partial pressure of 100 mbar, whereas the reduction from 600 mbar to 200 mbar led to a mild improvement at a first glance. In none of the batch processes with lower CO partial pressures did a lag phase occur, and the specific growth rates increased to 0.046 ± 0.009 h^{-1} with 200 mbar CO and 0.066 ± 0.0016 h^{-1} with 100 mbar. Analogue to the specific growth rate, the CO uptake rate also increased with decreasing CO inlet partial pressures, from 1.09 mmol L^{-1} h^{-1} with 600 mbar CO to 6.97 mmol L^{-1} h^{-1} with 200 mbar and 12.86 ± 0.09 mmol L^{-1} h^{-1} with 100 mbar. With a 100 mbar inlet CO, H_2 uptake was observed with a maximal rate at the 38th process hour of 22.14 ± 0.34 mmol L^{-1} h^{-1}.

Lowering the CO partial pressure to 100 mbar also benefited product formation, with emphasis on the strong acetate formation of 10.06 g L^{-1}. With 200 mbar, while low quantities of acetate were formed, ethanol was the main product formed within the analysed process time. A summary of the key results of these processes is shown in Table 4.

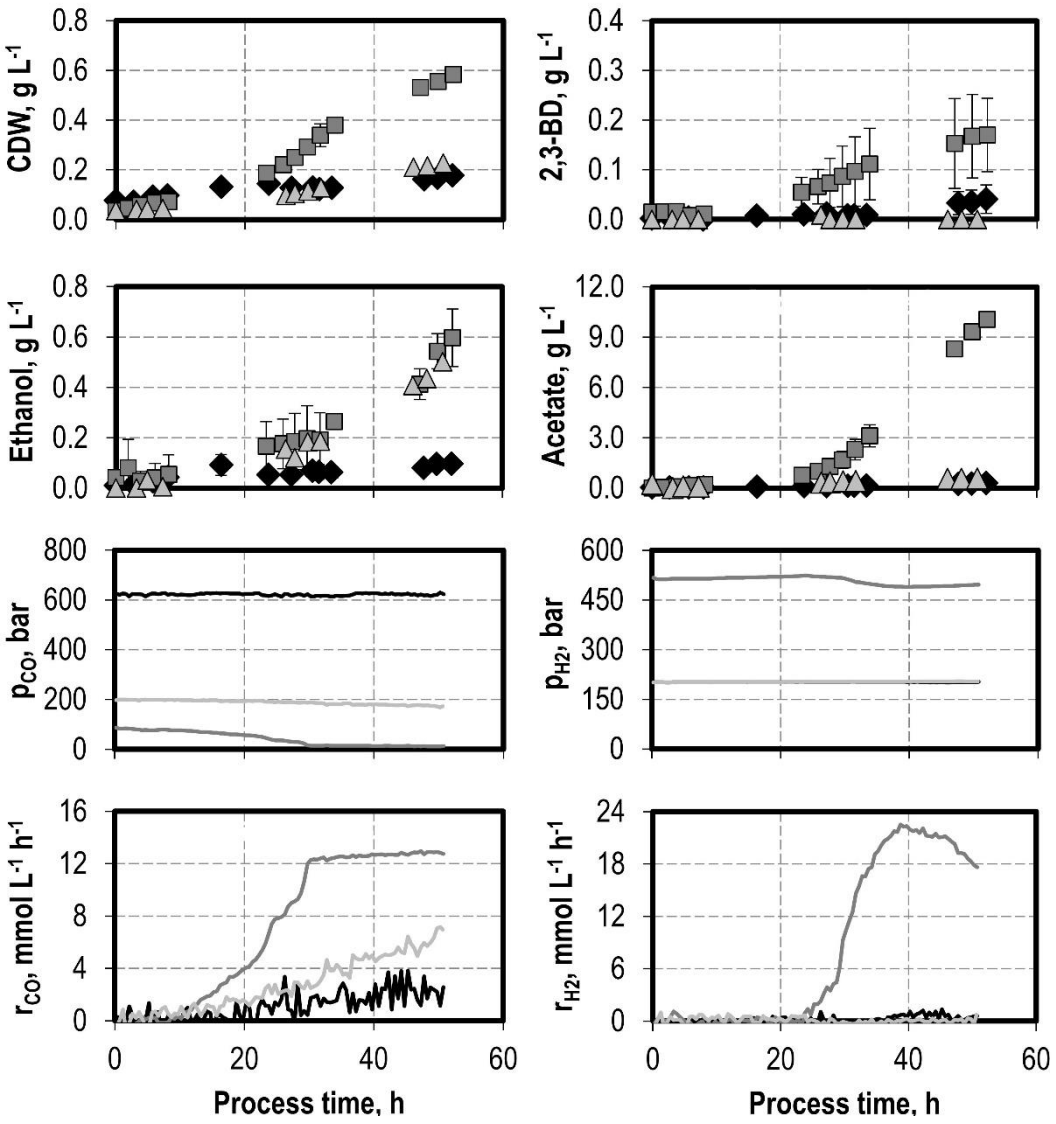

Figure 12 - Cell dry weight (CDW), 2,3-butanediol (2,3-BD), ethanol, and acetate concentrations, CO and H_2 partial pressure in the exhaust (p_{CO}, p_{H2}) and CO and H_2 uptake rates (r_{CO}, r_{H2}) of autotrophic batch processes with *Clostridium ljungdahlii* with inlet CO partial pressures of 600 mbar (black diamonds, black lines), 200 mbar (light grey triangles, light grey lines) and 100 mbar (grey squares, dark grey lines). Processes were conducted with pH 6.0, 37 °C, working volume of 1 L, volumetric power input of 3.5 W L^{-1} (800 rpm), gas flow of 5.0 NL h^{-1}. The processes with the inlet CO partial pressure of 600 mbar and 100 mbar were conducted in duplicate, and the error bars correspond to the standard deviations. For the uptake rates, values represent the mean without standard deviation.

Discussion

Using a CO-rich artificial syngas, *C. ragsdalei* was able to outperform *C. ljungdahlii* by fixating CO faster, while producing more ethanol and acetate. Moreover, *C. ljungdahlii* required an adaption phase until the 33rd process hour before CO uptake resumed. The specific growth rate of *C. ragsdalei* of 0.10 h^{-1} was similar to the one reported on the patent first describing

C. ragsdalei (0.099 h^{-1}, Huhnke et al., 2008). Comparatively, Maddipati et al. (2011) reported with a medium with 1 g L^{-1} yeast extract a specific growth rate of 0.059 h^{-1}, which could be increased to 0.076 h^{-1} by replacing the yeast extract with 20 g L^{-1} corn steep liquor. The specific growth rate obtained with *C. ljungdahlii* is lower than literature results. Hermann et al. (2020) reported in continuously gassed stirred-tank reactors specific growth rates of 0.058 ± 0.004 h^{-1} with a gas mixture of 39% (v/v) CO, 4% (v/v) CO_2 and 57% (v/v) Ar and 0.043 ± 0.007 h^{-1} with a gas mixture of 55% (v/v) CO, 30% (v/v) H_2, 5% (v/v) CO_2 and 10% (v/v) Ar.

Growth with *C. ljungdahlii* could be strongly increased upon reducing the CO inlet partial pressure, and the specific growth rates obtained with 200 mbar and 100 mbar inlet CO are similar or higher than those reported by Hermann et al. (2020). A possible reason for the discrepancy might lie in the different reactor configurations, since the published processes were conducted in a CSTR with 1.5 L working volume, 500 rpm stirrer speed and 1 six-blade Rushton impeller, whereas within this study batch processes were conducted with 1 L working volume, 1200 rpm stirrer speed and 2 six-blade Rushton impellers. With the latter configuration, a more efficient CO gas-liquid mass transfer is achieved, increasing dissolved CO concentration, and consequently increasing inhibitive effects, finally leading to lower specific growth rates.

Table 4 – Final cell dry weight (CDW) concentration, specific growth rate at the exponential growth phase and acetate, ethanol and 2,3-butanediol concentrations, and maximal CO and H_2 uptake rates (centered moving average with five values) in the batch processes with *C. ljungdahlii* depicted in Figure 12. Errors in the concentrations correspond to the standard deviation of replicates.

CO inlet partial pressure, mbar	600	200	100
CDW, g L^{-1}	0.18 ± 0.04	0.23 ± 0	0.58 ± 0.03
Specific growth rate, h^{-1}	0.023 ± 0.0004[1]	0.047 ± 0.009[1]	0.066 ± 0.0016[1]
Acetate, g L^{-1}	0.3 ± 0.09	0.58 ± 0	10.06 ± 0.15
Ethanol, g L^{-1}	0.1 ± 0.02	0.5 ± 0	0.6 ± 0.11
2,3-butanediol, g L^{-1}	0.04 ± 0.03	0 ± 0	0.17 ± 0.07
CO max. uptake rate, mmol L^{-1} h^{-1}	1.09	6.97	12.86 ± 0.09[2]
H_2 max. uptake rate, mmol L^{-1} h^{-1}	-	-	22.14 ± 0.34[2]

[1]Errors represent the standard error of the linear regression to obtain the specific growth rate.
[2]Values represent the mean of the five uptake rates around the maximum value, and error represent their standard deviation.

There is precedent for CO inhibition in syngas fermenting *clostridia.* Mayer et al. (2018) showed that an inlet CO partial pressure of 20 mbar led to the highest specific growth rate with *Clostridium aceticum*, with the value decreasing by 74% when the CO partial pressure

was increased to 300 mbar. The mechanism of the CO inhibition is not completely clear. Wang et al. (2013) assessed the CO inhibition of the hydrogenase/formate dehydrogenase complex HytA-E/FDH of *C. autoethanogenum,* a strain closely related to *C. ljungdahlii*, and observed that of all subunits of the HytA-E/FDH, only the hydrogenase HytA was inhibited by CO, and that the reduction of NADP and ferredoxin was inhibited by CO, but neither the reduction of methyl viologen with formate or with NADPH were. This indicates that the hydrogenase subunit HytA is involved in the electron transfer from ferredoxin and NADPH to formate, and consequently is the link to CO inhibition on the process.

The difference in the CO-rich processes with both strains is strongly affected by the lower biomass growth achieved with *C. ljungdahlii*. It can, additionally, be seen that the CO uptake rate with *C. ragsdalei* increased until the 32nd hours, whereas that with *C. ljungdahlii* increases throughout the whole process. Therefore, it is interesting to compare both processes with respect to the phase of increased activity *i.e.* in which the CO uptake rate increased. This is shown in Figure 13 by plotting the CDW, acetate, ethanol and 2,3-butanediol concentrations against the increasing CDW concentration within this phase.

As the CDW concentration and the CO uptake rate of the culture increased, *C. ragsdalei* formed mainly acetate and ethanol. *C. ljungdahlii,* differently, produced all three products equivalently. How both strains differently directed fixated carbon can be visualized by the CDW concentration of 0.56 g L^{-1} with *C. ljungdahlii* and 0.55 g L^{-1} with *C. ragsdalei*, which is represented with the dashed line in Figure 13. At this point, *C. ljungdahlii* produced 1.13 g L^{-1} acetate, 0.90 g L^{-1} ethanol and 1.28 g L^{-1} 2,3-butanediol, while *C. ragsdalei* produced 2.45 g L^{-1} acetate, 0.78 g L^{-1} ethanol and 0.08 g L^{-1} 2,3-butanediol, representing 1.45 g carbon fixated in the 3 products by *C. ragsdalei* and 1.61 g carbon fixated by *C. ljungdahlii*. Thus, while *C. ljungdahlii* fixated 0.54 g carbon less in acetate, it fixated 0.06 g more in ethanol and 0.64 g in 2,3-butanediol. Since the ethanol formation relative to biomass production was remarkably similar for both strains, the difference between both strains in the phase of increasing CO uptake lies in that *C. ljungdahlii* managed to strongly shift carbon to 2,3-butanediol formation.

Acetate and 2,3-butanediol are both derived from acetyl-CoA. The ATP generation per mol acetate with CO is 1.503 mol ATP (Richter et al., 2016), or 0.376 mol ATP mol^{-1} CO, and thus the ATP generation per mol acetyl-CoA from CO is 0.503 mol ATP, or 0.126 mol ATP mol^{-1} CO (equation 3.10). Using this relationship and combining equations 3.4, 3.5, 3.7, 3.14 and 3.12, the theoretical ATP generation per mol 2,3-butanediol from CO is 2.285 mol ATP with NADPH and 2.558 mol ATP with NADH as the reducing agents of the acetoin reduction, respectively. These values represent 0.208 mol ATP mol^{-1} CO and 0.233 mol ATP mol^{-1} CO, and thus the ATP yield on CO with acetate formation is 1.80 – 1.61-fold higher than that with

2,3-butanediol. Therefore, to support growth and 2,3-butanediol formation, more CO needs to be consumed, to supply both concurring processes.

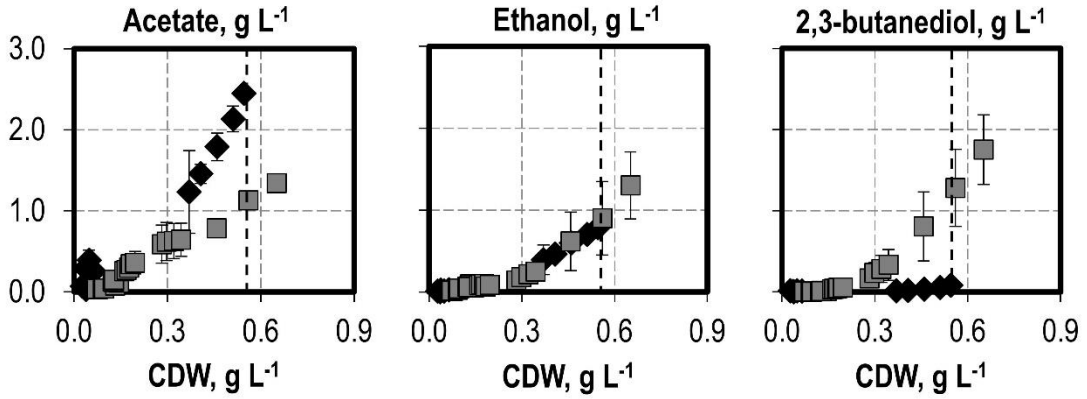

Figure 13 – Concentrations of acetate, ethanol and 2,3-butanediol vs. the cell dry weight (CDW) for the batch processes depicted in Figure 11 with *C. ljungdahlii* (grey squares) and *C. ragsdalei* (black diamonds) during the phase of increasing CO uptake rate. The dashed line represents the CDW value of 0.56 g L^{-1} for *C. ljungdahlii* and 0.55 g L^{-1} for *C. ragsdalei.* Error bars represent the standard deviations.

The results are insufficient to conclusively pinpoint the reason for the different product spectra, but plausibly the high *C. ragsdalei* activity curbed the formation of the alcohols. An increased acetate extracellular concentration increases the diffusion of acetic acid into the cell, which uncouples the proton motive force from ATP generation and increases the ATP costs for the cell activity (Valgepea et al. 2017). The reduction of acetate to ethanol or the production of 2,3-butanediol would deviate reducing agents required to maintain ATP generation, thus acetate is further produced in a self-reinforcing system. As acetate formation with *C. ljungdahlii* occurred at lower rates relative to biomass formation, no imbalance in the proton motive force occurred and reducing agents could also be employed in the production of more reduced products.

In most of the reported processes, only CO was consumed as gaseous substrate, but with *C. ljungdahlii* with an inlet CO partial pressure of 100 mbar, H_2 consumption was observed. H_2 uptake resumed at an outlet CO partial pressure of 42.8 mbar, after which the CO outlet partial pressure decreased to a minimum of roughly 11.5 mbar. The highest H_2 uptake rate achieved was 22.14 ± 0.34 mmol L^{-1} h^{-1} (average of the five values around the maximum), which is clearly higher than the maximal CO uptake rate achieved by *C. ragsdalei* of 15.37 mmol L^{-1} h^{-1}. This reflects the high hydrogenase activity of the most abundant protein in the proteome HytA-E (Wang et al., 2013; Richter et al., 2016).

The uptake of hydrogen did not strongly influence biomass formation, as can be visually identified in the plotted results (Figure 12). Its most clear influence lies in the increased acetate

production, which clearly accelerated as H_2 uptake resumed. The ATP generation from H_2 relative to one mol acetate is 36.4% lower than that with CO (Richter et al., 2016), and thus to keep a same level of cell activity the cells need to produce more acetate. In fact, given the ATP generation per mol acetate of 0.956 (Richter et al., 2016), and given that the acetate production from acetyl-CoA produces one mol of ATP, this results in a negative ATP generation per mol acetyl-CoA from CO of -0.044 mol ATP. Thus, with H_2 the cells need to produce acetate to support activity.

It could be demonstrated that *C. ragsdalei* performs better than *C. ljungdahlii* with a CO-rich syngas (600 mbar CO), achieving peak activity after 33 hours of batch process. Product formation in this case was shifted towards acetate, with an alcohol to acetate ratio of 0.406 g g^{-1}. *C. ljungdahlii* showed much slower growth in these conditions, however shifting carbon positively to alcohols, with an alcohol to acetate ratio of 2.28 g g^{-1}, being 2,3-butanediol the product with the highest final concentration. The growth of *C. ljungdahlii* could be increased almost threefold, regarding the specific growth rate, by reducing the CO inlet partial pressure to 100 mbar. This process also enabled the consumption of H_2, which showed higher uptake rates than CO and strongly shifted carbon to acetate production.

A Closer Look into CO and H_2 as Electron Donors

As syngas is composed mainly of CO, H_2 and CO_2, it is of interest to consume all three components in the syngas fermentation. However, the data showed that *C. ragsdalei* was not able to consume H_2 under the studied experimental setup, whereas the data with *C. ljungdahlii* indicated that H_2 was consumed once the outlet CO partial pressure was under 50 mbar. This motivated a more detailed study into the conditions which allow H_2 uptake in the presence of CO, and furthermore what are the implications for product formation. For such, batch processes were conducted with *C. ragsdalei* with a gas flow rate of 10 NL h^{-1} (working volume of 1 L) and a gas composition of 5% (v/v) CO, 47.5% (v/v) CO_2 and 47.5% (v/v) H_2. The CO concentration was chosen such that H_2 could be possibly directly used from process start, and the higher gas flow rate was chosen to technically allow the implementation of the desired CO inlet partial pressure, since CO volume flows lower than 0.5 NL h^{-1} were not possible with the equipment available. Additionally, the stirrer speeds of 800 rpm (3.5 W L^{-1}) and 1200 rpm (11.7 W L^{-1}) were implemented to evaluate if the CO threshold observed was due to gas-liquid mass transfer limitations. Three processes will be described in this section in more detail, two with stirrer speeds of 800 rpm and one with 1200 rpm. The CDW and product concentrations, as well as the CO and H_2 uptake rates in these processes are shown in Figure 14 up to the 60th process hour, since H_2 consumption was only observed within this process interval.

The CDW concentration evolved to similar maxima at the 33rd process hour of 0.49 g L^{-1} and 0.42 g L^{-1} (obtained through linear interpolation) with 800 rpm and 0.46 g L^{-1} with 1200 rpm. In one of the processes with 800 rpm, the CDW decreased after the 33rd hour, but no reason for this behaviour could be found. Acetate was the main product in all processes, reaching concentrations in the range of 8 g L^{-1}. Ethanol was also similarly built to concentrations in the range of 0.45 g L^{-1}; the ethanol concentration scattered in one of the batch processes with 800 rpm, but the reason for the scattering could not be found. Furthermore, negligible 2,3-butanediol was produced.

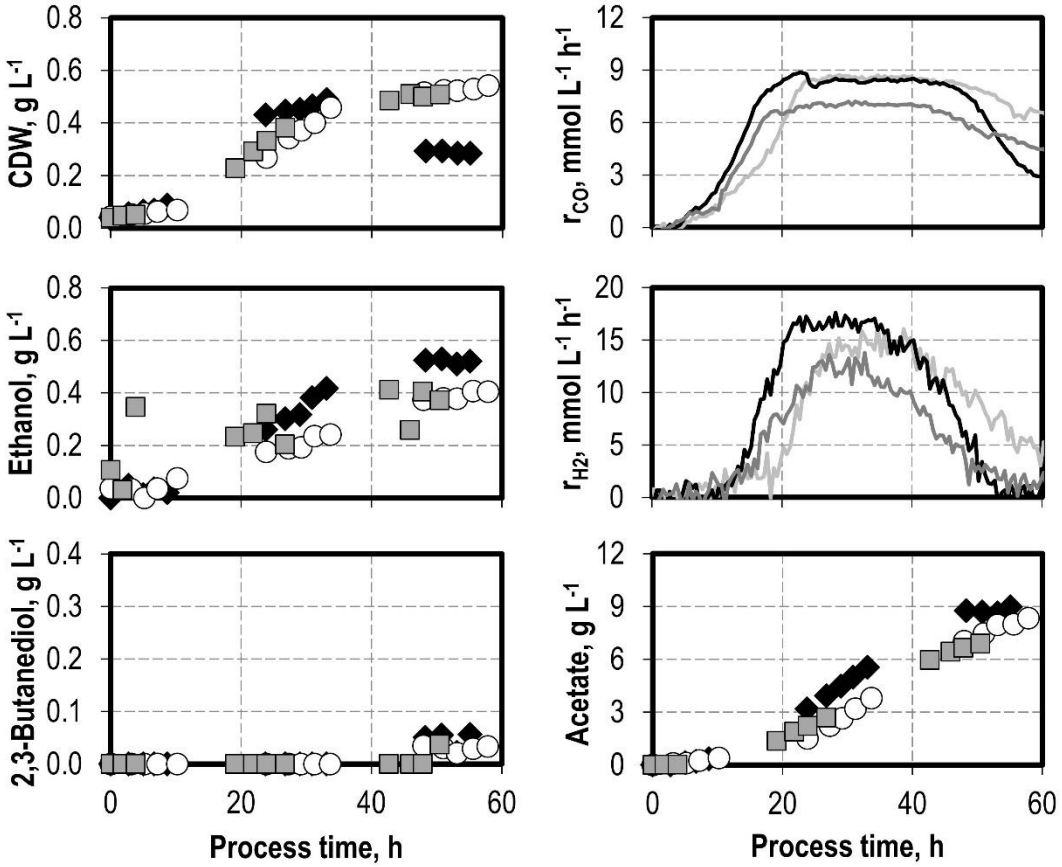

Figure 14 – Cell dry weight (CDW), CO uptake rate (r_{CO}), ethanol concentration, H_2 uptake rate (r_{H2}), acetate and 2,3-butanediol concentrations of autotrophic batch processes with *C. ragsdalei* with stirrer speed of 800 rpm (black diamonds, black lines; grey squares, grey lines) and 1200 rpm (white circles, light grey lines). Processes were conducted with pH 6.0, 37 °C, working volume of 1 L, gas flow rate of 10 NL h^{-1} and a gas composition of 5% (v/v) CO, 47.5% (v/v) CO_2 and 47.5% (v/v) H_2.

CO was initially consumed in exclusion of H_2 in all processes from process start. H_2 uptake resumed roughly in the 10th process hour in all processes, as the outlet CO partial pressures were 46 mbar and 47 mbar with 800 rpm and 49 mbar with 1200 rpm. A more detailed depiction of the H_2 uptake is shown in Figure 15, in which the H_2 uptake rates and the CO partial pressure in the exhaust are shown.

Discussion

The batch processes depicted in this subsection confirmed the capacity of *C. ragsdalei* to shift from CO uptake to its concomitant uptake with H_2. It also clearly showed that CO is initially the preferred electron donor, with H_2 uptake resuming when the outlet CO partial pressure was within the range of 46 – 49 mbar, as previously observed with *C. ljungdahlii*. This concomitant uptake has been little discussed in available literature. Whereas several publications show the consumption of both electron donors in processes with *C. ljungdahlii* and *C. ragsdalei* (Acharya et al., 2019; Devarapalli et al. 2017; Infantes et al., 2020; Liakakou et al., 2021; Maddipati et al., 2011; Richter et al., 2013), gassing and stirring conditions are very different, which hinders a closer look into the concomitant uptake of CO and H_2. Younesi et al. (2015) showed in anaerobic flasks that H_2 consumption occurred after CO was depleted from the gaseous phase, and only at H_2 partial pressures equal or higher than 0.32 atm. However, sampling occurred every 12 hours in the publication by Younesi et al. (2015), so the shift to H_2 uptake could not be adequately observed. The results here are consistent regarding the outlet CO partial pressure threshold, showing that sufficiently low CO partial pressures support H_2 uptake. Indeed, within this doctorate studies, 14 processes were conducted in which this shift was observed, which rendered a CO threshold of 47.1 ± 4 mbar for H_2 uptake.

The results also demonstrate that this CO threshold in not determined by mass transfer limitations, as no difference could be observed from the threshold observed with both studied stirrer speeds. A higher stirrer speed increases the mass transfer coefficient (Weuster-Botz and Takors, 2018), and thereby increases the mass transfer rate. Supporting this logic is the fact that the outlet CO partial further decreased and analogously the CO uptake rate further increased after H_2 uptake resumed, which would be inconsistent with a scenario of transfer limitation. This can be demonstrated by balancing the gas phase for the CO in the reaction system:

$$\frac{d(n_{CO})}{dt} = F_{in} \cdot c_{in,CO} - F_{out} \cdot c_{CO} - COTR \tag{5.1}$$

n_{CO} CO quantity, mol

$COTR$ CO transfer rate, mol h^{-1}

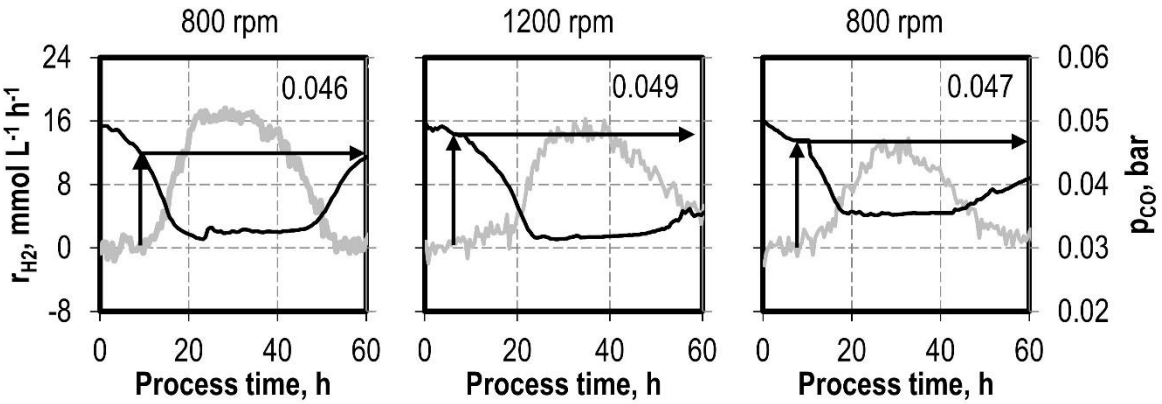

Figure 15 – Hydrogen uptake rate (r_{H2}, grey lines) and CO partial pressure in the exhaust (p_{CO}, black lines) of the processes shown in Figure 14. The stirrer rate of each process is identified above each graph. The black arrows represent the point in which H_2 uptake resumed and the corresponding CO partial pressure. The values represent this threshold CO partial pressure in bar.

When the CO partial pressure in the exhaust decreases, the difference in the molar flow of CO ($F_{in} \cdot c_{in,CO} - F_{out} \cdot c_{CO}$) increases. However, in this case, the relationship $d(n_{CO})/dt < 0$ applies. For this to occur, the CO transfer rate must further increase. Therefore, it can be concluded that no mass transfer limitations occur at the CO threshold concentration to H_2 uptake.

As previously discussed, the hydrogenase HytA-E transfers electrons from H_2 to drive the WLP, and this enzyme is strongly inhibited by CO (Wang et al., 2013; Richter et al., 2016). It can thus be assumed that the observed 47.1 ± 4 mbar CO in the used reactor setup corresponds to the liquid bulk CO concentration that enabled a sufficiently low intracellular CO concentration to permit measurable hydrogenase activity, and thus H_2 uptake. Wang et al. (2013) reported that the CO inhibition occurred in the formate reduction with ferredoxin and NADPH and hypothesized that growth with CO was still possible since the HytA-E/FDH is the most abundant protein in the proteome of *C. autoethanogenum.* However, considering the data on *C. ragsdalei* with a CO-rich gas (600 mbar), the specific growth rate (0.10 ± 0.006 h^{-1}) was unaffected by the higher CO partial pressure, since with a lower inlet CO partial pressure of 50 mbar the specific growth rate was 0.089 ± 0.010 h^{-1}. This implies that the formate reduction in the WLP was unaffected by the CO partial pressure of 600 mbar, or at least that it was not the rate limiting step. The data in this work is, however, insufficient to enable a conclusive hypothesis as to how the CO inhibition plays out and why *C. ljungdahlii* and *C. ragsdalei*, which use the same proteins to reduce CO_2 to formate, show different tolerances to CO.

6 Effect of Defined Impurities in the Syngas Fermentation[1]

While the use of artificial syngas contributes to better compare the performance of the strains *C. ljungdahlii* and *C. ragsdalei* and elucidate the concomitant uptake of CO and H_2, it does not contain possible impurities that might occur in real syngas, which could affect process performance. When considering an integrated process of biomass gasification for syngas production and subsequent fermentation, assessing how possible impurities impact the process is key to design necessary gas clean-up and conditioning steps. In this subsection, the syngas fermentation with *C. ragsdalei* with the addition of defined impurities will be presented and compared to the model acetogen *C. ljungdahlii*. For such, two nitrogen-based impurities, ammonia and nitrate, and one sulfur-based, hydrogen sulfide, were studied. Processes were conducted with 600 mbar CO, 200 mbar CO_2 and 200 mbar H_2 with *C. ragsdalei* and 200 mbar CO, 400 mbar N_2, 200 mbar CO_2 and 200 mbar H_2 with *C. ljungdahlii* to reduce the effect of CO inhibition in the latter case.

Ammonia

The effect of ammonia in the syngas fermentation with *C. ljungdhalii* and *C. ragsdalei* was studied through the addition of ammonium chloride prior to the inoculation of the batch process. This was intended to simulate the dilution of ammonia in the aqueous reaction medium, which at pH 6.0 leads to the complete conversion of dissolved ammonia to ammonium ions. The studied concentrations were the supplementation of 3.0 g NH_4Cl L^{-1} and 6.0 g NH_4Cl L^{-1} for both strains and 9.0 g NH_4Cl L^{-1} for *C. ragsdalei*.

The course of the CDW and product concentrations, as well as the CO uptake rates of these processes are shown in Figure 16. All batch processes with both strains showed a negative

[1] Some of the results of the chapter were published in:

Oliveira L, Rückel A, Nordgauer L, Schlumprecht P, Hutter E, Weuster-Botz D (2022) Comparison of syngas-fermenting *Clostridia* in stirred-tank bioreactors and the effects of varying syngas impurities. Microorganisms, 10, 681.

Oliveira L, Röhrenbach S, Holzmüller V, Weuster-Botz D (2022). Continuous sulfide supply enhanced autotrophic production of alcohols with *Clostridium ragsdalei*. Bioresources and Bioprocessing. 9, 15.

impact of the supplementation of ammonium, seen clearly in decreased CDW concentrations and CO uptake rates. With *C. ljungdahlii*, the supplementation of 3.0 g NH_4Cl L^{-1} led also to a decrease in the ethanol formation, while acetate was built equivalently to the process without extra ammonium chloride. With *C. ragsdalei*, the supplementation of NH_4Cl led to a decrease in acetate and ethanol formation, while 2,3-butanediol production was completely inhibited. 6.0 g L^{-1} NH_4Cl led to a complete growth inhibition for both strains and 9.0 g NH_4Cl L^{-1} also inhibited growth with *C. ragsdalei* in the first 60 hours of batch process; however, growth with 6.0 g NH_4Cl L^{-1} and 9.0 g NH_4Cl L^{-1} with *C. ragsdalei* did resume after the 100th process hour (data not shown), which indicates the possibility of adaption of the strain to a higher ammonium concentration.

Nitrate

While most of the organically bound nitrogen in biomass is converted to N_2, NH_3, HCN, and tar- and char-N during gasification, precedent for NO inhibition in a syngas fermentation process has been published, and NO would be in a thermodynamic equilibrium with nitrate and nitrite. Nitrate was chosen as a representative of an oxygenated nitrogen impurity. For such, nitrate was added to the bioreactor prior to the inoculation of the batch processes in form of $NaNO_3$ in the concentrations of 0.1 g $NaNO_3$ L^{-1} and 0.5 g $NaNO_3$ L^{-1} for *C. ljungdahlii* and *C. ragsdalei* and 0.2 g $NaNO_3$ L^{-1} for *C. ragsdalei*. The process results are shown in Figure 17.

The CDW concentration of *C. ljungdahlii* after 50 process hours was not altered by the addition of nitrate, with growth in the first 24 hours of process being positively impacted by the nitrate addition. Acetate formation decreased with 0.1 g L^{-1} $NaNO_3$, while it remained unaltered with 0.5 g L^{-1} $NaNO_3$. Nitrate also reduced ethanol formation and CO uptake in both studied concentrations. With *C. ragsdalei*, the addition of nitrate was detrimental to the process performance in all variables, with complete inhibition occurring already at the concentration of 0.2 g $NaNO_3$ L^{-1}. 0.1 g $NaNO_3$ L^{-1} decreased CDW and acetate formation and more strongly ethanol production, while it inhibited the formation of 2,3-butanediol. Analogously, no CO uptake was observed with the supplementation of 0.2 g $NaNO_3$ L^{-1} and 0.5 g $NaNO_3$ L^{-1}.

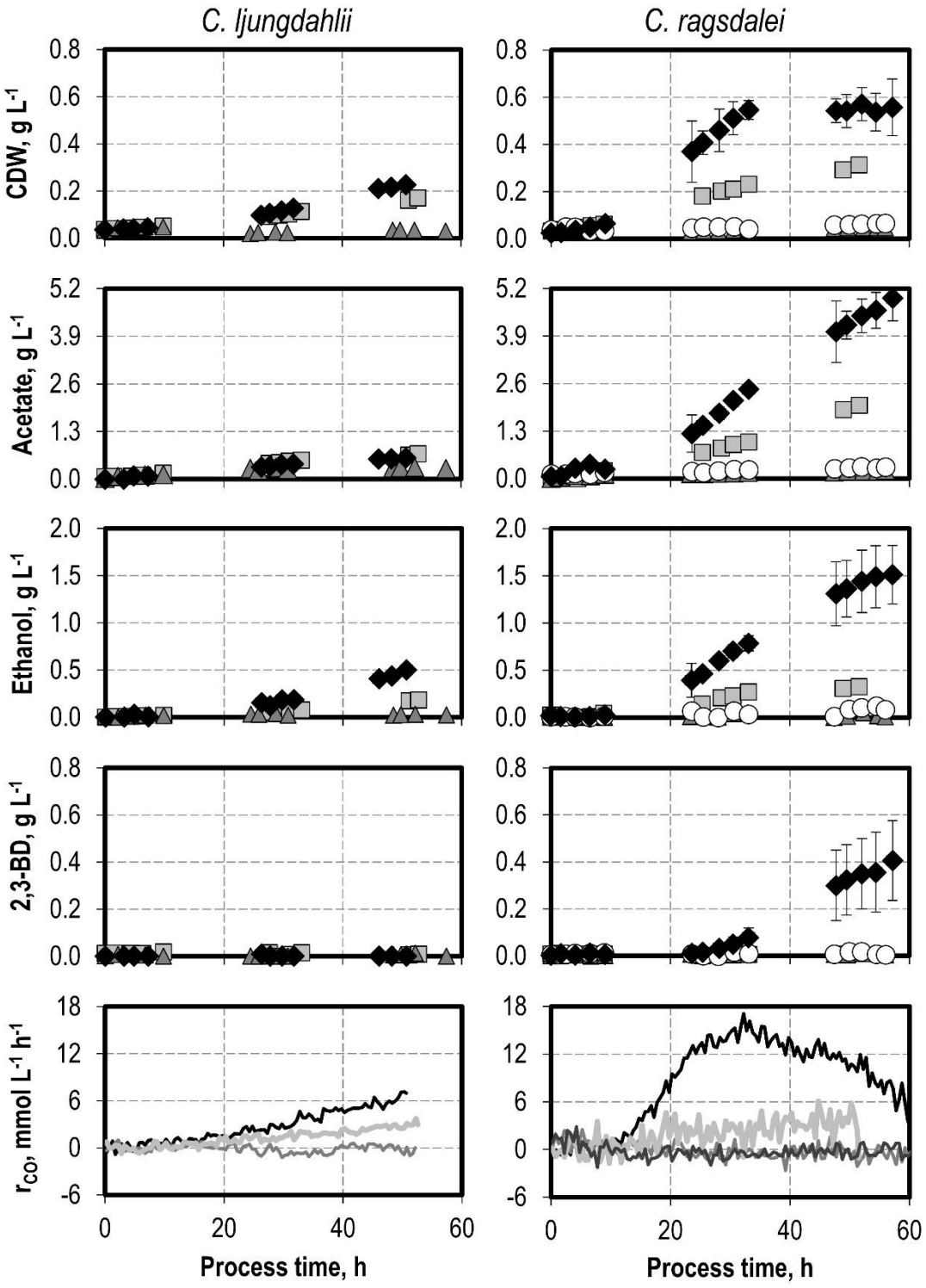

Figure 16 – Cell dry weight (CDW), product concentrations and CO uptake rates (r_{CO}) of the syngas fermentation with *C. ljungdahlii*, and *C. ragsdalei* with varying NH_4Cl concentrations. Reference process (black diamond, black top line), +3.0 g L^{-1} NH_4Cl (light grey square, light grey line), +6.0 g L^{-1} NH_4Cl (dark grey triangle, dark grey line), +9.0 g L^{-1} NH_4Cl (white circle, black bottom line). Processes were conducted with pH 6.0, 37 °C, working volume of 1 L, gas flow rate of 5 NL h^{-1} and overall pressure of 1 bar. Gas compositions were (*C. ragsdalei*) 600 mbar CO, 200 mbar CO_2, and 200 mbar H_2 and (*C. ljungdahlii*) 400 mbar N_2, 200 mbar CO, 200 mbar H_2, and 200 mbar CO_2.

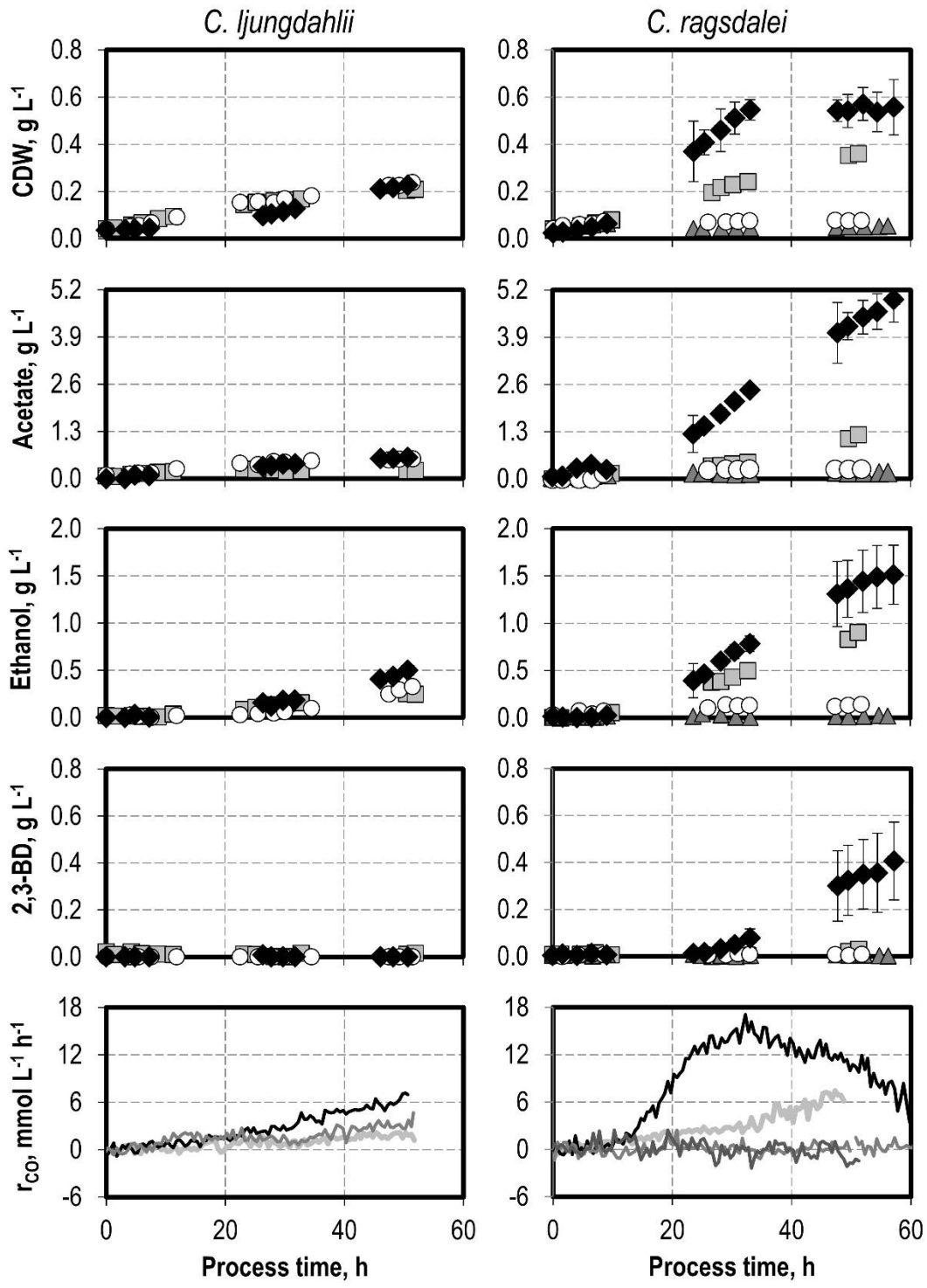

Figure 17 – Cell dry weight (CDW), product concentrations and CO uptake rates (r_{CO}) of the syngas fermentation with *C. ljungdahlii*, and *C. ragsdalei* with varying $NaNO_3$ concentrations. Reference process (black diamond, black top line), +0.1 g L^{-1} $NaNO_3$ (light grey square, light grey line), +0.2 g L^{-1} $NaNO_3$ (dark grey triangle, dark grey line), +0.5 g L^{-1} $NaNO_3$ (white circle, black bottom line). Processes were conducted with pH 6.0, 37 °C, working volume of 1 L, gas flow rate of 5 NL h^{-1} and overall pressure of 1 bar. Gas compositions were (*C. ragsdalei*) 600 mbar CO, 200 mbar CO_2, and 200 mbar H_2 and (*C. ljungdahlii*) 400 mbar N_2, 200 mbar CO, 200 mbar H_2, and 200 mbar CO_2.

Sulfide

Sulfur present in biomass is mainly converted to H_2S during gasification, component which was chosen as a sulfur-based impurity subject to this study. Since H_2S is a gas at the process temperature, thioacetamide was used to study the effect of H_2S in the syngas fermentation with *C. ljungdahlii* and *C. ragsdalei*. Thioacetamide splits into acetate, ammonium and H_2S in acidic milieus, and it was supplied prior to the batch process inoculation. The studied concentrations of H_2S were 0.1 g H_2S L^{-1} and 0.5 g H_2S L^{-1} and the process performance is graphically shown in Figure 18.

The addition of H_2S impacted the processes with *C. ljungdahlii* negatively, with the concentration of 0.5 g L^{-1} H_2S completely inhibiting biomass growth and CO uptake. With *C. ragsdalei*, a concentration of 0.5 g L^{-1} H_2S strongly inhibited biomass formation and CO uptake, while 0.1 g L^{-1} H_2S was very positive for the process performance. This addition of sulfur fomented biomass growth, increasing it from 0.57 g L^{-1} to 0.76 g L^{-1}, as well as increasing and prolonging high CO uptake rates and shifting carbon to alcohol formation, with both the ethanol and the 2,3-butanediol concentrations increasing by 50% and 83 %, respectively.

Discussion

When considering the coupling of biomass gasification and syngas fermentation, understanding which impurities might have an inhibitory effect is necessary to design a gas cleanup step. Moreover, identifying which strains are more resistant to impurities may impact the decision of which strain should be used in an industrial scale syngas fermentation unit. In this regard, this comprehensive comparison of the tolerance of the strains *C. ljungdahlii* and *C. ragsdalei* to two nitrogen-based impurities and one sulfur-based is of utmost relevance.

With few exceptions, all studied gas impurities and concentrations led to lower cell activity, measured by the CO uptake rate or biomass growth. This is clearly shown in Figure 19 and Figure 20, which depict the final CDW, acetate and total alcohol concentrations and the maximal CO uptake rate for all impurities and both strains.

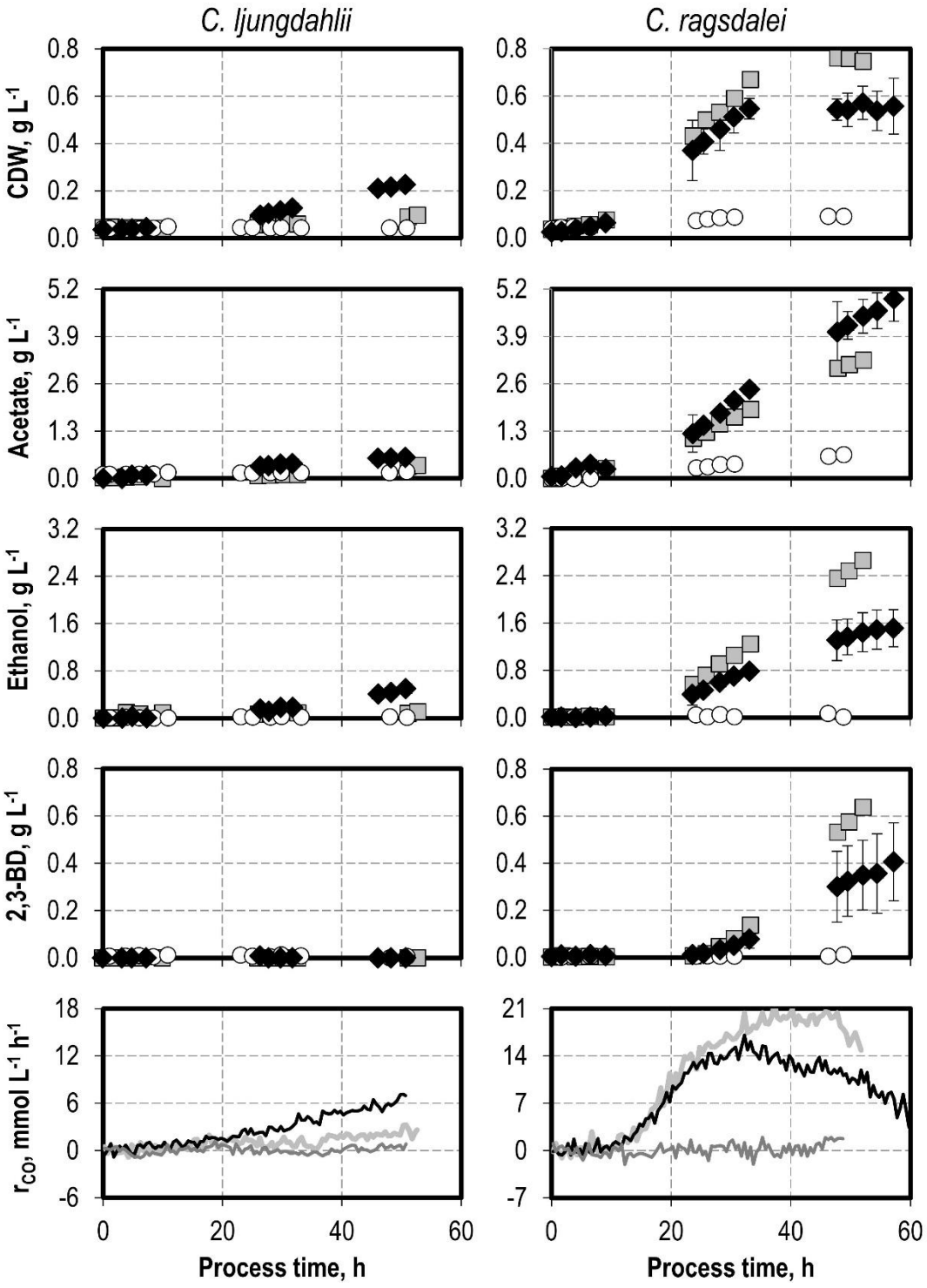

Figure 18 – Cell dry weight (CDW), product concentrations and CO uptake rates (r_{CO}) of the syngas fermentation with *C. ljungdahlii*, and *C. ragsdalei* with varying H_2S concentrations. Reference process (black diamond, black top line), +0.1 g L^{-1} H_2S (light grey square, light grey line), +0.5 g L^{-1} H_2S (white circle, black bottom line). Processes were conducted with pH 6.0, 37 °C, working volume of 1 L, gas flow rate of 5 NL h^{-1} and overall pressure of 1 bar. Gas compositions were (*C. ragsdalei*) 600 mbar CO, 200 mbar CO_2, and 200 mbar H_2 and (*C. ljungdahlii*) 400 mbar N_2, 200 mbar CO, 200 mbar H_2, and 200 mbar CO_2. H_2S was added as thioacetamide.

The inhibition concentrations which could be identified in this study were the supplementation of 3.0 g L^{-1} NH_4Cl for both strains, 0.2 g L^{-1} $NaNO_3$ for *C. ragsdalei* and 0.5 g L^{-1} H_2S for both strains. Considering a batch process of 60 hours and total dissolution of the components, these inhibiting concentrations would be achieved for a syngas containing 4560 ppm NH_3, 236 ppm NO_x and 540 ppm H_2S in a process with 60 hours, which apart from NO_X are concentrations within the range of published values for syngas derived from biomass, as shown in Table 1. Therefore, a successful coupling of biomass gasification and syngas fermentation would necessarily require a cleanup step.

As ammonia is present in uncleaned syngas from biomass, its influence in process performance should be considered, and the data presented here showed that high ammonium concentrations inhibit the process with both studied strains. In fact, Xu and Lewis (2012) reported that the hydrogenase activity of *C. ragsdalei* is inhibited by NH_4^+, which explains why the cell activity decreased in all cases. However, ammonium is also the main source of nitrogen in the implemented growth medium, with a concentration of 3.3 g L^{-1} ammonium chloride. Therefore, simply adjusting the ammonium concentration in the medium could eliminate the necessity of scrubbing ammonia from syngas, provided that a lower initial ammonium concentration does not slow cell activity. In fact, it has been demonstrated with *C. ragsdalei* that lowering the concentration of ammonium chloride from 2.5 g L^{-1} to 1.25 g L^{-1} had no observable difference in the biomass, ethanol, and acetate formation (Saxena and Tanner, 2012). Thus, the possibility of lowering the initial ammonium concentration in the medium and the adaptability shown by *C. ragsdalei* to higher ammonium concentrations indicate that ammonium toxicity might be easy to curb.

The results show that *C. ljungdahlii* is more tolerant than *C. ragsdalei* to nitrate. Nitrate is, however, less likely to be present in syngas as an oxygenated nitrogen species, as the reducing conditions of the gasification should hinder its production. Nitrate has also been shown to be beneficial in the fermentation of H_2/CO_2 with *C. ljungdahlii* (Emerson et al., 2019), with the hypothesized mechanism being that nitrate functions as an electron acceptor, thus decoupling energy conservation from carbon fixation and increasing ATP gain. This would occur through the reduction of nitrate to nitrite and subsequentially to ammonium with NADH. NADH would be produced from reduced ferredoxin and NADPH supplied by the hydrogenase from H_2, with ferredoxin reducing NAD over the Rnf complex and producing ATP and NADPH with ferredoxin producing NADH by electron bifurcation with the Nfn. To some extent, the results presented here are in accordance with these assumptions. Nitrite was produced in the processes with the addition of 0.1 g L^{-1} and 0.5 g L^{-1} $NaNO_3$ with *C. ljungdahlii*, as shown in Figure 21; with *C. ragsdalei*, nitrite was not measured. Moreover, carbon was shifted from product formation to biomass formation. However, final concentrations of products or biomass

did not increase, thus it cannot be stated that nitrate was beneficial. With *C. ragsdalei*, nitrate was clearly not beneficial, reducing cell activity with increasing initial nitrate concentrations.

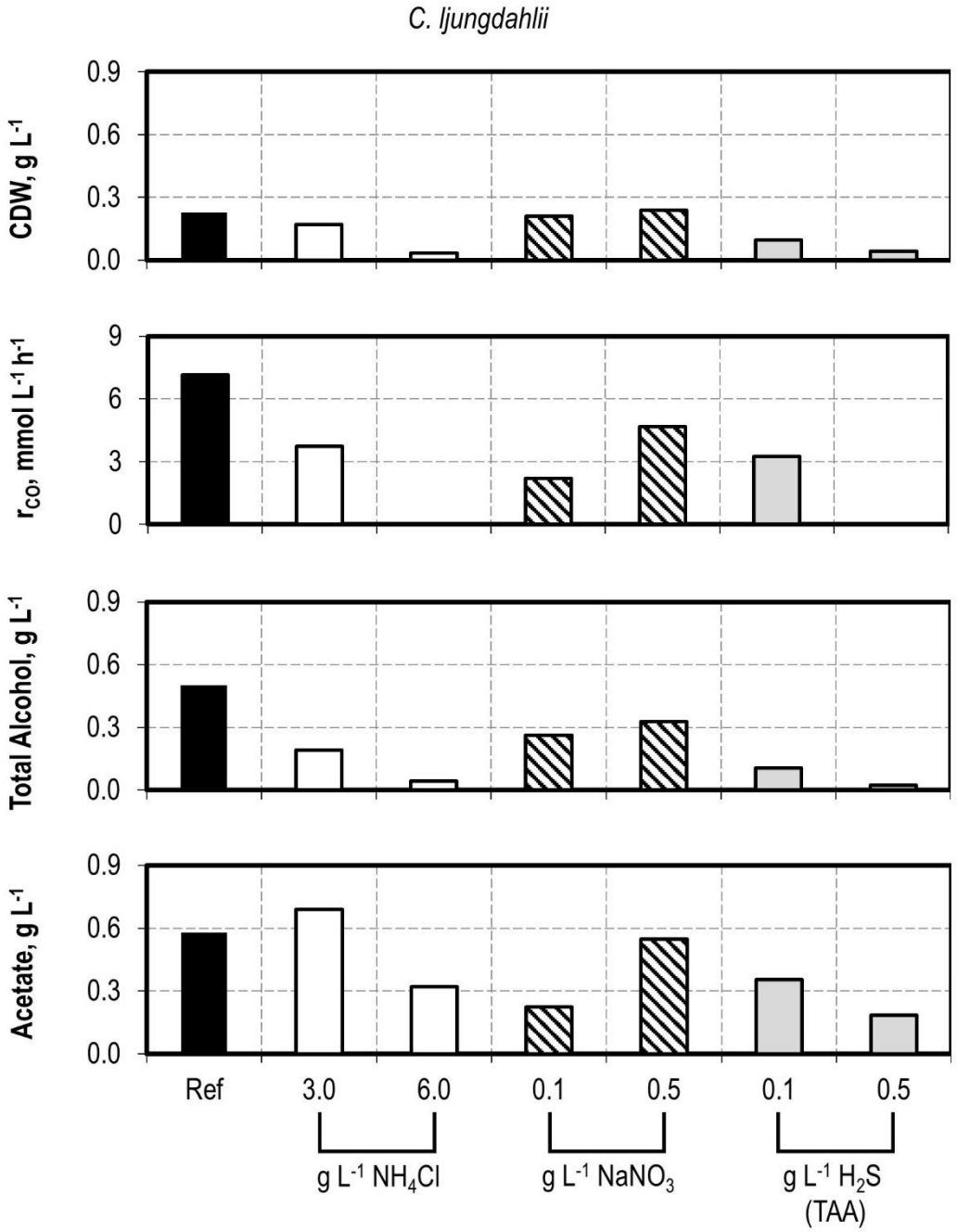

Figure 19 – Final concentration of cell dry weight (CDW), maximal CO uptake rate (r_{CO}), and final concentrations of total alcohol (ethanol and 2,3-butanediol) and acetate of the syngas fermentation with *Clostridium ljungdahlii* in continuously gassed batch processes, shown in Figure 16, Figure 17, and Figure 18, with the defined addition of NH_4Cl, $NaNO_3$ and H_2S as thioacetamide (TAA), in comparison to the process without the addition of impurities (Ref)

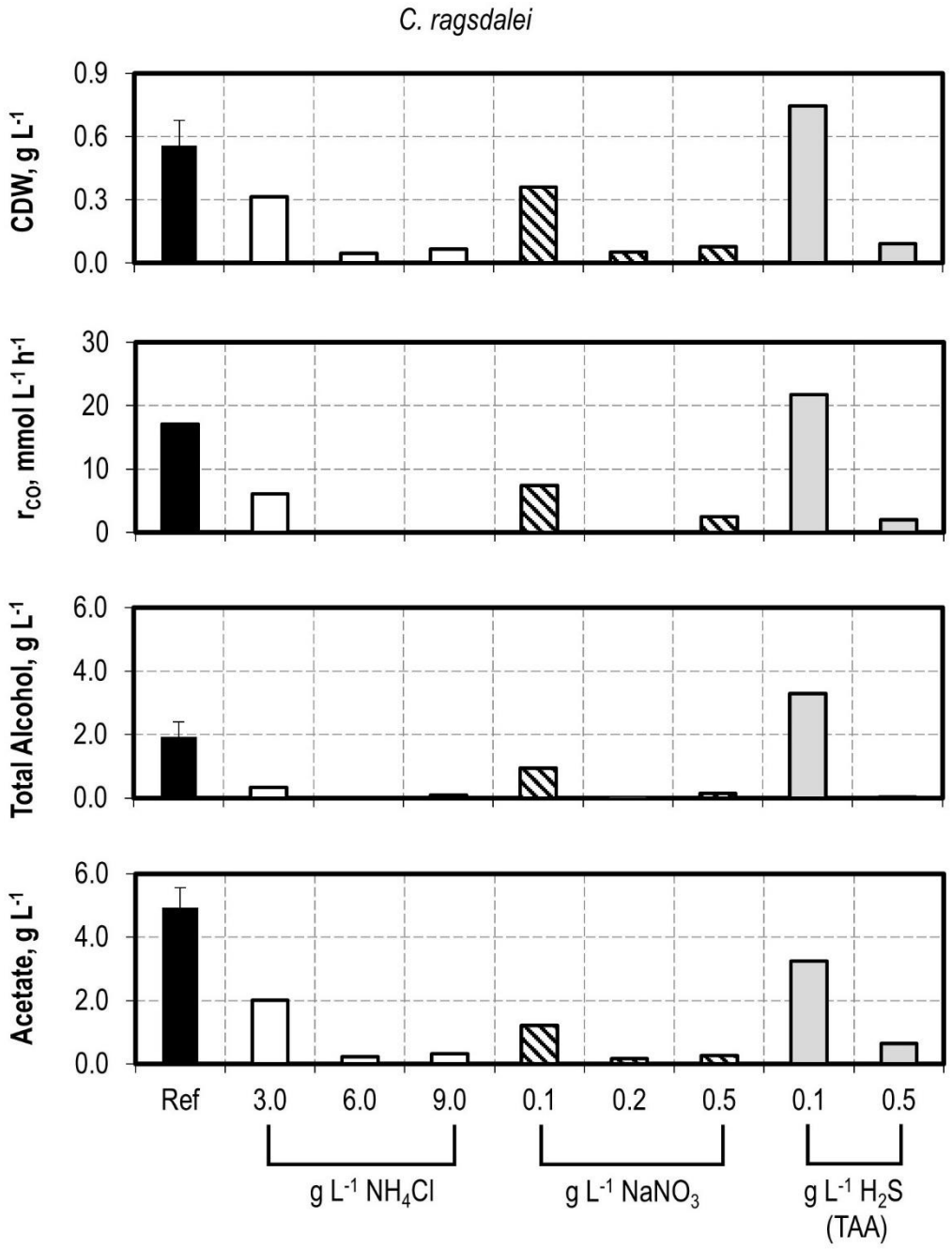

Figure 20 – Final concentration of cell dry weight (CDW), maximal CO uptake rate (r_{CO}), and final concentrations of total alcohol (ethanol and 2,3-butanediol) and acetate in the syngas fermentation with *Clostridium ragsdalei* in continuously gassed batch processes, shown in Figure 16, Figure 17, and Figure 18, with the defined addition of NH_4Cl, $NaNO_3$ and H_2S as thioacetamide (TAA), in comparison to the process without the addition of impurities (Ref). Error bars represent the standard deviation of the triplicate.

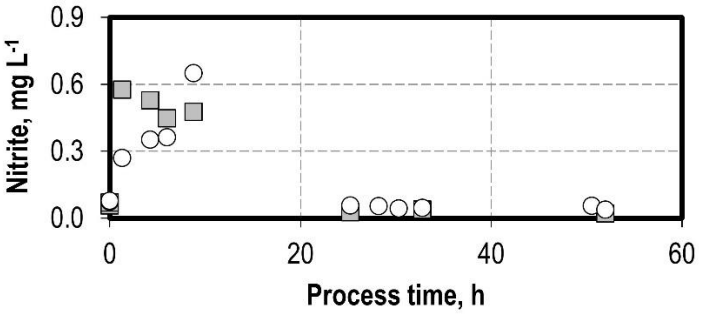

Figure 21 – Nitrite concentration in the autotrophic batch processes with addition of 0.1 g L^{-1} $NaNO_3$ (grey squares) and 0.5 g L^{-1} $NaNO_3$ (white circles) with *C. ljungdahlii* shown in Figure 17. Nitrite measurements were conducted with the method described in subsection 4.7.

H_2S, added as thioacetamide, showed a negative effect in the processes with *C. ljungdahlii*, whereas with *C. ragsdalei* an equivalent concentration of 0.1 g L^{-1} H_2S was beneficial for cell activity and alcohol production. Undissociated H_2S can permeate through the cell membrane and cause DNA damage and protein denaturation (O'Flaherty et al. 1998; Ntagia et al. 2020), which might be a reason for the overall negative effect of H_2S. However, sulfur is also a required nutrient for biomass formation, and the other sulfur sources in the medium implemented are sulfate, cysteine, or the sulfur present in the yeast extract, and at least sulfate is not accessible to *C. ljungdahlii*, since it cannot reduce it (Richter et al., 2016). Since *C. ragsdalei* produced more and faster biomass than *C. ljungdahlii*, it can be assumed that sulfide was a limiting factor for *C. ragsdalei*, and, once it was available, overall cell activity was increased. With *C. ljungdahlii*, however, as growth was already slower due to other reasons, a limitation in the sulfide availability was not manifested.

Analysis of Sulfide in the Syngas Fermentation

The supplementation of 0.1 g L^{-1} H_2S as thioacetamide increased cell activity and alcohol formation with *C. ragsdalei*, which could indicate a sulfur limitation in the process without additional H_2S. The sulfur sources in the medium for the syngas fermentation are cysteine, sulfur present in the yeast extract, and sulfate in the salts of the trace elements, with cysteine being the main sulfur source. Therefore, to better understand why the supplementation of H_2S improved cell activity, the cysteine concentration in the reaction broth and the H_2S concentration in the exhaust were measured with *C. ragsdalei* and *C. ljungdahlii*.

Figure 22 depicts the CDW and cysteine concentrations of batch three processes: *C. ljungdahlii* and 100 mbar inlet CO (process already presented in section 5); *C. ljungdahlii* and 450 mbar CO_2 and 550 mbar H_2 in the inlet; and *C. ragsdalei* and 600 mbar inlet CO (process also presented in section 5). In all processes, the cysteine concentration decreased to less than 0.04 g L^{-1} within the first 50 h; with *C. ragsdalei*, the cysteine concentration was 0.01 g L^{-1} already at the 24th process hour. Biomass growth continued in all processes after cysteine depletion.

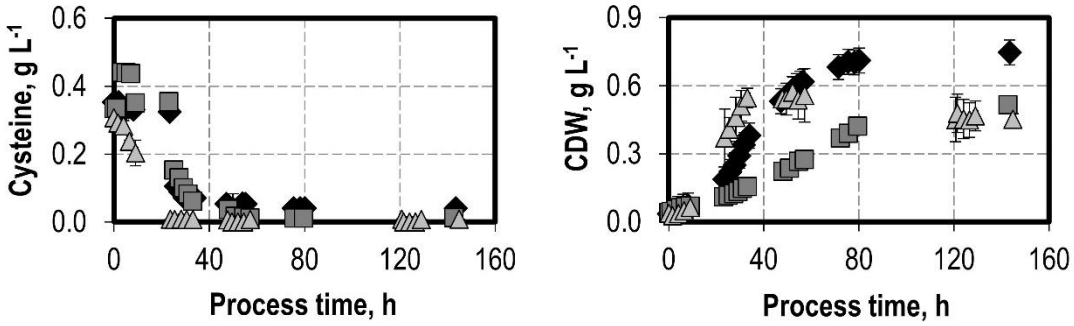

Figure 22 – Cell dry weight (CDW) and cysteine concentrations of the syngas fermentation with *C. ljungdahlii* and 100 mbar inlet CO (black diamonds); *C. ljungdahlii* and 450 mbar CO_2 and 550 mbar H_2 in the inlet (dark grey squares); and *C. ragsdalei* and 600 mbar inlet CO (grey triangles). Cysteine was measured with the method described in subsection 4.7. Batch processes were conducted with pH 6.0, 37 °C, working volume of 1 L, gas flow rate of 5 NL h^{-1}. Error bars correspond to the standard deviation of the processes carried out in duplicate (*C. ljungdahlii*, 100 mbar CO inlet) and triplicate (*C. ragsdalei*).

The H_2S concentration in the outlet was measured for the batch process with *C. ragsdalei*, and so the rate of H_2S stripping could be calculated. The H_2S stripping rate is shown in Figure 23 with the cysteine concentration and the cysteine depletion rate, which was calculated based on the nonlinear regression of the cysteine concentration according to equations 4.3 and 4.5. The nonlinear regression accurately described the measured cysteine concentrations with a residual sum of squares of 0.00023. The resulting cysteine depletion rate peaked with 0.023 g L^{-1} h^{-1} (0.146 mmol L^{-1} h^{-1}) at the 10.7th hour. The H_2S loss rate achieved its maximum of roughly 0.18 mmol L^{-1} h^{-1} at the 13th process hour and decreased sharply after the 16th process hour, concomitant with a low cysteine concentration and depletion rates. After the 40th hour, no H_2S loss or cysteine uptake was further measured.

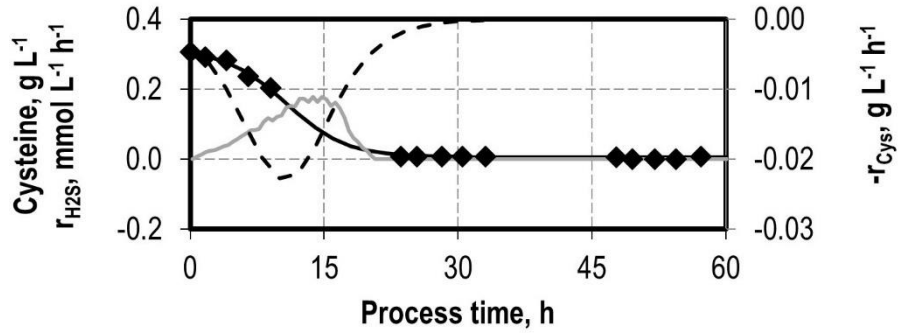

Figure 23 – Cysteine concentration (black diamonds), nonlinear regression of the cysteine concentration based on equation 4.3 (black line), cysteine negative depletion rate based on equation 4.5 ($-r_{Cys}$, black dashed line) and H_2S production rate in the exhaust (r_{H2S}, grey line) of the process with *C. ragsdalei* showed in Figure 22.

Discussion

Sulfur is a necessary element of the cell constitution and making it available for cell growth is key for a good process performance. However, ensuring sulfur availability is challenging, since *C. ljungdahlii* and *C. ragsdalei* do not assimilate sulfate (Richter et al., 2016). Cysteine is the most abundant source of sulfur in common syngas fermentation media, and the sulfur is accessed by releasing H_2S from the thiol group of cysteine with a L-cysteine desulfidase, as shown for *C. autoethanogenum*, a close relative to C*. ljungdahlii* and *C. ragsdalei,* (Gu et al., 2017; Bengelsdorf et al. 2016). Attempts to evaluate the effect of cysteine in the syngas fermentation have been made with *C. autoethanogenum* (Abubackar et al., 2012) and *C. ljungdahlii* (Infantes et al., 2020), but no substantial changes were observed. Meanwhile the cysteine concentration and the H_2S in the exhaust of the syngas fermentation has not been reported before. In this regard, the results presented here are novel by assessing if and to what extent cysteine is consumed in the syngas fermentation and by measuring sulfur losses through the gaseous phase.

The method used for measuring the cysteine concentration was proved appropriate. Despite its responsiveness also to sulfide ions, their effect was neglected, since the highest sulfide concentration measured in the process with *C. ragsdalei* was 0.4 mg L^{-1} at 9 h (data not shown), which would generate a neglectable absorption in the method.

If cysteine is broken down to release H_2S, a continuously gassed setup with pH 6.0 would inherently involve rapid stripping of H_2S. The extent to which H_2S is stripped has been shown by Hu et al. (2010) with the injection of 0.9 mM Na_2S in a cell-free continuously gassed STR at 37 °C, and sulfide was completely depleted to more than 95% after 150 minutes of stirring and gassing. Both strains rapidly broke drown cysteine, regardless of the presence of CO and

level of the specific growth rate. The cysteine depletion rate based on nonlinear regression led to a peak 2.5 hours prior to the peak H_2S loss rate in the exhaust, which strongly suggests a close correlation between both effects, the timely shift of H_2S stripping showed by Hu et al. (2010). This is a very strong indication that cysteine is broken down by the cells to access sulfur, thereby releasing H_2S, which is then stripped out of the reactor by the gassing. Overall, 74% (n/n) of the sulfur supplied as cysteine was lost through the exhaust as H_2S. This sulfur loss is a plausible reason why increasing the cysteine concentration did not have strong effects in the syngas fermentation with *C. ljungdahlii* (Infantes et al., 2020) and with *C. autoethanogenum* (Abubackar et al., 2012).

Despite the cysteine depletion, biomass formation continued in all processes. It is possible that the yeast extract in this case also serves as sulfur source, but available data are not sufficient to draw a conclusion in this regard.

Increasing Sulfide Availability with a Sulfide Feed

As cysteine is rapidly depleted from the reaction system and the supplementation of H_2S is beneficial for biomass and alcohol formation, better designing the sulfur availability in the syngas fermentation can be a key strategy to improve process performance.

For this purpose, batch processes were conducted with *C. ragsdalei* with a continuous Na_2S feed. Given that the process with *C. ragsdalei* presented in the previous subsection showed a cysteine depletion rate of 0.108 mmol L^{-1} h^{-1} over the first 23 process hours, the Na_2S feed rates implemented were 0.1 mmol S L^{-1} h^{-1} and 0.05 mmol S L^{-1} h^{-1}. The feed solutions consisted of 40 g L^{-1} and 20 g L^{-1} $Na_2S{\cdot}9H_2O$, respectively. The CDW and product concentrations, sulfur feed rates and CO uptake rates of the processes with the sulfide feed are shown in Figure 24.

The final CDW concentration achieved similar values in all processes, with 0.45 g L^{-1}, 0.50 g L^{-1} and 0.51 g L^{-1} for the processes without a sulfide feed and with feed rates of 0.05 mmol S L^{-1} h^{-1}, and 0.10 mmol S L^{-1} h^{-1}, respectively. The timely courses were, however, very distinct. Without and with a 0.05 mmol S L^{-1} h^{-1} feed rate, the CDW concentration increased until 58th process hour to 0.56 g L^{-1}, and 0.80 g L^{-1}, respectively, after which it decreased until the end of the process. With a 0.10 mmol S L^{-1} h^{-1} feed, biomass was formed throughout the whole process. The sulfide feed decreased the specific growth rates from 0.10 ± 0.006 h^{-1} with the sulfide feed, to 0.087 ± 0.004 h^{-1} and 0.062 ± 0.003 h^{-1} as the feed rate increased.

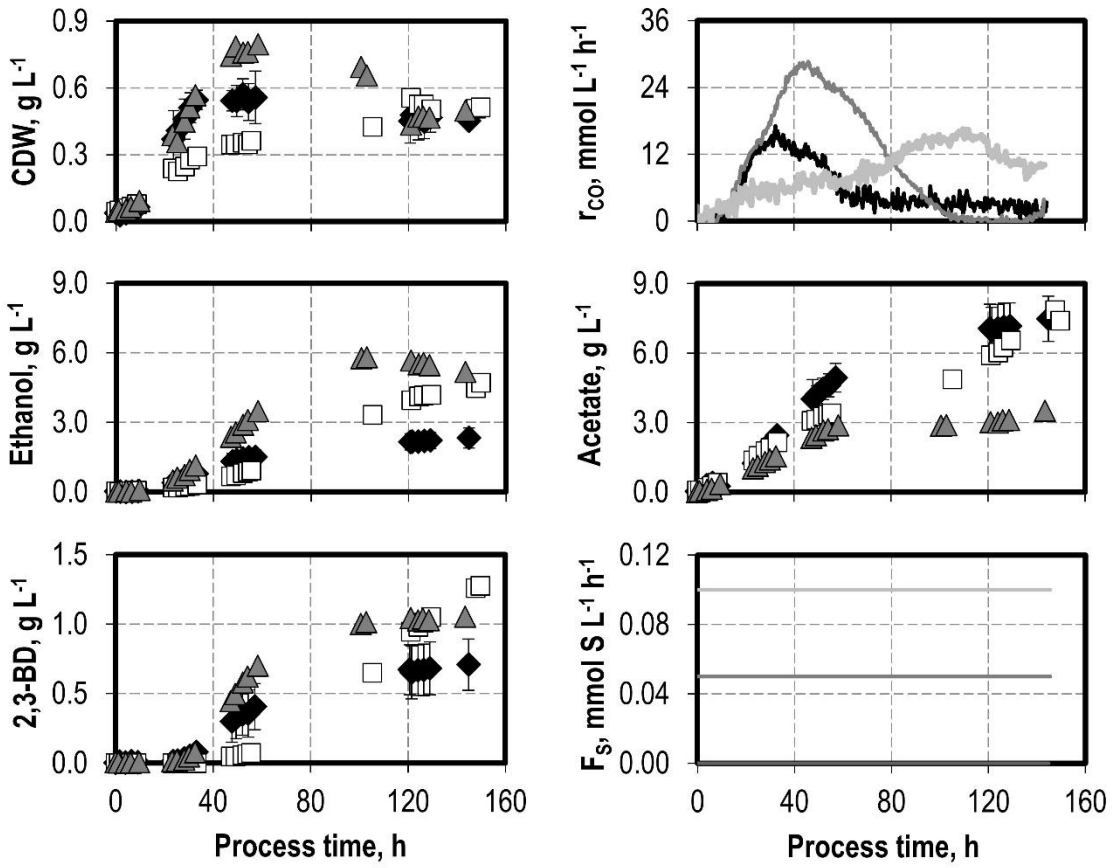

Figure 24 – Cell dry weight (CDW) concentration, CO uptake rate (r_{CO}), ethanol, acetate and 2,3-butanediol (2,3-BD) concentrations, and sulfide feed rate (F_S) of autotrophic batch processes with *C. ragsdalei* without a sulfide feed (black diamonds, black lines), with a sulfide feed of 0.05 mmol S L^{-1} h^{-1} (grey triangles, grey lines) and a sulfide feed of 0.10 mmol S L^{-1} h^{-1} (white squares, light grey lines). Processes were conducted with pH 6.0, 37 °C, working volume of 1 L, volumetric power input of 3.5 W L^{-1} (800 rpm), gas flow of 5.0 NL h^{-1}, a gas composition of 3:1:1 ($CO:H_2:CO_2$) and pressure of 1 bar.

This is reflected in the CO uptake rates. Without and with a 0.05 mmol S L^{-1} h^{-1} feed rate, the CO uptake rate peaked at 15.37 ± 1.35 mmol CO L^{-1} h^{-1} and 28.03 ± 0.50 mmol CO L^{-1} h^{-1} at the 32nd and 46th process hour, respectively. With a 0.10 mmol S L^{-1} h^{-1} feed, it peaked at 15.83 ± 0.70 mmol CO L^{-1} h^{-1} at the 110th hour. The values of uptake rates represent the average of the five measurements around the highest value and accordingly standard deviation. In none of the processes was H_2 consumed.

Product formation was strongly altered by the sulfide feed. Acetate formation reached similar values with the 0.10 mmol S L^{-1} h^{-1} feed rate but was more than halved with the lower feed rate, in relation to the process without a sulfide feed. In turn, the final concentration of ethanol increased to 5.18 g L^{-1} and 4.71 g L^{-1} with increasing sulfide feeds, a more than twofold increase. With the lower sulfide feed, ethanol concentration decreased after the 100th hour, concomitant with the biomass decline and absence of CO uptake. 2,3-butanediol final

concentration also increased with the sulfide feeds, reaching 1.05 g L^{-1} and 1.28 g L^{-1}. Similarly, no 2,3-butanediol formation was observed after the 100th hour with 0.05 mmol S L^{-1} h^{-1}. A summary of the process performance is presented in Table 5.

Table 5 - Final cell dry weight (CDW), specific growth rate at the exponential growth phase, acetate, ethanol and 2,3-butanediol concentrations, and maximal CO uptake rates (centered moving average with five values) in the batch processes with *C. ragsdalei* depicted in Figure 24. Errors in the concentrations correspond to the standard deviation of replicates.

Sulfide feed rate, mmol S L^{-1} h^{-1}	0.0	0.05	0.10
CDW, g L^{-1}	0.45 ± 0.03	0.5	0.51
Specific growth rate, h^{-1}	0.10 ± 0.006[1]	0.087 ± 0.004[1]	0.062 ± 0.003[1]
Acetate, g L^{-1}	7.48 ± 0.98	3.5	7.4
Ethanol, g L^{-1}	2.33 ± 0.43	5.18	4.71
2,3-butanediol, g L^{-1}	0.71 ± 0.18	1.05	1.28
CO max. uptake rate, mmol L^{-1} h^{-1}	15.3 ± 1.35[2]	28.03 ± 0.50[2]	15.83 ± 0.70[2]

[1]Errors represent the standard error of the linear regression to obtain the specific growth rate.
[2]Values represent the mean of the five uptake rates around the maximum value, and error represent their standard deviation.

As the 0.05 mmol S L^{-1} h^{-1} feed rate showed the highest cell activity with *C. ragsdalei*, it was replicated in a batch process with *C. ljungdahlii*, to assess if positive effects would also be observed. This was conducted in a process with 5 NL h^{-1} gassing with 100 mbar CO, 450 mbar CO_2 and 450 mbar H_2. The results are shown in Figure 25, with data from an analogue process without a sulfide feed as comparison (data also presented in section 5).

The sulfide feed slowed down the biomass formation in the first 60 process hours, leading to a decrease in the specific growth rate from 0.066 ± 0.0016 h^{-1} to 0.026 ± 0.0008 h^{-1}. However, biomass formation occurred until the 120th process hour, leading to a final CDW concentration of 1.46 g L^{-1}. The delayed biomass formation is reflected in the CO and H_2 uptake rates. The CO uptake rate reached its maximum later in process but remained close to maximum until the end of the process. H_2 uptake also resumed later in the process but reached higher values with a maximum of 40.66 ± 0.30 mmol L^{-1} h^{-1}. In the process without a sulfide feed, a discontinuity in the CO outlet partial pressures led to a discontinuity in the uptake rates, and the reason for this error could not be identified. Given that the H_2 uptake does not seem to be altered, it was assumed that a measurement error without any effect in the process performance occurred.

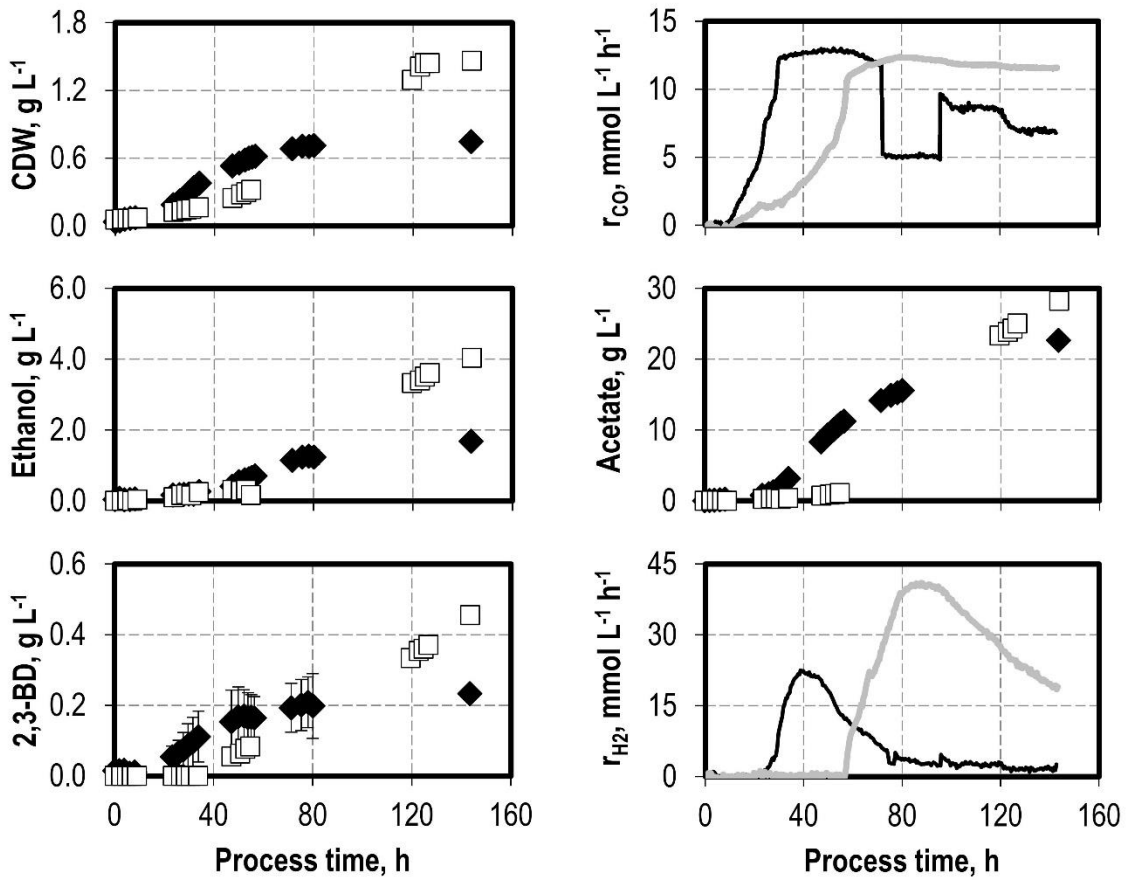

Figure 25 – Cell dry weight (CDW) concentration, CO uptake rate (r_{CO}), ethanol, acetate and 2,3-butanediol concentrations, and H_2 uptake rates (r_{H2}) of the syngas fermentation with *C. ljungdahlii* in batch mode without a sulfide feed (black diamonds, black lines) and with a sulfide feed of 0.05 mmol S L^{-1} h^{-1} (white squares, grey lines). Batch processes were conducted with pH 6.0, 37 °C, working volume of 1 L, volumetric power input of 3.5 W L^{-1} (800 rpm), gas flow of 5.0 NL h^{-1} with a gas compositions of 1:4.5:4.5: ($CO:H_2:CO_2$) and pressure of 1 bar.

The sulfide feed also led to an increase in the concentration of all products. The final concentration of acetate increased to 28.21 g L^{-1}, a 24.5% increase, while the increase in the ethanol and 2,3-butanediol concentrations were 2.4-fold, and twofold, respectively, more in line with the increase in the final CDW concentration. A summary of the key results from these processes with *C. ljungdahlii* is presented in Table 6.

Table 6 – Final cell dry weight (CDW) concentration, specific growth rate at the exponential growth phase, acetate, ethanol and 2,3-butanediol concentrations, and maximal CO and H_2 uptake rates (centered moving average with five values) in the batch processes with *C. ljungdahlii* depicted in Figure 25. Errors in the concentrations correspond to the standard deviation of replicates.

Sulfide feed rate, mmol S L^{-1} h^{-1}	0.0	0.05
CDW, g L^{-1}	0.75 ± 0.06	1.46
Specific growth rate, h^{-1}	0.066 ± 0.0016[1]	0.026 ± 0.0009[1]
Acetate, g L^{-1}	22.65 ± 0.71	28.21
Ethanol, g L^{-1}	1.69 ± 0.21	4.04
2,3-butanediol, g L^{-1}	0.23 ± 0.09	0.46
CO max. uptake rate, mmol L^{-1} h^{-1}	12.86 ± 0.09[2]	12.25 ± 0.018[2]
H_2 max. uptake rate, mmol L^{-1} h^{-1}	22.14 ± 0.34[2]	40.66 ± 0.30[2]

[1]Errors represent the standard error of the linear regression to obtain the specific growth rate.
[2]Values represent the mean of the five uptake rates around the maximum value, and error represent their standard deviation.

Discussion

Sulfur from cysteine is clearly lost in the continuously gassed syngas fermentation with *C. ljungdahlii* and *C. ragsdalei* through the exhaust as H_2S, requiring thus a more adequate concept for sulfur supply. Through the continuous feed of a Na_2S solution, sulfide can be supplied without the addition of carbon to the system. Here, results to the sulfide addition at rates of 0.05 mmol S L^{-1} h^{-1} and 0.10 mmol S L^{-1} h^{-1} in processes with *C. ragsdalei* and at a rate of 0.05 mmol S L^{-1} h^{-1} with *C. ljungdahlii* were presented and, overall, process performance was improved. This is the first time that the positive effect of adequately supplying sulfur was shown, as well as how process performance of the syngas fermentation with *C. ljungdahlii* and *C. ragsdalei* is changed by it.

Additional sulfide increased biomass formation over the whole process length, but this improvement is nuanced. Specific growth rates decreased with the sulfide feed in all cases, which was strongly demonstrated with 0.10 mmol S L^{-1} h-^{1} with *C. ragsdalei* and 0.05 mmol S L^{-1} h^{-1} with *C. ljungdahlii* with decreases of 38% and 60 %, respectively. This reflects the results presented previously in this section, whereby the supplementation of H_2S as thioacetamide was detrimental in most cases and *C. ljungdahlii* was less tolerant to a sulfide impurity. Possible mechanisms for sulfide inhibition have already been discussed.

With the sulfide feed rates of 0.05 mmol S L^{-1} h^{-1} and 0.10 mmol S L^{-1} h^{-1}, 7.2 mmol S^{2-} and 14.4 mmol S^{2-} were added to the reaction system over 144 h. Meanwhile, 5.43 mmol H_2S and 12.12 mmol H_2S were lost in the exhaust (data not graphically shown), which correspond to 56% (n/n) and 72% (n/n) losses of the sulfur supplied as Na_2S and cysteine. Considering the final free thiol concentration in the end of the processes, 37% (n/n) and 24% (n/n) of the sulfur supplied as Na_2S and cysteine could not be measured either as H_2S in the exhaust or as free thiol. These differences are not justified by the fixation of sulfur in biomass, which considering a sulfur fraction of 1% (w/w) in biomass (Metcalf & Eddy Inc. et al, 2014) and a CDW concentration of 0.5 g L^{-1}, corresponds to a fixation of only 0.15 mmol sulfur, less than 1% of the sulfur supplied. A possible reason for this discrepancy might lie in the formation of insoluble sulfide, such as zinc sulfide and nickel sulfide since both zinc and nickel ions are present in the medium composition.

To try to infer what effects did the sulfide produce on the cell, let us consider the process phase with increased overall activity *i.e.*, increasing CO uptake rate. A key benefit of the sulfide feed was prolonging this phase, which was achieved by enabling further CDW formation and led overall to a higher uptake of CO in this phase. This is shown in Table 7, with the values for the CO uptake within this phase of increasing CO uptake rate and the phase length. While the length of the phase of increasing CO uptake rate was 32 h without a sulfide feed, the sulfide feed rate of 0.05 mmol L^{-1} h^{-1} increased the phase length to 46 hours. This led to an increase in the CO uptake within this phase from 167.52 mmol to 611.50 mmol. With a feed rate of 0.10 mmol L^{-1} h^{-1}, phase length and CO uptake were also substantially increased, however with the detriment of a much slower growth. This overall benefit lastly relates to overcoming a sulfur limitation and enabling higher CDW concentrations.

Table 7 – CO uptake in the phase of increasing CO uptake rate and phase length of the processes with a sulfide feed with *C. ragsdalei* presented in Figure 24.

	Sulfide feed rate, mmol S L^{-1} h^{-1}		
	0.0	0.05	0.10
CO uptake, mmol	167.52	611.50	809.15
Phase length, h	32	46	110

Besides this overall effect of increasing CO uptake in the most active phase, carbon was directed differently in each process with *C. ragsdalei*, which can be seen in Figure 26, where the CDW and product concentrations are plotted against the overall CO absorbed within this phase. A strong similarity can be seen within all processes in the relationship between CO uptake and alcohol formation, with greater divergences seen for acetate and CDW. Ethanol

formation and CO uptake showed a linear relationship within the processes, with the slopes being 4.30 ± 0.15 g $mmol^{-1}$ CO L^{-1} (coefficient of correlation 0.991), 3.92 ± 0.15 g $mmol^{-1}$ CO L^{-1} (coefficient of correlation 0.987) and 4.04 ± 0.10 g $mmol^{-1}$ CO L^{-1} (coefficient of correlation 0.990) for the processes without a sulfide feed and with 0.05 mmol S L^{-1} h^{-1} and 0.10 mmol S L^{-1} h^{-1}, respectively. This indicates that the sulfide feed did not alter the activities of the enzymes directly involved in ethanol production, and the increase in the concentration was derived from the higher CDW. For 2,3-butanediol this analysis is more difficult, since a great gap is seen in the higher values and the 2,3-butanediol production without a sulfide feed in the phase of increasing CO uptake rate was small.

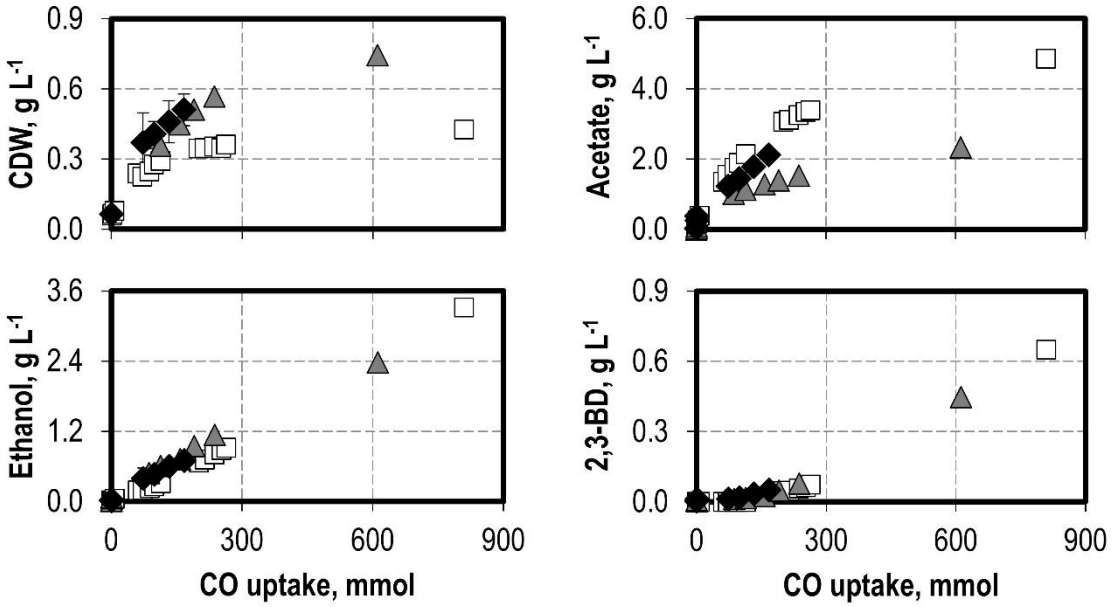

Figure 26 – Cell dry weight (CDW) concentration, acetate, ethanol and 2,3-butanediol (2,3-BD) concentrations *vs* the total CO uptake within the process phase of increasing CO uptake rates of the batch processes with *C. ragsdalei* presented in Figure 24: no sulfide feed (black diamonds), 0.05 mmol S L^{-1} h^{-1} (grey triangles) and 0.10 mmol S L^{-1} h^{-1} (white squares).

Important amounts of product were also produced after the CO uptake rates peaked. To analyse this, the integral production rates of CDW and products for the phases of increasing CO uptake rates and that of decreasing rates are shown in Table 8. While no sulfide feed was beneficial for CDW and acetate production in the phase of increasing activity, with integral production rates of 0.402 g L^{-1} h^{-1} and 1.679 g L^{-1} h^{-1}, respectively, the sulfide feed of 0.05 mmol S L^{-1} h^{-1} led to the highest ethanol and 2,3-butanediol productivities, with increases of 218% and 570% in relation to no-feed. After the CO uptake rates peaked, the sulfide feed led in both cases to a higher ratio of alcohol per acetate produced, with 0.42 $g_{alcohol}$ $g^{-1}_{acetate}$ without the sulfide feed, 2.92 $g_{alcohol}$ $g^{-1}_{acetate}$ with 0.05 mmol S L^{-1} h^{-1} and 0.80 $g_{alcohol}$ $g^{-1}_{acetate}$ with 0.10 mmol S L^{-1} h^{-1}. In absolute term, the alcohol rates were also higher with the sulfide feed. This

is especially interesting for the processes without and with the lowest sulfide feed, in which biomass decrease was observed. Without biomass formation, ATP consumption relates to maintenance, so the lower sulfide feed enabled the supply of ATP while mainly producing alcohols. The ATP yield per mol CO decreases slightly if acetate or ethanol is produced, with 0.376 mol ATP mol^{-1} CO for acetate (Richter et al., 2016) and 0.342 mol ATP mol^{-1} CO for ethanol, while with 2,3-butanediol the ATP yield decreases to 0.233 – 0.208 mol ATP mol^{-1} CO, as discussed in section 5. The ATP yield on CO for ethanol was calculated combining equations 3.4, 3.5, 3.7 and 3.11. The small difference in the ATP yield from acetate to ethanol, but the big one to 2,3-butanediol, might explain why the integral production rate of ethanol with the lower sulfide feed could be twofold than that without the sulfide feed, but the 2,3-butanediol rate remained similar.

Table 8 – Production rates of cell dry weight (CDW), acetate, ethanol and 2,3-butanediol for the phases of increasing CO uptake rates (r_{CO}) and decreasing rates of the batch processes with *C. ragsdalei* shown in Figure 24. The phase lengths are presented in Table 7.

		Integral production rate, g L^{-1} d^{-1}			
Sulfide feed rate, mmol S L^{-1} h^{-1}		CDW	Acetate	Ethanol	2,3-butanediol
Before $r_{CO, max}$	0.00	0.402	1.679	0.552	0.040
	0.05	0.378	1.188	1.208	0.227
	0.10	0.097	1.109	0.756	0.148
After $r_{CO, max}$	0.00	-0.012	1.122	0.341	0.138
	0.05	-0.061	0.291	0.699	0.151
	0.10	0.047	1.369	0.753	0.338

In summary with *C. ragsdalei*, a sulfide feed of 0.05 mmol S L^{-1} h^{-1} increased the maximal achieved CDW concentration by 45% (0.74 g L^{-1}) and the ethanol and 2,3-butanediol concentration in the phase of increasing CO uptake rates. This was achieved by both extending length of this phase and increasing the ethanol and 2,3-butanediol integral production rates. Moreover, the sulfide feed increased with both feed rates the alcohol to acetate ratio, from 0.406 g g^{-1} to 1.78 g g^{-1} and 0.81 g g^{-1} with 0.05 mmol S L^{-1} h^{-1}, and 0.10 mmol S L^{-1} h^{-1}, respectively.

With *C. ljungdahlii*, the improvements in process performance from the sulfide feed are different than that with *C. ragsdalei*. Whereas the sulfide feed strongly curbed the specific growth rate, the final CDW and 2,3-butanediol concentrations and maximal H_2 uptake rates roughly doubled, whereas the final ethanol concentration increased by 2.4-fold, thus increasing the alcohol to acetate ratio from 0.085 g g^{-1} to 0.159 g g^{-1}.

The mechanisms with which the sulfide feed improved the process performance is unclear. The overall effects observed here were:

- Increase in achievable CDW concentration;
- Increase in alcohol concentration and alcohol to acetate ratios.

The increase in the achievable CDW concentration is most likely due to overcoming a sulfur limitation, as it could be successfully demonstrated that cysteine is quickly depleted in the continuously gassed process and the sulfur is mostly lost in the exhaust. Indications of sulfur limitation have been published for data with *C. ljungdahlii* based on the upregulation of genes for the uptake and metabolism of sulfur compounds (Aklujkar et al. 2017) and the overabundance of sulfur related proteins in the proteome and depletion of sulfur containing amino acids in the metabolome of *C. ljungdahlii* (Richter et al., 2016).

The reason for the increased alcohol production cannot be fully answered with the available data, but only hypothesis can be elaborated. One aspect that can be excluded from this analysis is a more reduced state in the bioreactor, which could foment the reduction of acetate. In fact, the redox potential (RP), as is shown in Figure 27, was more negative without the addition of sodium sulfide, and the highest with the highest sulfide feed rate. This is in accordance with published data in which the RP was less negative with the addition of cysteine and Na_2S than without it (Yang et al., 2022). Additionally, it was not expected that the addition of Na_2S would further decrease the RP, since it is a weaker reductant than cysteine (Kabil and Banerjee, 2010).

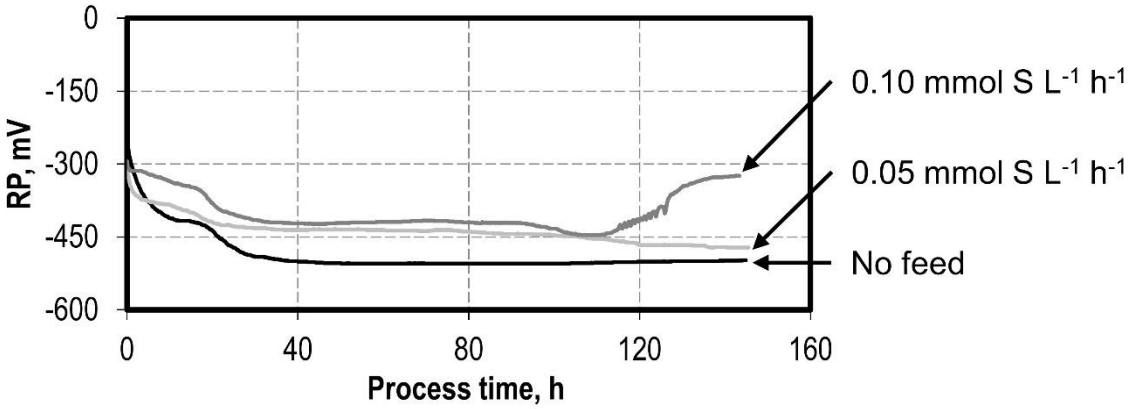

Figure 27 – Redox potential (RP) of the syngas fermentation with *C. ragsdalei* without and with a sulfide feed of 0.05 mmol L^{-1} h^{-1} and 0.10 mmol L^{-1} h^{-1}. The processes were presented in Figure 24.

Another aspect to consider is whether H_2S can serve as electron donor to support the production of more reduced products by regenerating a reducing agent. No results have been

published in this regard. Furthermore, the very similar relationship between the ethanol concentration and the CO consumed with and without the sulfide feed, showed in Figure 26, indicates no direct involvement of sulfide in the ethanol formation. To finally exclude this possibility, the use of H_2S as an electron donor will be analysed on a thermodynamical basis considering the anaerobic sulfite reductase (ASR), which both *C. ljungdahlii* and *C. ragsdalei* possess (Bengelsdorf et al. 2016), and reversibly reduces sulfite to sulfide by

$$H_2SO_3 + 3H_2 \leftrightarrow H_2S + 3H_2O \qquad \Delta G^0 = -174{,}0\ kJ\ mol^{-1} \qquad (5.2)$$

(Barton and Fauque, 2009)

The reducing agent of this reaction is unknown (Barton and Fauque, 2009). Considering NADH, NADPH and ferredoxin as reducing agents, the standard Gibbs free energies of reaction would be

$$H_2SO_3 + 3NADPH + 3H^+ \leftrightarrow H_2S + 3H_2O + 3NADP^+ \qquad \Delta G^0 = -120{,}0\ kJ\ mol^{-1} \qquad (5.3)$$

$$H_2SO_3 + 3Fd^{-2} + 6H^+ \leftrightarrow H_2S + 3H_2O + Fd \qquad \Delta G^0 = -195{,}0\ kJ\ mol^{-1} \qquad (5.4)$$

$$H_2SO_3 + 3NADH + 3H^+ \leftrightarrow H_2S + 3H_2O + 3NAD^+ \qquad \Delta G^0 = -120{,}0\ kJ\ mol^{-1} \qquad (5.5)$$

based on equation 5.2 and the Gibbs free energies of the redox reactions of NAD^+, $NADP^+$ and ferredoxin from Schuchmann and Müller (2014). Thus, under standard conditions, H_2S as electron donor through the anaerobic sulfite reductase is thermodynamically unfeasible. Does this change under the real process conditions? Considering the use of NADH, the Gibbs free energy can be calculated by

$$\Delta G'_T = \sum v_i \cdot \Delta G^0_{T,i} + R \cdot T \cdot ln \frac{[H_2S] \cdot [H_2O]^3 \cdot [NAD]^3}{[H_2SO_3] \cdot [H^+]^3 \cdot [NADH]^3} \qquad (5.6)$$

$\Delta G'_T$	Transformed Gibbs free energy of the reaction, kJ mol^{-1}
v_i	Stoichiometric coefficient of species *i*
$\Delta G^0_{T,i}$	Standard Gibbs free energy of the reaction corrected for temperature and pH, kJ mol^{-1}
R	Gas constant, kJ K^{-1} mol^{-1}
T	Temperature, K
[ ]	Concentration, M

Neglecting the effect of temperature on the first term of equation 5.6, the difference in the standard and the transformed free energies, considering equal H_2S and sulfite concentrations, would be:

$$\Delta G'_T - \Delta G'^{,0} \sim R \cdot T \cdot ln \frac{[10^{-7}]^3 \cdot [NAD]^3}{[H^+]^3 \cdot [NADH]^3} \quad (5.7)$$

Valgepea et al. (2017) reported ratios of NADH to NAD^+ from 0.01 to 0.03; considering a NADH/NAD^+ ratio of 0.02 and a pH of 6.0 at temperature 37 °C, the change in the free energy is 12.44 kJ mol^{-1}, which is insufficient to turn the reduction of NAD^+ with H_2S to a feasible reaction. A conclusive answer to this question, however, would require the measurement of sulfite in the processes, which was not conducted within these studies.

Excluding more reduced conditions in the reactor, and a direct involvement of H_2S as electron donor, it is to assume that the sulfide incurred changes on a biological level that improved alcohol formation, but the available data is insufficient to identify possible changes. To elucidate this, ideally a proteome analysis should be conducted, to evaluate if the proteins involved in alcohol production are more abundant with the sulfide feed, as well as assessing how the ratios NADH/NAD^+ and NADPH/$NADP^+$ changed under these conditions. In this regard, Richter et al. 2016 published a broad set of data of a 2 bioreactor cascade with *C. ljungdahlii*. In the first bioreactor, at pH 5.5 and biomass and acetate were built and in the second at pH 4.5 and ethanol was produced. Proteome and metabolome analysis were conducted in each bioreactor, to compare the differences between the acid or alcohol production in the proteome and metabolome level. It was observed that enzymes involved in the WLP, energy conservation and anabolism were not differently regulated in both reactors. Furthermore, the NADPH/$NADP^+$ ratio did not change substantially, according to the authors, from 0.062 in the first reactor to 0.045 in the second. The biggest differences lied in the upregulation of enzymes related to nutrient limitation and the NADH/NAD^+ ratio. Of the ten most upregulated enzymes in the second reactor, 6 were related to sulfur metabolism or uptake, and the NADH/NAD^+ ratio increased from 0.001 in the first to 0.03 in the second. With this, the authors concluded that ethanol formation in the second reactor was fomented by the unchanged proteome with respect to the WLP and alcohol production which kept the generation of reducing agents, but due to a nutrient limitation, these were not directed to anabolism but to acetate reduction.

Extrapolating these observations to the results presented here, a closer look into the alcohol production in the exponential growth phase in the process without and with a sulfide feed of 0.05 mmol S L^{1-} h^{-1} with *C. ragsdalei* is relevant. This is shown in Figure 28 with the ethanol and 2,3-butanediol concentrations plotted against the CDW concentration for both processes in the exponential growth phase, as well as the rate of H_2S loss in the exhaust. The latter was correlated to the CDW in the unmeasured intervals by a nonlinear regression based on equation 4.3 of the CDW concentration and the time for each data set. The residual sum of

squares was 2.68 10^{-4} and 3.60 10^{-3} for the process without and with the sulfide feed, respectively.

The sulfide feed increased the ethanol yield to biomass, while the yield of 2,3-butanediol was similar. A key difference in the ethanol production lies in the available sulfur, as shown by the H_2S in the exhaust: whereas without a sulfide feed no H_2S was seen in the exhaust already at CDW concentrations below 0.3 g L^{-1}, H_2S was observed throughout the whole process, even though at substantially lower rates than those fed (0.011 mmol S L^{-1} h^{-1} *vs.* 0.05 mmol S L^{-1} h^{-1}). This indicates a different relationship between nutrient limitation and ethanol production than that reported by Richter et al. (2016), with ethanol formation being fomented once the sulfur limitation was curbed. However, it is important to note that the pH was substantially different in the processes here described and the pH 4.5 employed by Richter et al. (2016), which *per se* is a driver of ethanol formation. Thus, it is expected that the sulfide feed, by overcoming the sulfur limitation in the end of the exponential growth phase, changes the abundance of key enzymes required for ethanol production. Which enzymes these are, the data here does not offer basis for hypothesizing.

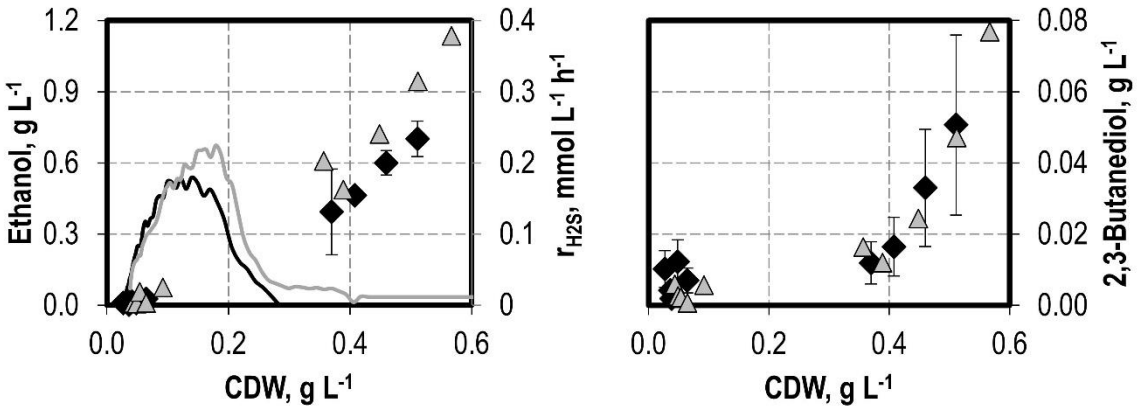

Figure 28 – Ethanol, 2,3-butanediol (2,3-BD) concentrations and the H_2S production rate (r_{H2S}) *vs* the cell dry weight (CDW) concentration within the exponential growth phases of the processes with *C. ragsdalei* presented in Figure 24: no sulfide feed (black diamonds, black line), 0.05 mmol S L^{-1} h^{-1} (grey triangles, grey line).

2,3-butanediol behaved differently than ethanol in this phase, and indeed the implementation of a sulfide feed did not alter the 2,3-butanediol biomass related yield. This indicates that 2,3-butanediol formation is in the exponential phase closely tied to biomass formation.

7 Increasing Alcohol Formation[2]

The goal of the syngas fermentation is to convert syngas into valuable products. With *C. ljungdahlii* and *C. ragsdalei*, these are ethanol and 2,3-butanediol. In the last section, it was shown that applying a sulfide feed substantially changed the outcomes of the syngas fermentation with *C. ljungdahlii* and *C. ragsdalei*. It enabled an increase in the achievable CDW concentration, prolonged the phase length of increasing activity i.e. increasing CO uptake rate and increased alcohol to acetate ratios. In relation to alcohol formation, these improvements were more pronounced with *C. ragsdalei.*

C. ragsdalei also showed a higher tolerance to high CO partial pressures, and therefore it was chosen as the best strain to further improve alcohol production through changes in process parameters. In this section, results to the process performance of *C. ragsdalei* with different pH profiles and lower temperatures will be presented and discussed. Furthermore, results to the combination of the best pH and temperature with the sulfide feed of 0.05 mmol S L^{-1} h^{-1} will be shown, assessing whether combined benefits could be achieved.

7.1 Individual Effect of Temperature and pH on the Syngas Fermentation

The syngas fermentation with *C. ragsdalei* and related strains is commonly conducted at 37 °C. By lowering the temperature to 32 °C and 27 °C, the batch process outcomes were substantially changed, as can be seen in Figure 29.

The CDW concentration was increased in both processes with lower temperatures, both regarding the final as well as the maximal CDW concentration. The highest CDW concentration was achieved with 32 °C with 0.79 g L^{-1}. The specific growth rate was unchanged at 32 °C, but decreased to 0.065 ± 0.001 at 27 °C. It is to highlight that at both lower temperatures, the CDW concentration did not decrease once the CO uptake rate started to decline, as is the case at 37 °C.

[2] Some of the results of the chapter were published in:

Oliveira L, Röhrenbach S, Holzmüller V, Weuster-Botz D (2022). Continuous sulfide supply enhanced autotrophic production of alcohols with *Clostridium ragsdalei*. Bioresources and Bioprocessing. 9, 15.

The maximal CO uptake rate was also unchanged by lowering the temperature to 32 °C with 15.08 ± 0.23 mmol L^{-1} h^{-1} (15.3 ± 1.35 mmol L^{-1} h^{-1} at 37 °C) but decreased at 27 °C to 11.23 ± 0.32 mmol L^{-1} h^{-1}, analogous to the lower specific growth rate. Differently than at a higher temperature, the CO uptake rate was maintained higher for longer at lower temperatures, with both processes achieving final CO uptake rates of roughly 7 mmol L^{-1} h^{-1}.

Lowering the temperature decreased acetate formation, with both processes achieving similar final acetate concentrations of 5.40 g L^{-1} and 5.88 g L^{-1} at 32 °C and 27 °C, respectively. In turn, alcohol formation was fomented in both cases. The final ethanol concentration increased slightly at 27 °C to 3.02 g L^{-1}, but substantially to 5.34 g L^{-1} at 32 °C, an increase of 132% in comparison to the process at a higher temperature. 2.3-butanediol was also produced at higher quantities at lower temperatures, increasing from 0.71 g L^{-1} to 1.35 g L^{-1} at 32 °C and 1.13 g L^{-1} at 27 °C. A summary of the key results of the processes with lower temperatures is presented in Table 9.

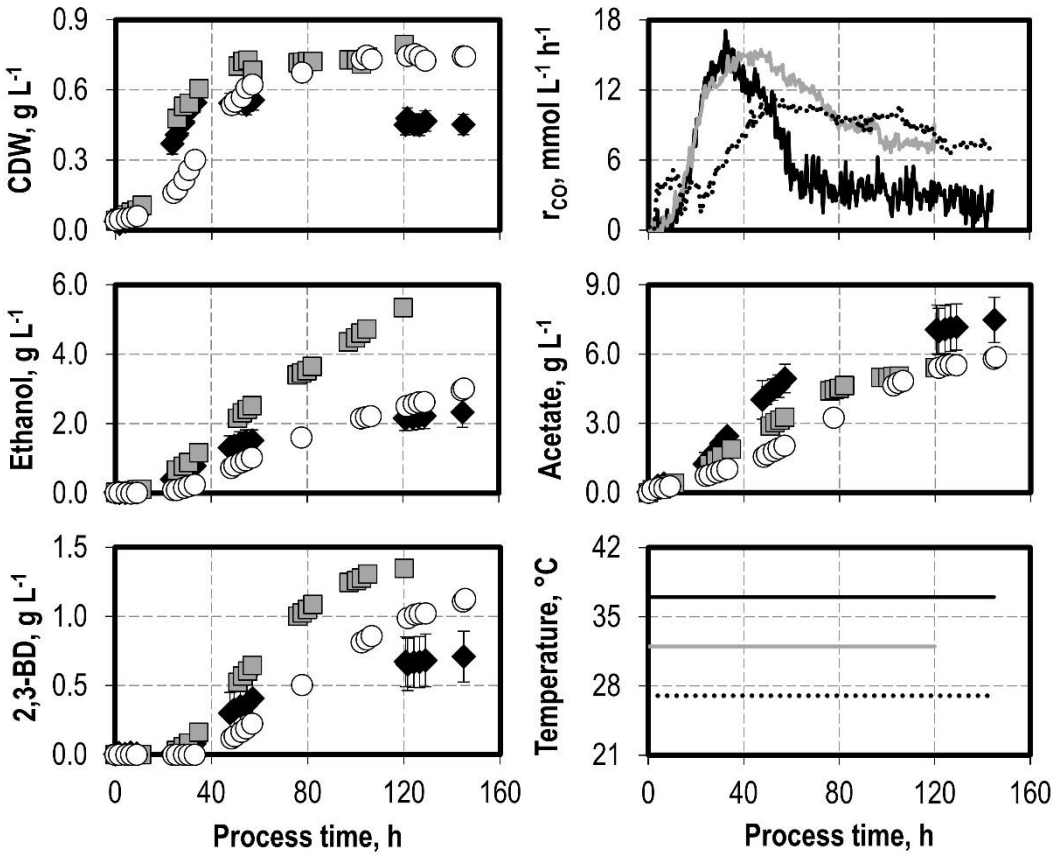

Figure 29 – Cell dry weight (CDW) concentration, CO uptake rate (r_{CO}), ethanol, acetate and 2,3-butanediol concentrations, and temperature of the syngas fermentation with *C. ragsdalei* at 37 °C (black diamonds, black lines), 32 °C (grey squares, grey lines) and 27 °C (white circles, dotted lines). Batch processes were conducted with pH 6.0, working volume of 1 L, volumetric power input of 3.5 W L^{-1} (800 rpm), gas flow of 5.0 NL h^{-1} with 3:1:1 ($CO:H_2:CO_2$) and pressure of 1 bar.

Table 9 – Final cell dry weight (CDW) concentration, specific growth rate at the exponential growth phase, acetate, ethanol and 2,3-butanediol concentrations, and maximal CO uptake rates (centered moving average with five values) in the batch processes with *C. ragsdalei* with different temperatures depicted in Figure 29. Errors in the concentrations correspond to the standard deviation of replicates.

Temperature, °C	37	32	27
CDW, g L^{-1}	0.45 ± 0.03	0.79	0.74
Specific growth rate, h^{-1}	0.10 ± 0.006[1]	0.094 ± 0.003[1]	0.065 ± 0.001[1]
Acetate, g L^{-1}	7.48 ± 0.98	5.4	5.88
Ethanol, g L^{-1}	2.33 ± 0.43	5.34	3.02
2,3-butanediol, g L^{-1}	0.71 ± 0.18	1.35	1.13
CO max. uptake rate, mmol L^{-1} h^{-1}	15.3 ± 1.35[2]	15.08 ± 0.23[2]	11.23 ± 0.32[2]

[1]Errors represent the standard error of the linear regression to obtain the specific growth rate.
[2]Values represent the mean of the five uptake rates around the maximum value, and error represent their standard deviation.

To assess the individual effect of pH on the syngas fermentation with *C. ragsdalei*, processes were conducted at an initial pH of 6.0 without pH control until a desired pH was achieved. These pH levels were pH 5.5, pH 5.0 and a process without pH control. Process performances are shown for these processes in Figure 30.

pH 5.5 and pH 5.0 were achieved in the processes around the 33rd process hour, whereas in the process with uncontrolled pH, a minimum of pH 4.024 was achieved in the 107th h. The courses of the CDW concentration were very similar in all processes within the first 33 hours, even though the pH profiles were different. This is also clear in the very similar specific growth rates, which ranged from a maximum of 0.10 ± 0.006 h^{-1} with pH 6.0 to a minimum of 0.094 ± 0.001 h^{-1} with uncontrolled pH. The highest final CDW concentrations were observed with pH 5.5 (0.72 g L^{-1}) and 5.0 (0.73 g L^{-1}). Analogous to the specific growth rates, the CO uptake rates were very similar, ranging from a maximal rate of 15.34 ± 0.58 mmol L^{-1} h^{-1} with pH 5.0 and the lowest maximal rate of 14.15 ± 0.66 mmol L^{-1} h^{-1} with pH 5.5. After peaking between the 30th and 40th process hour, the CO uptake rates sharply decreased in all processes. CO uptake rates at the process end also varied with pH, being the highest with pH 5.5 (2.83 ± 0.66 mmol L^{-1} h^{-1}) and lowest with uncontrolled pH (0.50 ± 0.10 mmol L^{-1} h^{-1}).

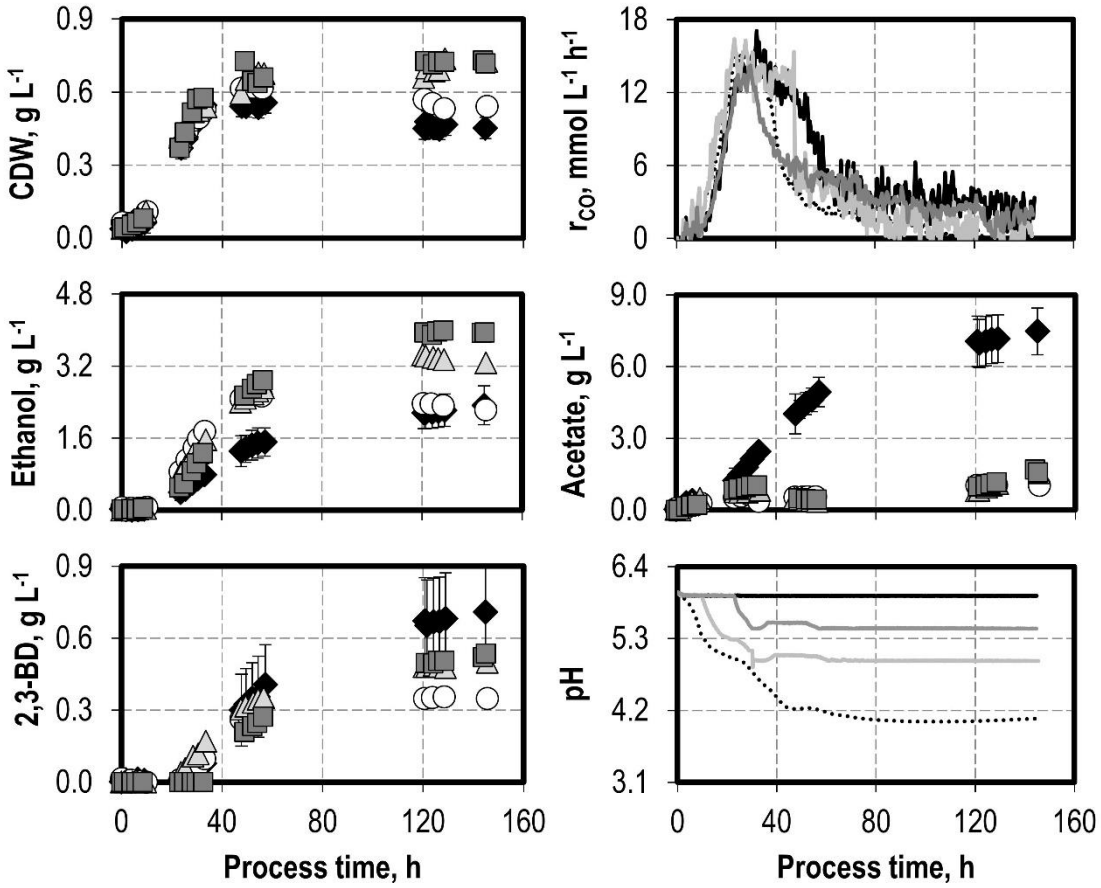

Figure 30 – Cell dry weight (CDW) concentration, CO uptake rate (r_{CO}), ethanol, acetate and 2,3-butanediol concentrations, and pH of the syngas fermentation with *C. ragsdalei* at final pH 6.0 (black diamonds, black lines), pH 5.5 (dark grey squares, dark grey lines), pH 5.0 (light grey triangles, light grey lines) and pH uncontrolled (white circles, dotted lines). Batch processes were conducted with initial pH 6.0, at 37 °C, working volume of 1 L, volumetric power input of 3.5 W L^{-1} (800 rpm), gas flow of 5.0 NL h^{-1} with 3:1:1 ($CO:H_2:CO_2$) and pressure of 1 bar.

Acetate formation decreased strongly in all processes with pH lower than pH 6.0, varying however little in between the lower levels. Ethanol formation, in turn, was substantially increased at lower pH. Until the 55-57th process hour, ethanol formation in all process with lower pH were clearly higher than the 1.51 g L^{-1} with pH 6.0. After this, the ethanol concentration with uncontrolled pH declined. The highest concentration of 3.95 g L^{-1} ethanol was achieved with pH 5.5. 2,3-butanediol showed a clear inverse relationship to pH, with the highest concentration seen with pH 6.0 and the lowest with uncontrolled pH. A summary of these key results is shown in Table 10.

Table 10 – Final cell dry weight (CDW) concentration, specific growth rate at the exponential growth phase and acetate, ethanol and 2,3-butanediol concentrations, and maximal CO uptake rates (centered moving average with five values) in the batch processes with *C. ragsdalei* with different pH profiles depicted in Figure 30. Errors in the concentrations correspond to the standard deviation of replicates.

pH	6.0	5.5	5.0	Uncontrolled
CDW, g L^{-1}	0.45 ± 0.03	0.72	0.73	0.54
Specific growth rate, h^{-1}	0.10 ± 0.006[1]	0.098 ± 0.002[1]	0.097 ± 0.002[1]	0.094 ± 0.001[1]
Acetate, g L^{-1}	7.48 ± 0.98	1.57	1.56	1.04
Ethanol, g L^{-1}	2.33 ± 0.43	3.95	3.27	2.23
2,3-butanediol, g L^{-1}	0.71 ± 0.18	0.54	0.50	0.35
$r_{CO,\,max}$, mmol L^{-1} h^{-1}	15.3 ± 1.35[2]	14.15 ± 0.66[2]	15.34 ± 0.58[2]	14.91 ± 0.34[2]

[1]Errors represent the standard error of the linear regression to obtain the specific growth rate.
[2]Values represent the mean of the five uptake rates around the maximum value, and error represent their standard deviation.

Discussion

In this section, the effects of lowering the process pH or temperature on the outcomes of the syngas fermentation and, most of all, on alcohol formation were assessed with *C. ragsdalei*. The results presented here are important since they compare several pH levels and temperatures in a more relevant setup: a continuously gassed stirred-tank reactor. Overall, both strategies had a positive effect, above all on ethanol formation.

The temperature effect on alcohol formation in the syngas fermentation has been only sparsely published. Ramió-Pujol et al. (2015) and Shen et al. (2017) published a positive influence of a temperature decrease from 37 °C to 25 °C in the syngas fermentation with *C. carboxidivorans* in anaerobic flasks. Kundiyana et al. (2011) also reported an improvement in ethanol production at 32 °C rather than 37 °C with *C. ragsdalei*, however, due to experiment design, the positive effect of the lower temperature cannot be separated from the removal of buffer, so that a causality cannot be established. In fact, the highest ethanol concentrations reported by Kundiyana et al. (2011) were obtained at initial pH 6.0, 32 °C and absence of buffer and pH 7.0, 37 °C and absence of buffer, which are more an indication of the positive effect of not buffering that of the lower temperature. Shen et al. (2020) took a closer look at the improvements seen with the lower temperature with *C. carboxidivorans* by Shen et al. (2017) and conducted a transcriptome analysis of processes with *C. carboxidivorans* at 37 °C and 25 °C. It was observed that the gene expression of enzymes in the WLP and ethanol formation were not upregulated at lower temperatures, despite the higher alcohol

concentrations. Rather, they observed enriched pathways in carbohydrate and amino acid metabolism, with the most enriched pathway being cysteine and methionine metabolism.

To the results presented here, lowering the temperature to 32 °C had clear benefits in the biomass formation: the specific growth rate did not decrease from 37 °C, the maximal achieved CDW concentration could be maintained throughout the process. This was reflected in CO uptake rates that could be sustained higher for longer, which had implications in overall product formation. To further compare the processes, it is worth dividing the processes in two phases: a first phase of increasing activity, measured by increasing CO uptakes rates, and a second phase of decreasing activity, determined by decreasing CO uptake rates. For each phase, the integral production rate was calculated for CDW, acetate, ethanol and 2,3-butanediol, which is shown in Table 11.

The temperature of 32 °C showed a clear outperformance regarding alcohol production, achieving the highest integral production rates in both phases for both alcohols. More importantly, this process managed to keep the productivity of both ethanol and 2,3-butanediol in both phases, even though the productivity of CDW and acetate formation decreased strongly in the second phase. The decrease in the CDW production was roughly 90%, so product formation served for ATP and redox maintenance. Interestingly, there was a slight increase in the alcohol production rates in this second phase (8.8% for ethanol and 16.3% for 2,3-butanediol). As acetate yields more ATP from CO (see discussion in section 5), the lower acetate production coupled with the higher CO uptake rates at 32 °C and absence of biomass formation enabled the cells to produce comparatively more alcohol in the second than in the first phase.

Table 11 – Production rates of cell dry weight (CDW), acetate, ethanol and 2,3-butanediol for the phases of increasing CO uptake rates (r_{CO}) and decreasing rates of the batch processes with different temperatures with *C. ragsdalei,* shown in Figure 29.

		Integral production rate, g L^{-1} d^{-1}			
	Temperature, °C	CDW	Acetate	Ethanol	2,3-Butanediol
Before $r_{CO, max}$	37	<u>0.402</u>	<u>1.679</u>	0.552	0.040
	32	0.330	1.353	<u>1.017</u>	<u>0.246</u>
	27	0.261	0.825	0.409	0.076
After $r_{CO, max}$	37	-0.012	<u>1.122</u>	0.341	0.138
	32	0.032	0.878	<u>1.106</u>	<u>0.286</u>
	27	<u>0.045</u>	1.052	0.548	0.248

By further decreasing the temperature to 27 °C, overall process performance decreased. CDW, acetate and ethanol productivities decreased in the first phase, comparing to the process at 37 °C. In the second phase, however, acetate formation slightly decreased but the productivity of alcohols increased, alongside a small biomass formation.

To better understand the mechanisms which led to the improvement in alcohol production, the product concentrations were plotted against the CDW concentrations during the phase of increasing activity. This is shown in Figure 31. A very strong similarity is seen for both alcohols between temperatures, with the differences being present at higher CDW concentrations. For acetate, in turn, no clear relationship can be established, apart from a greater similarity between the processes at lower temperatures. Thus, a key difference in the improvement in the alcohol production lies in the late stages of the phase of increasing CO uptake rates. Lowering the temperature enabled a prolonging of this phase at a stage of substantially increased alcohol yield. This can be qualitatively visualized in Figure 31 by the asymptotic lines drawn for ethanol and 2,3-butanediol. This indicates that the benefits of the lower temperatures do not lie in metabolic changes during the exponential growth phase, but rather how the cells adapt at the final stages of the phase of increasing activity.

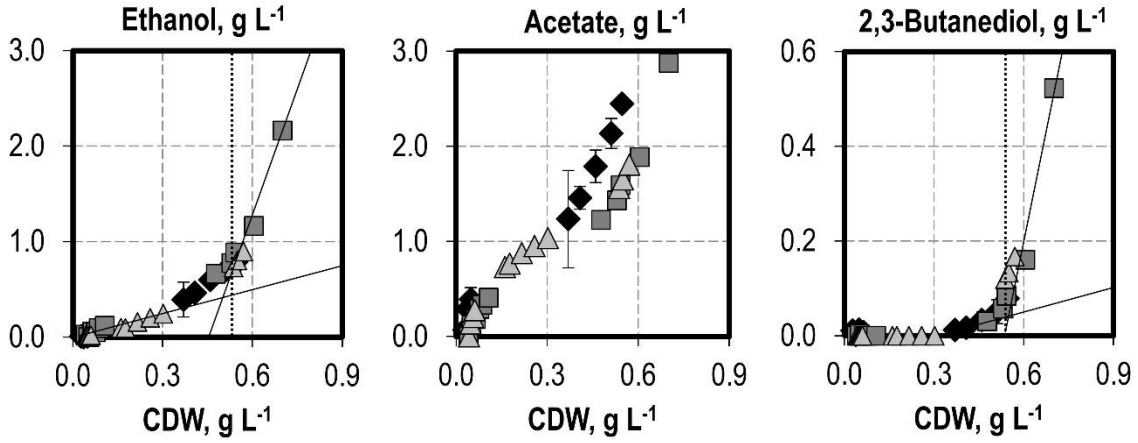

Figure 31 – Product concentration *vs.* the cell dry weight (CDW) for the phase of increasing CO uptake rates with different temperatures with *C. ragsdalei,* shown in Figure 29. Lines were visually drawn to represent asymptotes in the biomass related yield.

Lowering the process pH incurred in changes beyond the broadly reported increase in ethanol production. The CO uptake rates were very similar in all processes; however, with higher pH, the phase length of increasing activity i.e., increasing CO uptake rates, was higher and consequently the overall CO uptake also increased.

Analogue to the discussion on the effect of lower temperatures, the integral production rates of CDW and products for the phase of increasing CO uptake and decreasing CO uptake rates

are shown in Table 12. As the overall activity increased, biomass formation was very similar between all processes, with an average productivity of 0.437 ± 0.025 g L^{-1} d^{-1} within the different pH profiles. The acetate and ethanol production rates in this phase showed how intertwined both components are, and how lower pH levels trigger acetate reduction to ethanol. The highest acetate production rate was obtained with pH 6.0 and the lowest with the uncontrolled pH. For ethanol, the trend is the inverse, with the higher pH being detrimental for ethanol formation. This is well in accordance with various published results and confirms the metabolic shift induced by lower pH, which forces the acetate reduction to ethanol by increasing the concentration of undissociated acetic acid (Richter et al., 2016). Considering equation 3.15 and Figure 4, a pH reduction from pH 6.0 to pH 5.5 leads to an increase of 2.8-fold in the fraction of undissociated acetic acid, and a reduction from pH 6.0 to pH 5.0 an increase of 6.73-fold. Applying these ratios to the productivity values, the production rate of undissociated acetic acid increased with lower pH by 36.7% with pH 5.5 and 158% with pH 5.0, reflecting the increase in the ethanol productivities (51.8% for pH 5.5 and 95.1% for pH 5.0). Since the initial pH in all processes was pH 6.0, it was not expected that these increases in the undissociated acetic acid and ethanol productivities would be equal, but they show the trend. 2,3-butanediol production in this first phase was negligible.

In the second process phase, the divergence between processes was higher. pH 6.0 further fomented acetate formation, and pH 5.5 enabled the highest ethanol production. Uncontrolled pH led to a strong sharp decrease in overall activity, with the lowest production rate of all products. 2,3-butanediol showed in this phase a clear relationship to pH: with decreasing pH, the 2,3-butanediol production decreased. This is the first time that this relationship is shown, and it partially contradicts previous assumptions to the triggers of 2,3-butanediol production; indeed, Köpke et al. (2011) hypothesized that 2,3-butanediol production is triggered as an offload of reducing agents and as deacidification from pyruvic acid, since 2,3-butanediol production is derived from pyruvate. The results presented here indicate that the offload of reducing agents is the main driver for 2,3-butanediol production, and that deacidification is prioritized through acetate reduction. Therefore, ethanol and 2,3-butanediol production possibly compete for reducing agents.

Table 12 – Production rates of cell dry weight (CDW), acetate, ethanol and 2,3-butanediol for the phases of increasing CO uptake rates (r_{CO}) and decreasing rates of the batch processes with different pH profiles with *C. ragsdalei,* shown in Figure 30.

		Integral production rate, g L^{-1} d^{-1}			
	pH	CDW	Acetate	Ethanol	2,3-butanediol
Before $r_{CO, max}$	6.0	0.402	<u>1.679</u>	0.552	0.040
	5.5	<u>0.461</u>	0.810	0.838	0.000
	5.0	0.449	0.643	1.077	<u>0.093</u>
	Uncontrolled	0.436	0.594	<u>1.245</u>	0.055
After $r_{CO, max}$	6.0	-0.012	<u>1.122</u>	0.341	<u>0.138</u>
	5.5	0.030	0.119	<u>0.606</u>	0.112
	5.0	<u>0.042</u>	0.166	0.413	0.080
	Uncontrolled	0.012	0.077	0.171	0.058

7.2 Combining Strategies to Increase Alcohol Production

Individually lowering the process temperature to 32 °C and lowering the pH to pH 5.5 showed clear benefits to the process performance. These conditions overcame the decrease in CDW concentration observed in the later phases of the process and increased the alcohol to acetate ratio. More concretely, a lower temperature enabled a more than twofold increase in the final ethanol concentration, while with pH 5.5 the ethanol to acetate ratio increased eightfold. Separately, it was shown that a sulfide feed of 0.05 mmol S L^{-1} h^{-1} increased biomass and alcohol formation, whereby the maximal CO uptake rate and the alcohol to acetate ratio also increased. Therefore, combining these strategies might allow for synergetic effects, and further improve process performance. In this section, results to the combination of these strategies will be presented. The process conditions applied were:

- temperature of 32 °C and pH 5.5,
- 0.05 mmol S L^{-1} h^{-1} sulfide feed and pH 5.5,
- 0.05 mmol S L^{-1} h^{-1} sulfide feed and temperature of 32 °C.

Sulfide was added as Na_2S from a 20 g L^{-1} $Na_2S{\cdot}H_2O$ solution.

The CDW and product concentrations, as well as the CO uptake rates of the process with pH 5.5 and temperature of 32 °C are presented in Figure 32. For visual comparison, the processes with the temperature of 37 °C and pH 5.5 and pH 6.0, and temperature of 32 °C at pH 6.0 are also presented.

Combining pH 5.5 and a temperature of 32 °C avoided the recurring CDW decrease, which is in line with the processes at pH 5.5 and that with 32 °C. The final CDW concentration decreased in comparison to both batch processes at pH 5.5 or with 32 °C to 0.67 g L^{-1} and the specific growth rate decreased to 0.085 ± 0.002 h^{-1}. Product concentrations were in between both batch processes, with the final ethanol concentration achieving 4.23 g L^{-1}. The maximal CO uptake rate was 15.71 ± 0.37 mmol L^{-1} h^{-1}, achieved at the 33rd process hour, slightly higher than the other two processes. A summary with the key variables of this process and those at pH 5.5 and temperature of 32 °C is shown in Table 13.

Table 13 – Final cell dry weight concentration (CDW), specific growth rate, final concentrations of acetate, ethanol and 2,3-butanediol and maximal CO uptake rate ($r_{CO, max}$) of the syngas fermentation with *C. ragsdalei* at pH 5.5 and temperature of 32 °C, shown in Figure 32.

pH	5.5	5.5	6.0	6.0
Temperature, °C	32	37	32	37
CDW, g L^{-1}	0.67	0.72	0.79	0.45 ± 0.03
Specific growth rate, h^{-1}	0.085 ± 0.002[1]	0.098 ± 0.002[1]	0.094 ± 0.003[1]	0.10 ± 0.006[1]
Acetate, g L^{-1}	4.81	1.57	5.4	7.48 ± 0.98
Ethanol, g L^{-1}	4.23	3.95	5.34	2.33 ± 0.43
2,3-butanediol, g L^{-1}	0.82	0.54	1.35	0.71 ± 0.18
$r_{CO, max}$, mmol L^{-1} h^{-1}	15.71 ± 0.37[2]	14.15 ± 0.66[2]	15.08 ± 0.23[2]	15.3 ± 1.35[2]

[1]Errors represent the standard error of the linear regression to obtain the specific growth rate.
[2]Values represent the mean of the five uptake rates around the maximum value, and error represent their standard deviation.

The sulfide feed of 0.05 mmol S L^{-1} h^{-1} was combined with pH 5.5, a lower temperature of 32 °C, and both lower pH and temperature simultaneously. The courses of the CDW and product concentrations, and the CO uptake rates are shown in Figure 33. The process with the sulfide feed, pH 6.0 and temperature of 37 °C was added as comparison.

Lowering the pH to 5.5 with the sulfide feed led to strong decreases in the CDW concentration and CO uptake rates. It could also not avoid a decline in the CDW concentration once the peak of 0.58 g L^{-1} was achieved at the 52nd process hour. This decline was however to a lesser extent than with a pH of 6.0. The CO uptake ceased around the 105th process hour, after which no net acetate or 2,3-butanediol was built and the ethanol concentration slightly decreased. Acetate formation was kept low, while ethanol and 2,3-butanediol concentrations decreased in comparison to the process with a sulfide feed with pH 6.0 at 37 °C.

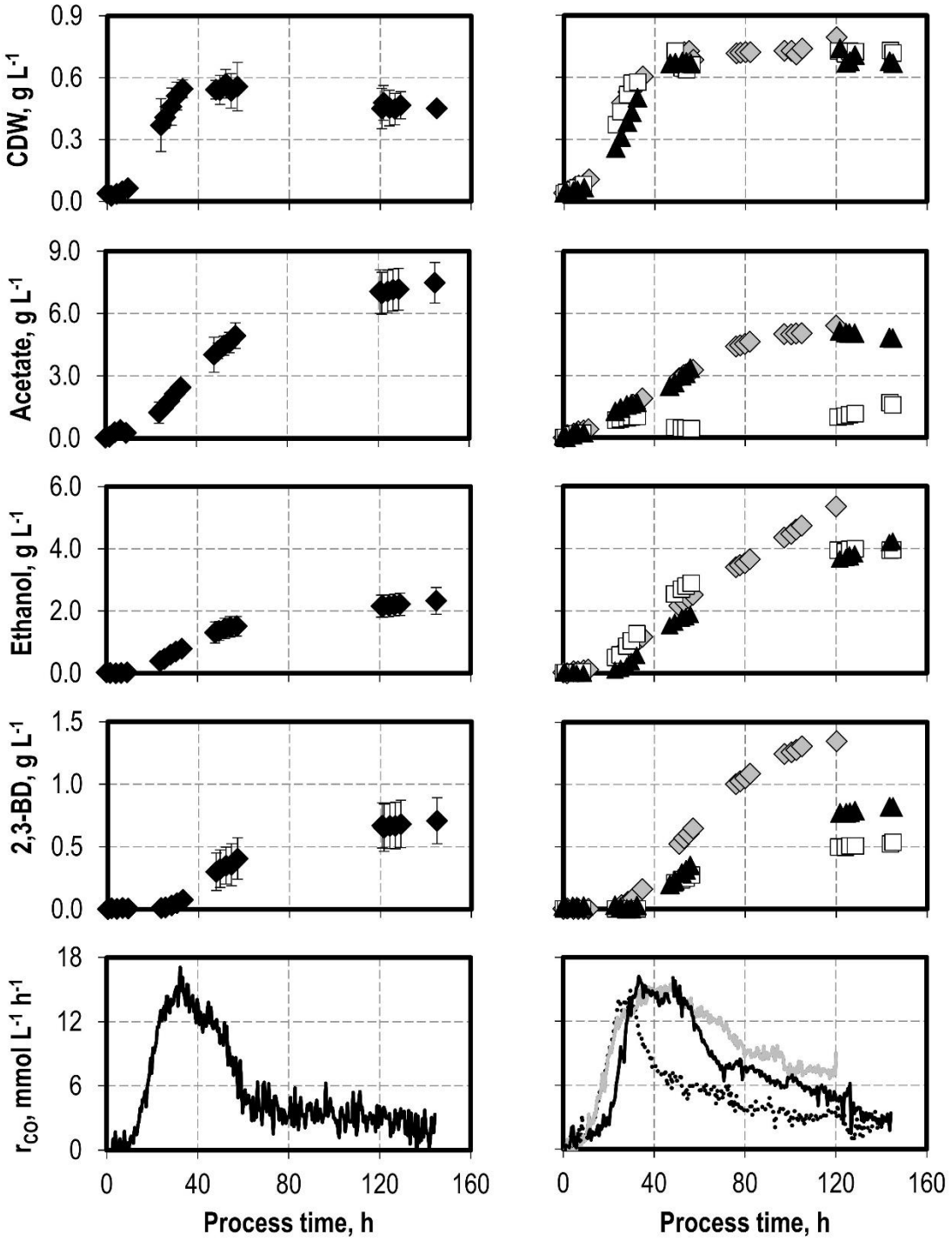

Figure 32 – Cell dry weight (CDW), acetate, ethanol and 2,3-butanediol (2,3-BD) concentrations and CO uptake rates (r_{CO}) of the syngas fermentation with *C. ragsdalei*. Process conditions were: **left**, pH 6.0 and 37 °C (black diamonds, black lines); **right**, pH 5.5 (white squares, dotted black line), 32 °C (grey diamonds, grey line) and combined pH 5.5 and 32 °C (black triangles, black line). Other general process conditions were: working volume of 1 L, volumetric power input of 3.5 W L^{-1} (800 rpm), gas flow of 5.0 NL h^{-1} with 3:1:1 ($CO:H_2:CO_2$) and pressure of 1 bar.

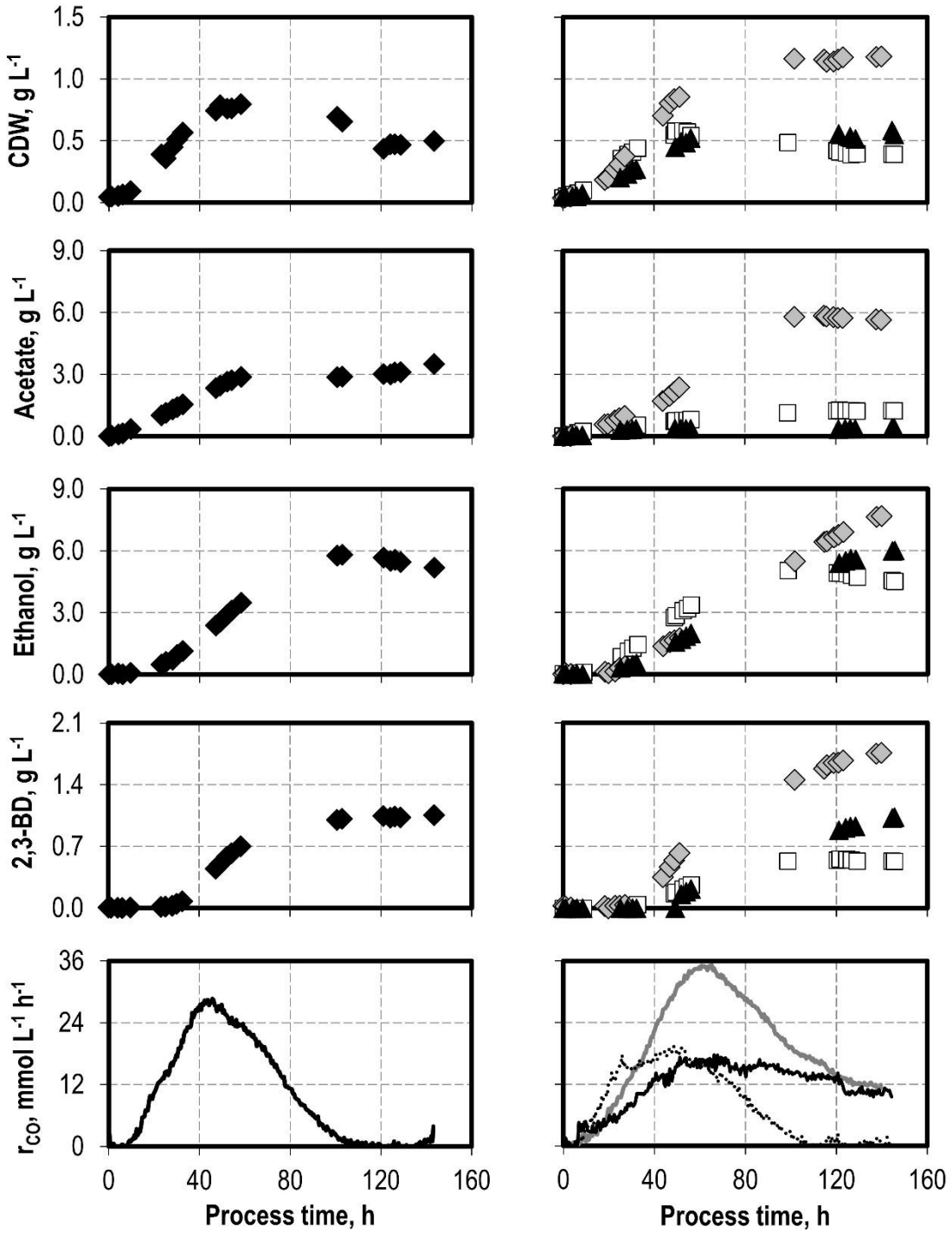

Figure 33 – Cell dry weight (CDW), acetate, ethanol and 2,3-butanediol (2,3-BD) concentrations and CO uptake rates (r_{CO}) of the syngas fermentation with *C. ragsdalei* with a sulfide feed of 0.05 mmol L^{-1} h^{-1}. Process conditions were: **left**, pH 6.0 and 37 °C (black diamonds, black lines); **right**, pH 5.5 (white squares, dotted black line), 32 °C (grey diamonds, grey line) and combined pH 5.5 and 32 °C (black triangles, black line). Other general process conditions were: working volume of 1 L, volumetric power input of 3.5 W L^{-1} (800 rpm), gas flow of 5.0 NL h^{-1} with 3:1:1 ($CO:H_2:CO_2$) and pressure of 1 bar.

Decreasing the temperature to 32 °C with the sulfide feed led to a substantial increase in all relevant absolute values. While the specific growth rate remained roughly unchanged at 0.085

± 0.001 h^{-1}, the maximal and final CDW concentration was increased to 1.18 g L^{-1} and the maximal CO uptake rate increased to 34.9 ± 0.14 mmol L^{-1} h^{-1}, which represent increases of 47.5% and 25 %, respectively, from the maximal values achieved at a higher temperature. The final concentration of all products increased, with prominence to the final ethanol and 2,3-butanediol concentrations of 7.67 g L^{-1}, and 1.76 g L^{-1}, respectively. The alcohol to acetate ratio, however, decreased by 6% to 1.67 g g^{-1}.

Lowering both pH and temperature to pH 5.5 to 32 °C slowed biomass formation, decreasing the specific growth rate to 0.061 ± 0.003 h^{-1}, but a decrease in the CDW concentration could be avoided. The maximal CO uptake rate was the lowest from the processes with the sulfide feed (16.88 ± 0.67 mmol L^{-1} h^{-1}), but it did not decrease as sharply after peaking, with the CO uptake rates at process end ranging around 10 mmol L^{-1} h^{-1}. Acetate formation was substantially reduced, with the highest concentration throughout the process being 0.40 g L^{-1}, the lowest in all processes presented in this subsection. Alcohol formation slightly increased, with the final ethanol concentration increasing to 6.0 g L^{-1} and the 2,3-butanediol concentration being roughly unchanged (1.03 g L^{-1}). A summary of the key results of the processes combining the sulfide feed with changes in process parameters is shown in Table 14.

Table 14 – Final cell dry weight concentration (CDW), specific growth rate, final concentrations of acetate, ethanol and 2,3-butanediol and maximal CO uptake rate ($r_{CO, max}$) of the syngas fermentation with *C. ragsdalei* with a sulfide feed of 0.05 mmol S L^{-1} h^{-1} and different process conditions, depicted in Figure 33.

Sulfide feed rate of 0.05 mmol L^{-1} h^{-1}				
pH	5.5	5.5	6.0	6.0
Temperature, °C	32	37	32	37
CDW, g L^{-1}	0.55	0.39	1.18	0.50
Specific growth rate, h^{-1}	0.061 ± 0.003[1]	0.081 ± 0.002[1]	0.085 ± 0.001[1]	0.087 ± 0.004[1]
Acetate, g L^{-1}	0.40	1.23	5.64	3.50
Ethanol, g L^{-1}	6.00	4.49	7.67	5.18
2,3-butanediol, g L^{-1}	1.03	0.53	1.76	1.05
$r_{CO, max}$, mmol L^{-1} h^{-1}	16.88 ± 0.67[2]	18.94 ± 0.46[2]	34.9 ± 0.14[2]	28.03 ± 0.50[2]

[1]Errors represent the standard error of the linear regression to obtain the specific growth rate.
[2]Values represent the mean of the five uptake rates around the maximum value, and error represent their standard deviation.

Discussion

It was shown in section 6 how the sulfide feed of 0.05 mmol L^{-1} h^{-1} can improve CDW and alcohol formation, and similarly in subsection 7.1 with the individual lowering of the process pH to pH 5.5 and the temperature to 32 °C. Each strategy had its idiosyncratic effects. The sulfide feed increased CO uptake rates and the formation of both alcohols, but it could not avoid a decrease in the CDW concentration as the CO uptake rates decreased. Lowering the temperature to 32 °C did not increase the maximal CO uptake rate, but curbed its strong decrease after peaking, enabling cell activity for longer, while also fomenting a higher production of both alcohols. With a pH 5.5, the decrease in CDW was avoided as well and the maximal CO uptake rate was unchanged with an increase in the formation of ethanol, but overall CO uptake decreased, as well as 2,3-butanediol production was negatively impacted. These key changes in the overall process performance can be qualitatively seen in Table 15, which highlights the complementarity of each strategy. In this section, these strategies were combined, to assess whether beneficial effects could be added, while negative effects could be curbed.

Table 15 – Qualitative assessment of changes in the key performance parameters of the syngas fermentation, using the individual strategies of decreasing process pH, temperature or implementing a sulfide feed. Increases are depicted by the "**+**" symbol, decreases by the "**-**" symbol, and similar values by the "**≈**" symbol.

pH	5.5	6.0	6.0
Temperature, °C	37	32	37
S. feed, mmol L^{-1} h^{-1}	0	0	0.05
Increase in $r_{CO,\ max}$	**≈**	**≈**	**++**
Increase in overall CO uptake	-	**+**	**+**
Ethanol formation	+	**++**	**++**
2,3-butanediol formation	-	**++**	+
Alcohol to acetate ratio	**+++**	+	++

By Table 15, lowering simultaneously the pH and temperature to pH 5.5 and 32 °C should have no impact in the maximal CO uptake rate and support ethanol formation with a high alcohol to acetate ratio, while the effect on the overall CO uptake and 2,3-butanediol would be unclear. In practice, the maximal CO uptake remained roughly unchanged and the overall CO uptake remained in the range between both processes, corroborating with the qualitative analysis. The final concentration of ethanol was closer to that of the process at pH 5.5,

whereas acetate production was very similar to the process with the lower temperature. 2,3-butanediol formation lied in between both processes with individual changes. In fact, combining the lower pH and temperature led to a decrease in the alcohol to acetate ratio to 1.05 g g^{-1}, in comparison to 2.86 g g^{-1} at pH 5.5 and 1.24 g g^{-1} with 32 °C.

Taking a closer look at ethanol production, Figure 34 shows the ethanol concentration of the processes with pH 5.5, with temperature of 32 °C and with both parameters combined and the ethanol production rates. To obtain the production rates, the data were fitted with a nonlinear regression according to equation 4.3 for the process with pH 5.5 and according to equation 4.4 for the other two processes. The highest rate was achieved with lowering both pH and temperature to pH 5.5 and 32 °C, with a maximal rate of 2.26 g L^{-1} d^{-1}. The combination of a lower temperature and pH led to a lagged initiation of the ethanol formation, while the interval of high production rates was very reduced. For most of the process, however, the ethanol production rate was constant, but this value was lower when both pH 5.5 and temperature of 32 °C were combined than only with the lowering of the temperature, being the constant ethanol production rates 0.69 g L^{-1} d^{-1}, and 1.07 g L^{-1} d^{-1} respectively. Thus, regarding the ethanol production rates, combining the lower pH and temperature led to a worsening of the individual benefits: the higher rate of the lower pH was kept for a lower period, while the constant rate of the lower temperature decreased by 35.3 %.

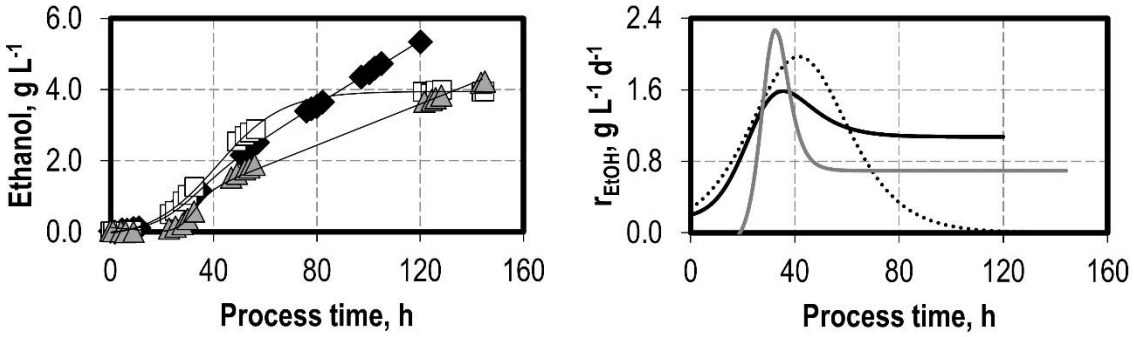

Figure 34 – Ethanol concentration, nonlinear regression of the ethanol concentration (left, black lines) and ethanol production rates (r_{EtOH}, right) of the processes with *C. ragsdalei* with pH 5.5 (white squares, dashed line), temperature of 32 °C (black diamonds, black line) and both pH 5.5 and temperature of 32 °C (grey triangles, grey line), depicted in Figure 32. Residual sum of squares of the nonlinear regressions are given in Table 23.

While ethanol production was impacted negatively by lowering both pH and temperature, 2,3-butanediol formation was a balanced mixture of both strategies. Furthermore, the process with both lower pH and temperature showed how intertwined 2,3-butanediol and ethanol formation can be. The production rates of both alcohols are shown in Figure 35 for the processes with lower pH, lower temperature and both parameters combined. While the process at 32 °C sustained high rates for both alcohols almost simultaneously, at pH 5.5 in both cases, 2,3-

butanediol production resumes as the ethanol production rate approached its peak. Combining both lower pH and temperature led to a clear distinction of ethanol and 2,3-butanediol production. This reinforces the argument from subsection 7.1, by which the formation of ethanol and 2,3-butanediol compete for reducing agents once the lower pH foment ethanol formation, if an increase in the CO uptake rates does not occur to supply sufficient reducing agents for both processes.

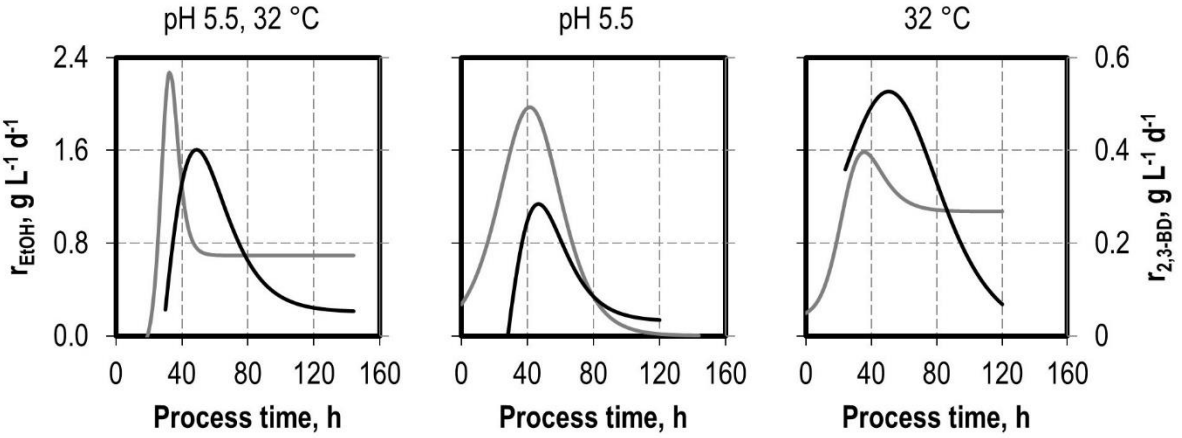

Figure 35 – Production rates of ethanol (r_{EtOH}, black lines) and 2,3-butanediol ($r_{2,3\text{-}BD}$, grey lines) of the processes with *C. ragsdalei* depicted in Figure 32 with pH 5.5, temperature of 32 °C and both pH and temperature at pH 5.5 and 32 °C. Residual sum of squares of the nonlinear regressions are given in Table 23.

Both temperature and pH were individually and simultaneously combined with a sulfide feed of 0.05 mmol S L^{-1} h^{-1}. By Table 15, the sulfide feed and lower pH had complementary effects, most evident on the extent of CO uptake, while the lower temperature and the sulfide feed impacted the process similarly.

In practice, coupling the sulfide feed with the lower pH led to mixed results. Lowering the pH with the sulfide reduced the extent to which the CDW concentration decreased after peaking, and the alcohol to acetate ratio increased to 4.08 g g^{-1}, in comparison to 2.86 g g^{-1} at pH 5.5 and 1.78 g g^{-1} only with the sulfide feed. In turn, the maximal CDW achieved was lower than in the process with the sulfide feed at pH 6.0, as well as the final concentrations of both alcohols. Furthermore, the sulfide feed had no effect in the final 2,3-butanediol concentration in relation to the process with lower pH, thus not being able to counter the negative effects of a lower pH, as did the lower temperature. The processes with a sulfide feed and both pH levels shared the similarity of a complete halt in the CO uptake around the 100th process hour. These halts were not associated with the CDW decrease but occurred rather after the CDW stabilized already at a lower level. Once the CO uptake stopped, the concentrations of CDW, acetate and 2,3-butanediol stabilized, while that of ethanol decreased. Pinpointing the reason for the

decline in the ethanol concentration is not possible with the available data, but it is most likely due to the evaporation of ethanol. Another possible reason, even though it is not supported by the data, is that ethanol was reassimilated. Indeed, Liu et al. (2020) showed that *C. ljungdahlii* produced acetate from the reassimilation of ethanol. They argued that the pathway for ethanol oxidation was through the aldehyde:ferredoxin oxidoreductase (AOR) based on the ratios of $NADH/NAD^+$ and $NADPH/NADP^+$. In this case, however, it would have been expected that in the processes presented here, as the ethanol concentration decreased, the acetate concentration would increase, which was not observed.

Looking more closely into the alcohol production in this process, Figure 36 contains the production rates of ethanol and 2,3-butanediol for the processes with pH 6.0 and pH 5.5 with and without a sulfide feed and temperature of 37 °C. For the process without the sulfide feed, the ethanol nonlinear regression was only conducted until the 66th hour since both used equations could not properly described the whole process. After the 66th hour, a linear correlation was stablished, resulting in a constant production rate.

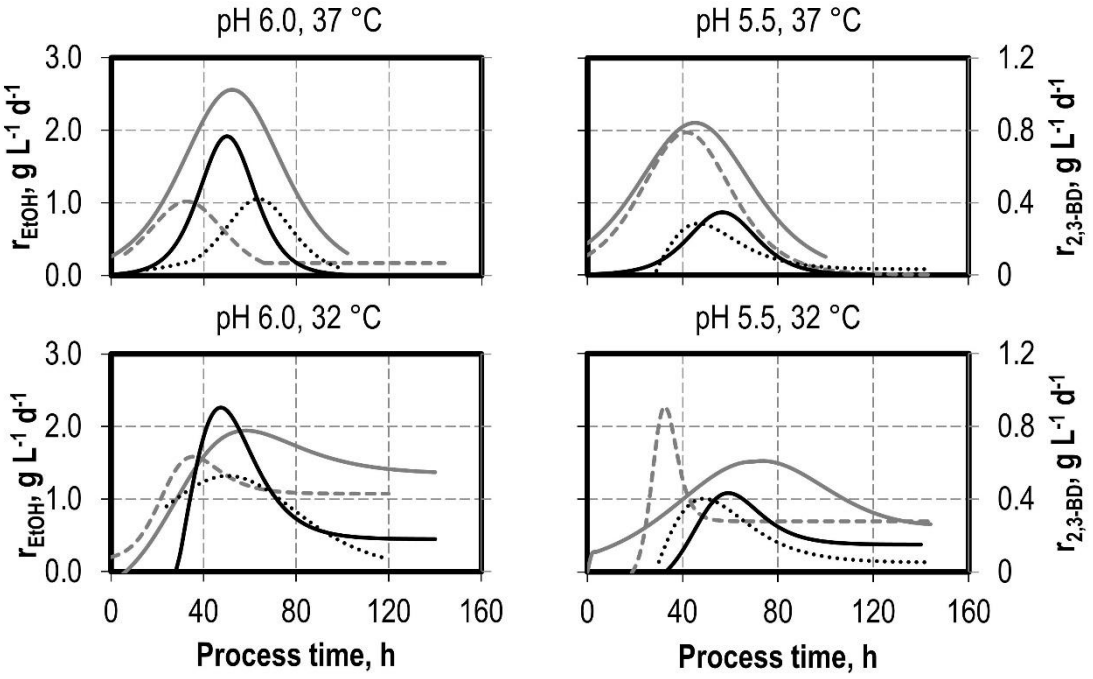

Figure 36 – Ethanol and 2,3-butanediol production rates (Ethanol: r_{EtOH}, black lines and black dotted lines; 2,3-butanediol: $r_{2,3-BD}$, grey lines and grey dashed lines) of processes with *C. ragsdalei* without and with a sulfide feed and different pH and temperature levels. The process data were shown in Figure 32 and Figure 33. Specific aspects of the nonlinear regressions are discussed in the text. The residual sum of squares of the nonlinear regressions are given in Table 23.

The production rates show that the sulfide feed had a more pronounced effect in the process with pH 6.0 than with pH 5.5. At pH 6.0, the sulfide feed increased both maximal rates strongly

and caused that the peaks were almost simultaneous, with the production rate of ethanol peaking at the 54 h and that of 2,3-butanediol at the 52 h, both peaking shortly after the CO uptake rate peaked at 46 h. At pH 5.5, the sulfide feed had little effect in the productions rate, slightly increasing the maximal rates and slightly broadening the productive time.

To further look for clues to the effect of sulfide at a lower pH, the concentrations of the products against the CDW concentrations for the processes at pH 5.5 with and without the sulfide feed are shown in Figure 37 for the process interval in which the CO uptake rate increased. Differently than the information from the production rates, it can be clearly seen that the sulfide feed fundamentally changed the product spectrum in the phase of increasing activity. Acetate formation relative to biomass decreased, while ethanol and 2,3-butanediol formation increased. Moreover, the increase in the alcohol formation surpassed the decrease in acetate production, which given the stoichiometries of acetate and alcohol formation (equations 3.2, 3.8 and 3.10) and that ethanol is formed from the reduction of acetate (equation 3.15) indicate a higher CO uptake and uptake rate. In fact, the maximal CO uptake increased from 14.05 ± 0.66 mmol L^{-1} h^{-1} to 18.94 ± 0.46 mmol L^{-1} h^{-1}, while the phase length in which the CO uptake rate went from 30 h to 48.8 h.

These improvements are also nuanced since the specific growth rate decreased from 0.098 ± 0.002 h^{-1} to 0.081 ± 0.002 h^{-1} with the implementation of the sulfide feed at pH 5.5. Furthermore, the CO uptake rate peaked without the sulfide prior to the peak in the CDW concentration, while with the sulfide both peaked roughly simultaneously. Nevertheless, the sulfide feed enabled higher CO uptake and higher alcohol to acetate ratios in the phase of increasing CO uptake rate, despite the lower specific growth rates and maximal CDW concentration. The higher CO uptake rate at lower CDW concentration indicates that a higher activity or abundance of the carbon monoxide dehydrogenase (CODH) with the sulfide feed, but the results available are not sufficient for a definite conclusion.

Finally, it appears that the sulfide feed at pH 5.5 changed the process in the following manner: it increased the CO uptake, which increased the availability, initially, of reduced ferredoxin. As less biomass was formed, and consequently less ATP was consumed in anabolism, ferredoxin was directed to ethanol formation. Furthermore, by overcoming the sulfur limitation and enabling higher CO uptake rates for longer, a higher overall CO uptake occurred, directed to ethanol formation due to the ferredoxin availability.

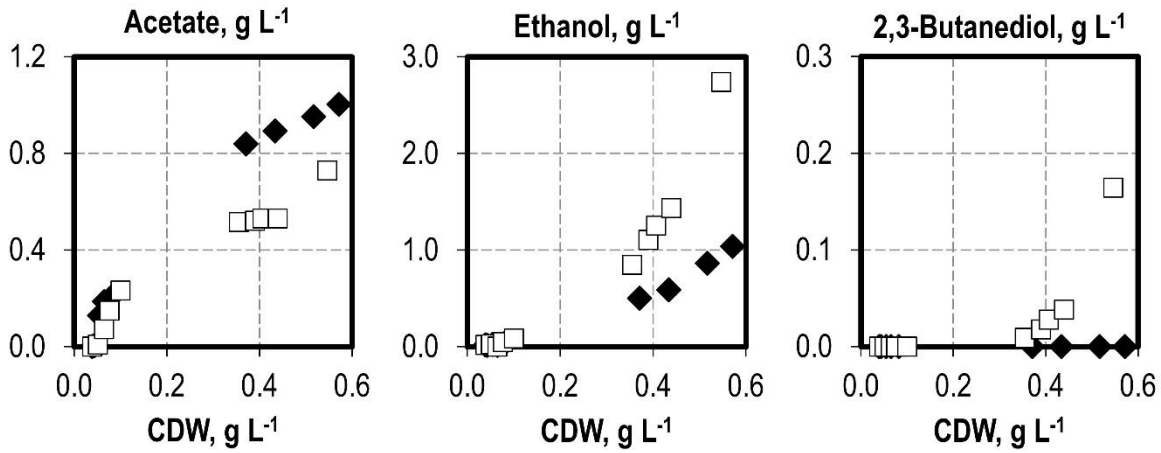

Figure 37 – Product concentration *vs.* the cell dry weight (CDW) for the phase of increasing CO uptake rates with *C. ragsdalei* from processes with pH 5.5 without (black diamonds) and with (white squares) a 0.05 mmol S L^{-1} h^{-1} sulfide feed. These processes were depicted in Figure 32 and Figure 33.

The alcohol production with the sulfide at a temperature of 32 °C was strongly fomented, as shown in Figure 36 by the production rates of ethanol and 2,3-butanediol for the processes with and without the sulfide feed. The higher maximal ethanol production rate with the sulfide feed occurred later in the process, as with all processes with the sulfide feed in comparison to those without it. The sulfide feed enabled both an increase in the maximal ethanol and 2,3-butanediol production rates of 22% and 71 %, respectively, as well as increased the constant production rates in the last section of the process by 27.5% for ethanol and 117% for 2,3-butanediol.

During the phase of increasing activity (increasing CO uptake rate), the profile of product formation relative to the CDW concentration was similar for both processes at 32 °C without and with the sulfide feed, as shown in Figure 38. To account for a value of CDW, acetate, ethanol and 2,3-butanediol at the 62th process hour (peak in the CO uptake rate) of the process with the sulfide feed, the concentrations were estimated by nonlinear regression. The residual sum of squares of these nonlinear regressions are given in Table 23. The profiles of the curves show little difference until the CDW of 0.6 g L^{-1}, indicating at first no metabolic change from the sulfide feed. From that process time, both processes diverged strongly. Without the sulfide feed, the CO uptake rate stabilized until the 50th hour and during this phase the product yield relative to biomass of all products increased, mostly due to a very low increase in CDW formation. With the sulfide feed, CDW formation continued, supported by a further increase in the CO uptake rate until the 62th process hour. In this process, the phase between the CDW of 0.6 g L^{-1}, estimated by the nonlinear regression to have been at the 39th process hour, and

the peak of the CO uptake rate comprised both maxima in the ethanol and 2,3-butanediol production rates, as shown in Figure 36.

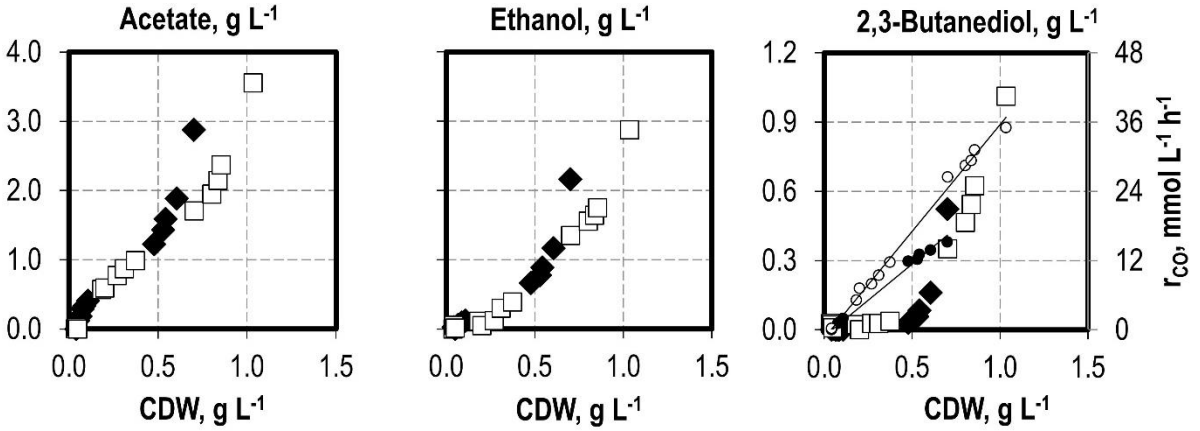

Figure 38 – Product concentration and CO uptake rates (r_{CO}) *vs.* the cell dry weight (CDW) for the phase of increasing CO uptake rates with *C. ragsdalei* from processes with 32 °C without (Products: black diamonds, CO uptake rate: black circles) and with (Product: white squares, CO uptake rate: white circles) a 0.05 mmol S L^{-1} h^{-1} sulfide feed. These processes were depicted in Figure 32 and Figure 33. The lines for the CO uptake rates serve as visual aid and do not represent linear regressions.

Thus, it appears that no metabolic shift occurred within the phase of increasing CO uptake rate, due to the similar relationship of product and biomass formation. At the later stages of this phase, the biomass related yield increased without sulfide, due to a slowing in biomass formation. The main difference appears on the side of CO uptake, which occurred at higher rates with the sulfide feed relative to biomass, again suggesting an increased activity of the CODH. Considering the whole process length, the alcohol to acetate ratio was increased from 1.24 g g^{-1} to 1.67 g g^{-1} with the sulfide feed at 32 °C, with the increase driven by a higher production of both alcohols, while the final acetate concentrations remained very similar (5.4 g L^{-1} and 5.64 g L^{-1}, without and with the sulfide feed).

Revisiting Table 15, it can be concluded that combining the lower temperature and the sulfide feed led to an addition of the individual benefits, curbing the disadvantages of the individual processes.

- The alcohol to acetate remained in similar values to the process with sulfide feed at 37 °C (1.78 g g^{-1}), which is higher than without it at 32 °C (1.24 g g^{-1}).
- No decrease in the CDW concentration occurred, as was observed with the sulfide feed at 37 °C.
- CO uptake rates were increased, further than only with the sulfide feed.
- More products and biomass were built in comparison to both processes.

Combining the pH 5.5 and temperature 32 °C without a sulfide feed led to the higher acetate production of the lower temperature and the lower ethanol production of the lower pH. Upon implementation of the sulfide feed, the process was substantially changed. Most remarkably, it increased the alcohol to acetate ratio to 17.57 g g^{-1} from 1.05 g g^{-1} with pH 5.5 and 32 °C. This was achieved by an increase in both the final ethanol as well as 2,3-butanediol concentrations, while the acetate concentration was kept to a minimum.

Looking closer into the alcohol production, Figure 36 shows the production rates of both alcohols for the processes with pH 5.5 and 32 °C with and without a sulfide feed. Without a sulfide feed, the maximal ethanol production rate was 2.26 g L^{-1} d^{-1}, and this rapidly decreased to a stable value of 0.70 g L^{-1} d^{-1}. In turn, with the sulfide feed the maximal ethanol production rate decreased to 1.53 g L^{-1} d^{-1} but remained higher over most of the process. Regarding 2,3-butanediol, the profile of the production rates was very similar, but the sulfide feed enabled a stabilization of the rate at roughly 0.15 g L^{-1} d^{-1}, while the absence of the sulfide feed led to a value of roughly 0.05 g L^{-1} d^{-1}. Analogous to the process at 32 °C, the sulfide feed inverted the chronological order of the peaks in the ethanol and 2,3-butanediol production rates, indicating that with the sulfide feed reducing agents are more abundant to allow for the non-competitive formation of both alcohols.

Analysing the product formation during the phase of increasing activity in comparison with the process without the sulfide feed, strong changes can be observed for ethanol and acetate, as can be seen in Figure 39. Due to the sulfide feed, acetate was already produced at lower quantities in the early stages of the process, and inversely more ethanol was produced. 2,3-butanediol was clearly produced in both processes once biomass formation was almost stopped, which occurred at a lower CDW with the sulfide feed. These changes in the behaviour of acetate and ethanol formation in the early stages is very distinct from the other analysis done in this work, in which most of the difference occurred at the end stages of the exponential growth phase or the phase with increasing CO uptake rate. This implies that a stronger metabolic shift occurred under the conditions of pH 5.5, temperature 32 °C and the sulfide feed. In fact, as of the CDW concentration of 0.27 g L^{-1} with the sulfide feed, no net acetate was produced until the end of the phase of increasing CO uptake rate, so growth was coupled mainly to ethanol formation.

The CO uptake rate relative to biomass formation was very similar for both processes until the CDW of 0.5 g L^{-1}, so, differently than in the other two cases, it cannot be assumed that the activity or abundance of the carbon monoxide dehydrogenase (CODH) strongly increased with the sulfide feed. Given similar CO uptake rates relative to the CDW, since the sulfide feed led to a slower growth, more CO was consumed to generate the same CDW concentration, so

the resulting reducing agents from CO which could not be employed in biomass formation were redirected to ethanol production.

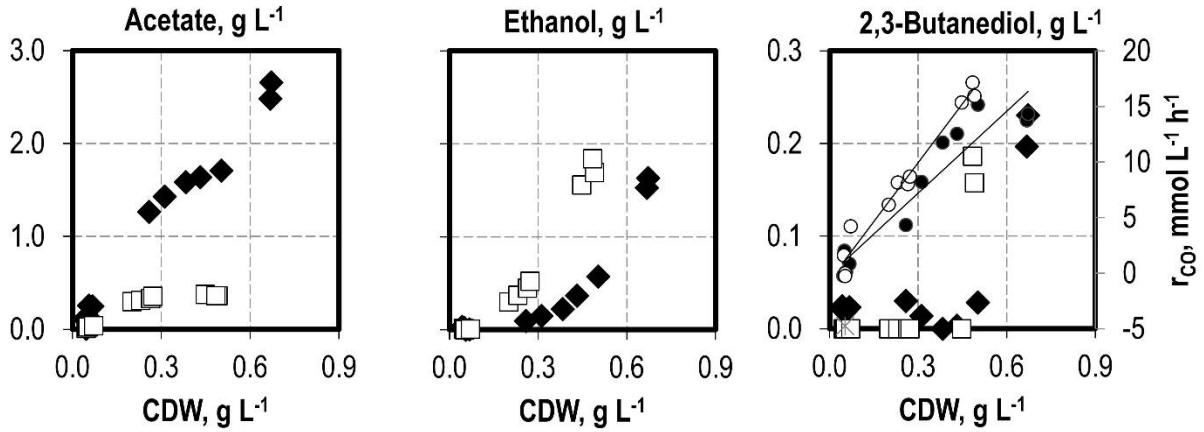

Figure 39 – Product concentration and CO uptake rates (r_{CO}) *vs.* the cell dry weight (CDW) for the phase of increasing CO uptake rates with *C. ragsdalei* from processes with pH 5.5 and 32 °C without (Products: black diamonds, CO uptake rate: black circles) and with (Product: white squares, CO uptake rate: white circles) a 0.05 mmol S L^{-1} h^{-1} sulfide feed. These processes were depicted in Figure 32 and Figure 33. The lines for the CO uptake rates serve as visual aid only.

After the CO uptake rate peaked, the sulfide feed enabled higher CO uptakes rates for longer, and this CO was almost completely converted to alcohol formation. Considering the alcohol to acetate ratio in the process phase starting from the peak in the CO uptake rate until the end of the process, the ratio was 2.68 g g^{-1} at 32 °C (with the concentration of the products at the peak of the CO uptake rate being estimated by the nonlinear regression), 6.56 g g^{-1} with pH 5.5 (calculated only until the CO uptake rate reached null) and 118.41 g g^{-1} with pH 5.5 at 32 °C.

What enabled this almost complete shift to alcohol production cannot be fully answered with the available data, but clues can be obtained from the production rates relative to the CDW concentration, as shown in Table 16. Despite not leading to the highest concentration of CDW and alcohols, the combination of the pH 5.5 and temperature of 32 °C led to the highest ethanol and 2,3-butanediol production rates relative to CDW, both the maximal production rate as well as the final production rate (for the processes which showed a constant production rate). The highest maximal ethanol production rate *per* CDW was 4.12 g g^{-1}_{CDW} d^{-1}, obtained without the sulfide feed and with pH 5.5 and 32 °C, which indicates that these conditions enabled the highest activity in the pathway for ethanol formation. Interestingly, relative to CDW, the 2,3-butanediol production rate was the highest with pH 5.5 and 32 °C and the sulfide feed, indicating that higher concentrations were mainly limited by the low CDW achieved.

Considering the late stages in the processes, there was also a much smaller divergence between the production rates relative to CDW for ethanol than for 2,3-butanediol formation. This indicates that in this stage, the pathway for ethanol production is limited, and higher concentrations could only be achieved if higher CDW were available. In turn, 2,3-butanediol formation was still affected by process conditions, and changes in process parameters could further improve the 2,3-butanediol productivity.

Table 16 – Maximal and final production rates of ethanol (r_{EtOH}) and 2,3-butanediol ($r_{2,3,BD}$) for the processes with *C. ragsdalei* with the presented conditions. Production rates were obtained with nonlinear regression, as described in the text, and the processes were presented in Figure 32 and Figure 33.

pH	5.5	6.0	5.5	5.5
Temperature, °C	37	32	32	32
S. feed, mmol L^{-1} h^{-1}	0.05	0.05	0	0.05
Max. r_{EtOH}, g L^{-1} d^{-1}	2.102	1.943	<u>2.265</u>	1.526
Max. $r_{2,3BD}$, g L^{-1} d^{-1}	0.346	<u>0.903</u>	0.401	0.433
Max. r_{EtOH} per CDW, g g^{-1}_{CDW} d^{-1}	3.845	1.878[1]	<u>4.118</u>	3.152[1]
Max. $r_{2,3BD}$ per CDW, g g^{-1}_{CDW} d^{-1}	0.633	0.872[1]	0.729	<u>0.896</u>[1]
Final r_{EtOH}, g L^{-1} d^{-1}	-	<u>1.370</u>	0.694	0.656
Final $r_{2,3BD}$, g L^{-1} d^{-1}	-	<u>0.180</u>	0.053	0.151
Final r_{EtOH} per CDW, g g^{-1}_{CDW} d^{-1}	-	1.161	1.036	<u>1.193</u>
Final $r_{2,3BD}$ per CDW, g g^{-1}_{CDW} d^{-1}	-	0.153	0.079	<u>0.275</u>

[1]Value of CDW used obtained from the nonlinear regression of the CDW in the processes.

In summary, implementing a sulfide feed of 0.05 mmol S L^{-1} h^{-1} in combination with different pH values and temperatures led to substantial changes in the syngas fermentation with *C. ragsdalei*, as depicted by the key parameters shown in Figure 40 and Figure 41. It led to an increase in the maximal CO uptake rate, the final alcohol concentrations, and the alcohol to acetate ratio in all studied pH levels and temperatures. The maximal production rate of 2,3-butanediol also increased in all conditions with the sulfide, and the maximal production of ethanol was only lower after the implementation of the sulfide feed at pH 5.5 with 32 °C. The final CDW increased in both processes at pH 6.0 and decreased at pH 5.5, while the specific growth rate decreased in all processes.

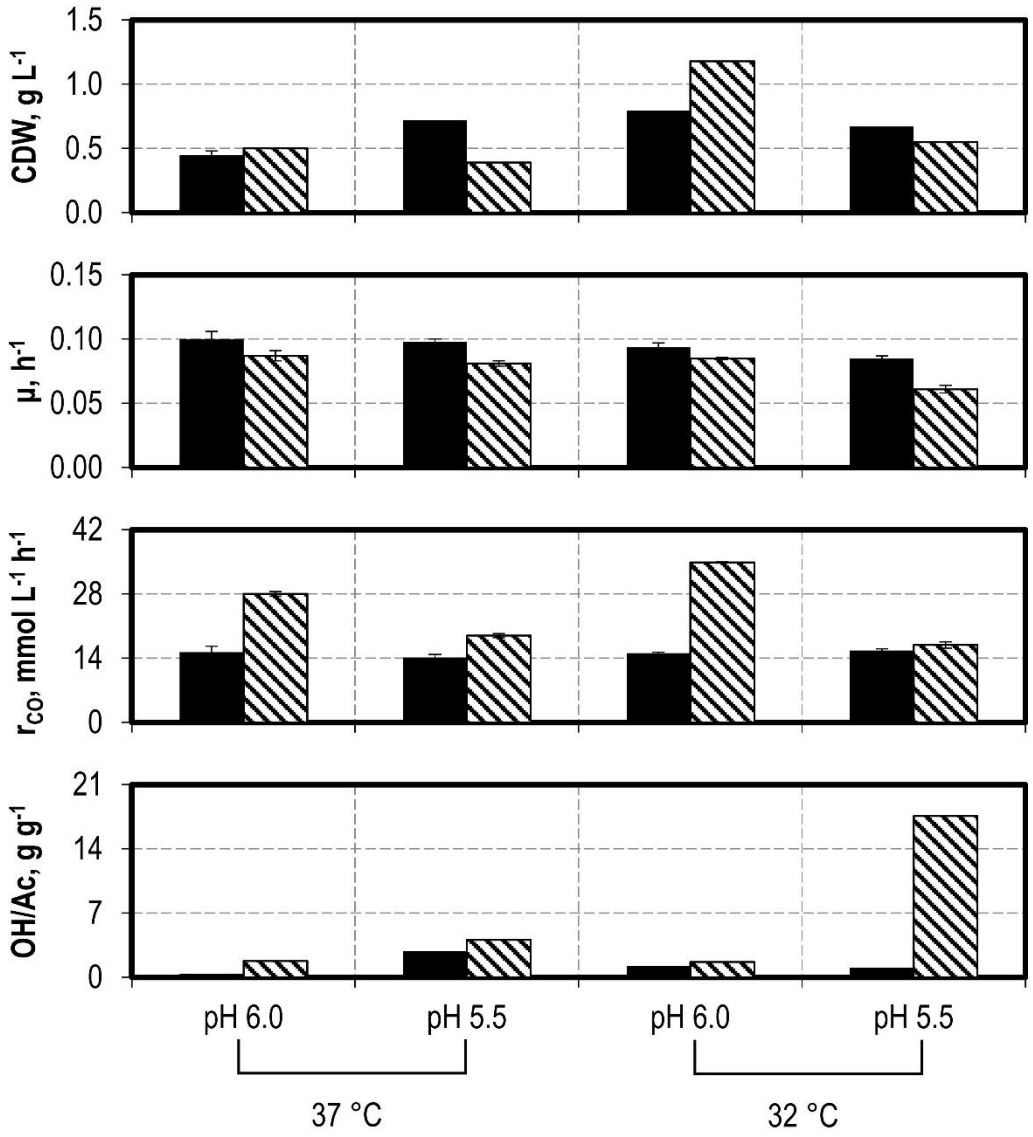

Figure 40 – Influence of decreasing the pH from pH 6.0 to pH 5.5, the temperature from 37 °C to 32 °C and implementing a sulfide feed in the syngas fermentation with *C. ragsdalei*: final cell dry weight concentration (CDW), specific growth rate (μ), maximal CO uptake rate (r_{CO}) and alcohol to acetate ratio (OH/Ac). Black bars: processes without a sulfide feed; Bar with diagonal stripes: processes with a sulfide feed of 0.05 mmol Na_2S L^{-1} h^{-1}.

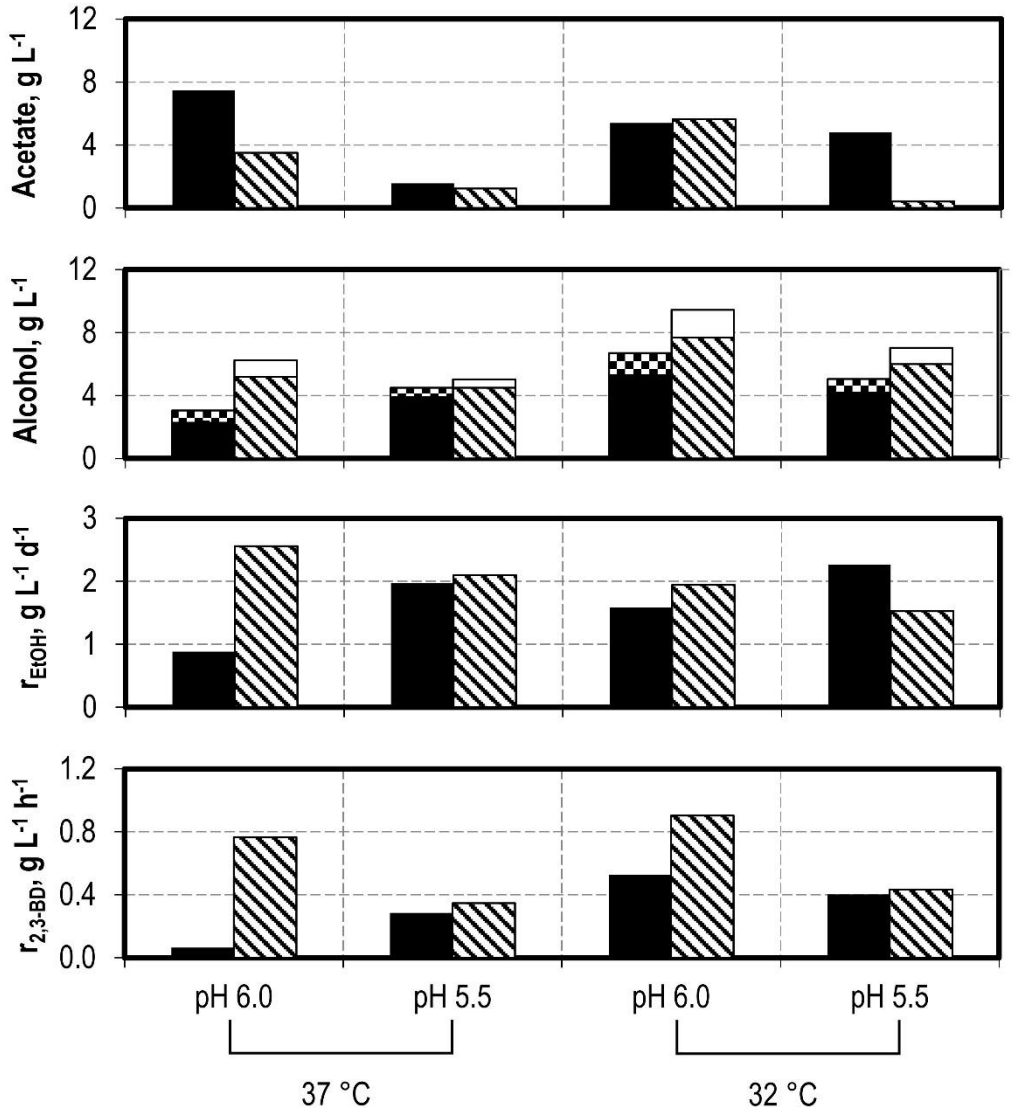

Figure 41 – Influence of decreasing the pH from pH 6.0 to pH 5.5, the temperature from 37 °C to 32 °C and implementing a sulfide feed in the syngas fermentation with *C. ragsdalei*: final acetate concentration, alcohol concentration (Ethanol: lower bars; 2,3-butanediol: upper bars), maximal ethanol production rate (r_{EtOH}) and maximal 2,3-butanediol production rate ($r_{2,3\text{-}BD}$). Black bars (and chequered for 2,3-butanediol): processes without a sulfide feed; Bar with diagonal stripes (and white for 2,3-butanediol): processes with a sulfide feed of 0.05 mmol Na_2S L^{-1} h^{-1}.

7.3 Combining Strategies at a Lower CO Partial Pressure

It could be successfully shown that lowering the process pH or temperature to pH 5.5 or 32 °C improved alcohol production. Adding a sulfide feed to these process alterations led to improvements in CO uptake rates and final alcohol concentrations, with the highest alcohol to acetate ratio being 17.58 g g^{-1} with the conditions pH 5.5, 32 °C and the sulfide feed of 0.05 mmol S L^{-1} h^{-1}. These results were, however, obtained with a syngas composition of 600 mbar CO, 200 mbar CO_2 and 200 mbar H_2, and in none of the processes H_2 was consumed. Notwithstanding, to achieve higher carbon conversions in the syngas fermentation, the uptake of H_2 is required to reduce CO_2, which is also a base constituent of syngas and is unavoidably produced using CO as electron donor.

The batch processes with *C. ragsdalei* in which H_2 was consumed involved phases of very low CO partial pressures and, more importantly, strongly favoured acetate formation, as shown in section 5. To investigate if alcohol formation with H_2 consumption can be improved, processes were conducted with a gas volume flow of 1.5 NL h^{-1} (working volume of 1 L) and a gas composition of 1:1:1 for CO, CO_2 and H_2. Further process changes were also implemented: a sulfide feed of 0.05 mmol L^{-1} h^{-1}, alone or in combination with lower pH levels of pH 5.5 and pH 5.0 or a lower temperature of 32 °C.

Figure 42 shows the results of the batch processes with gas flow 1.5 NL h^{-1} without and with a sulfide feed of 0.05 mmol S L^{-1} h^{-1}. For visual comparison, the process with 5 NL h^{-1} and no sulfide feed is also presented. All processes showed a peak in the CDW concentration, after which it decreased. The final CDW concentrations decreased to 0.30 g L^{-1} with the lower gas flows in both processes independently of sulfide feed, but the maximal CDW concentration of 0.77 g L^{-1} was achieved with the lower gas flow and the sulfide feed at the 74th process hour. This process also showed a sharp decrease in the CDW concentration between the 80th and 120th process hour. The specific growth rates remained unchanged by lowering the gas flow and composition with 0.099 ± 0.002 h^{-1} but decreased with the addition of the sulfide feed to 0.083 ± 0.005 h^{-1}.

The maximal CO uptake rates were similar in all batch processes and were constrained by the amount of CO supplied into the system. H_2 consumption was observed in both processes with the lower gas flow. With the sulfide feed, both the maximal H_2 uptake and the overall H_2 uptake increased in comparison to the analogous process without the sulfide feed, by 20.7% and 46.7 %, respectively.

The acetate concentrations increased by lowering the gas flow in both cases. With the sulfide feed, the acetate concentration sharply decreased from 14.02 g L^{-1} to 11.04 g L^{-1}

simultaneously to the decrease in the CDW concentration. Lowering the gas flow led to a similar final ethanol concentration, while combining the sulfide feed with the lower gas flow led to an increase from 2.08 g L^{-1} to 3.64 g L^{-1}. The 2,3-butanediol concentration remained unchanged by lowering the gas flow, but strongly decreased by adding the sulfide feed. A summary of the key parameters of these processes is shown in Table 17.

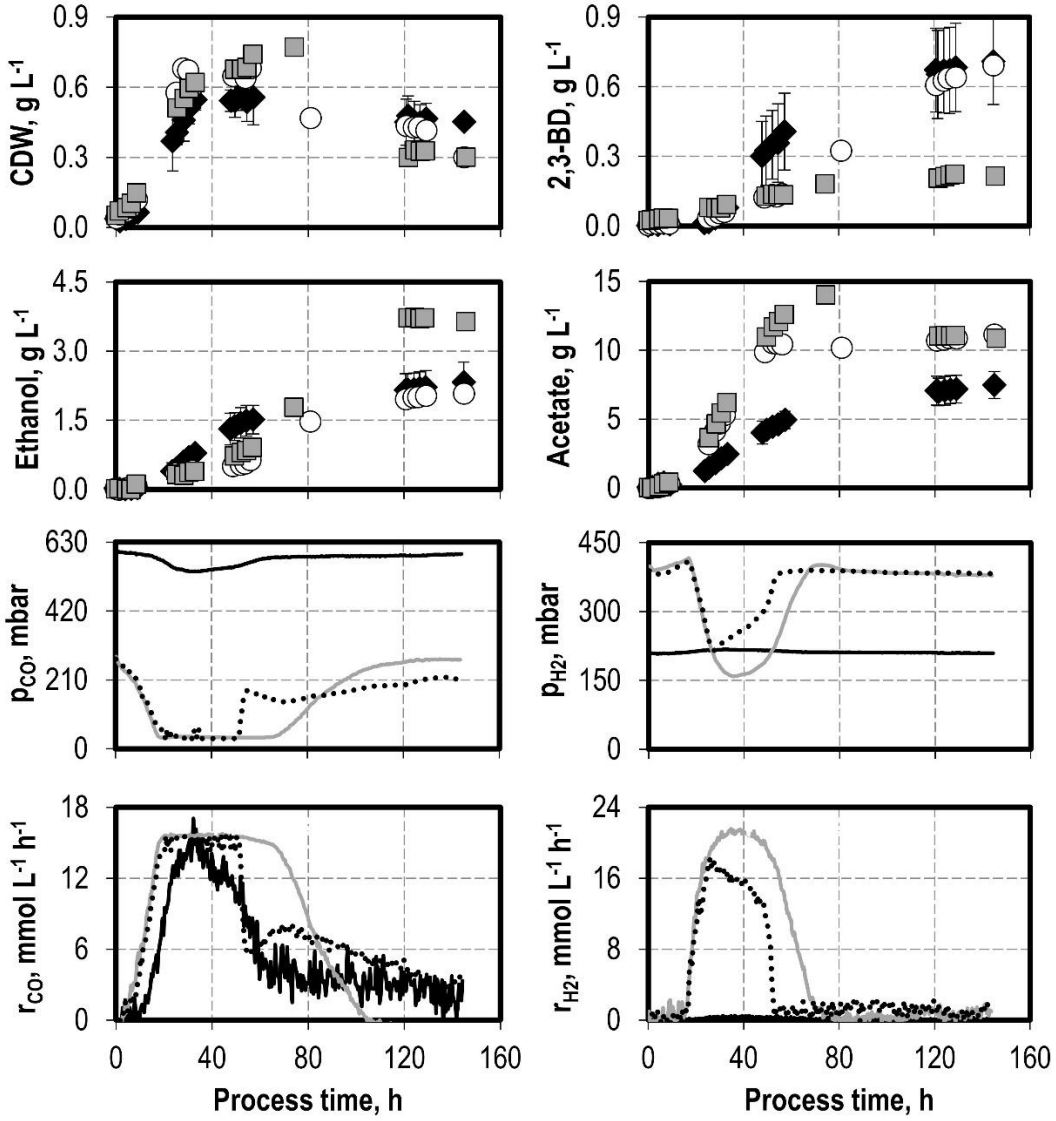

Figure 42 – Cell dry weight (CDW), 2,3-butanediol (2,3-BD), ethanol, and acetate concentrations, CO and H_2 partial pressures in the exhaust (p_{CO}, p_{H2}) and uptake rates (r_{CO}, r_{H2}) of the syngas fermentation with *C. ragsdalei* with a CO inlet partial pressure of 600 mbar (black diamonds, black lines), 333 mbar (white circles, dotted lines) and 333 mbar with a sulfide feed rate of 0.05 mmol S L^{-1} h^{-1} (grey squares, grey lines). Batch processes were conducted with pH 6.0, working volume of 1 L, volumetric power input of 3.5 W L^{-1} (800 rpm) and pressure of 1 bar. Processes with 600 mbar inlet CO had a gas flow of 5.0 NL h^{-1} with 3:1:1 ($CO:H_2:CO_2$), and processes with 333 mbar inlet CO had a gas flow of 1.5 NL h^{-1} with 1:1:1 ($CO:H_2:CO_2$)

Table 17 – Final cell dry weight (CDW) concentration, specific growth rate at the exponential growth phase, acetate, ethanol and 2,3-butanediol concentrations, and maximal CO and H_2 uptake rates (r_{CO}, r_{H2}; centered moving average with five values) in the processes with *C. ragsdalei* with gas flows, compositions and sulfide feed depicted in Figure 42. Errors in the concentrations correspond to the standard deviation of replicates.

Gas flow, NL h^{-1}	5.0	1.5	1.5
Sulfide feed, mmol S L^{-1} h^{-1}	0	0	0.05
CDW, g L^{-1}	0.45 ± 0.03	0.3	0.3
Specific growth rate, h^{-1}	0.10 ± 0.006[1]	0.099 ± 0.002[1]	0.083 ± 0.005[1]
Acetate, g L^{-1}	7.48 ± 0.98	11.16	10.87
Ethanol, g L^{-1}	2.33 ± 0.43	2.08	3.64
2,3-butanediol, g L^{-1}	0.71 ± 0.18	0.69	0.22
$r_{CO, max}$, mmol L^{-1} h^{-1}	15.3 ± 1.35[2]	16.00 ± 1.12[2]	14.85 ± 0.05[2]
$r_{H2, max}$, mmol L^{-1} h^{-1}	-	17.67 ± 0.41[2]	21.33 ± 0.18[2]

[1]Errors represent the standard error of the linear regression to obtain the specific growth rate.
[2]Values represent the mean of the five uptake rates around the maximum value, and error represent their standard deviation.

To increase alcohol concentration with a gas flow of 1.5 NL h^{-1}, further batch processes were conducted at a temperature of 32 °C, pH 5.5 and pH 5.0 with a sulfide feed of 0.05 mmol S L^{-1} h^{-1}. The CDW and product concentrations, as well as the CO and H_2 uptake rates of these processes are shown in Figure 43.

All processes avoided the sharp decrease in the CDW concentration and stop of the CO uptake rate, as observed in the process with the sulfide feed at 37 °C and pH 6.0, shown in Figure 42. Very similar timely courses and final CDW concentrations were achieved in these processes, with however bigger differences in the specific growth rates. All specific growth rates decreased, with the lowest observed in the process at pH 5.0 of 0.067 ± 0.0026 h^{-1}. Analog to the CDW concentration, the courses of the CO uptake rates were also very similar, with the maximal CO uptake rates ranging from 17.01 ± 0.04 mmol L^{-1} h^{-1} (with 32 °C) to 15.45 ± 0.12 mmol L^{-1} h^{-1} (with pH 5.5). H_2 uptake was observed in all processes at lower rates, with the highest uptake seen with 32 °C (14.6 ± 0.05 mmol L^{-1} h^{-1}), whereby overall H_2 uptake decreased in comparison with the process at 37 °C and pH 6.0.

Lowering the temperature to 32 °C led to a decrease in the concentration of all products, as well as a decrease in the alcohol to acetate ratio. Lowering the pH to 5.5 enabled a slight increase in the final concentration of ethanol to 3.82 g L^{-1}, while less 2,3-butanediol was produced. Further lowering the pH to pH 5.0 substantially increased the ethanol concentration to 7.05 g L^{-1}, and slightly increased the 2,3-butanediol concentration to 0.32 g L^{-1}, concomitant

to a decrease in the acetate concentration to 2.06 g L^{-1}, which resulted in an alcohol to acetate ratio of 3.58 g g^{-1}, the highest amongst the processes with a gas flow of 1.5 g L^{-1}. A summary of the key parameters of these processes is shown in Table 18.

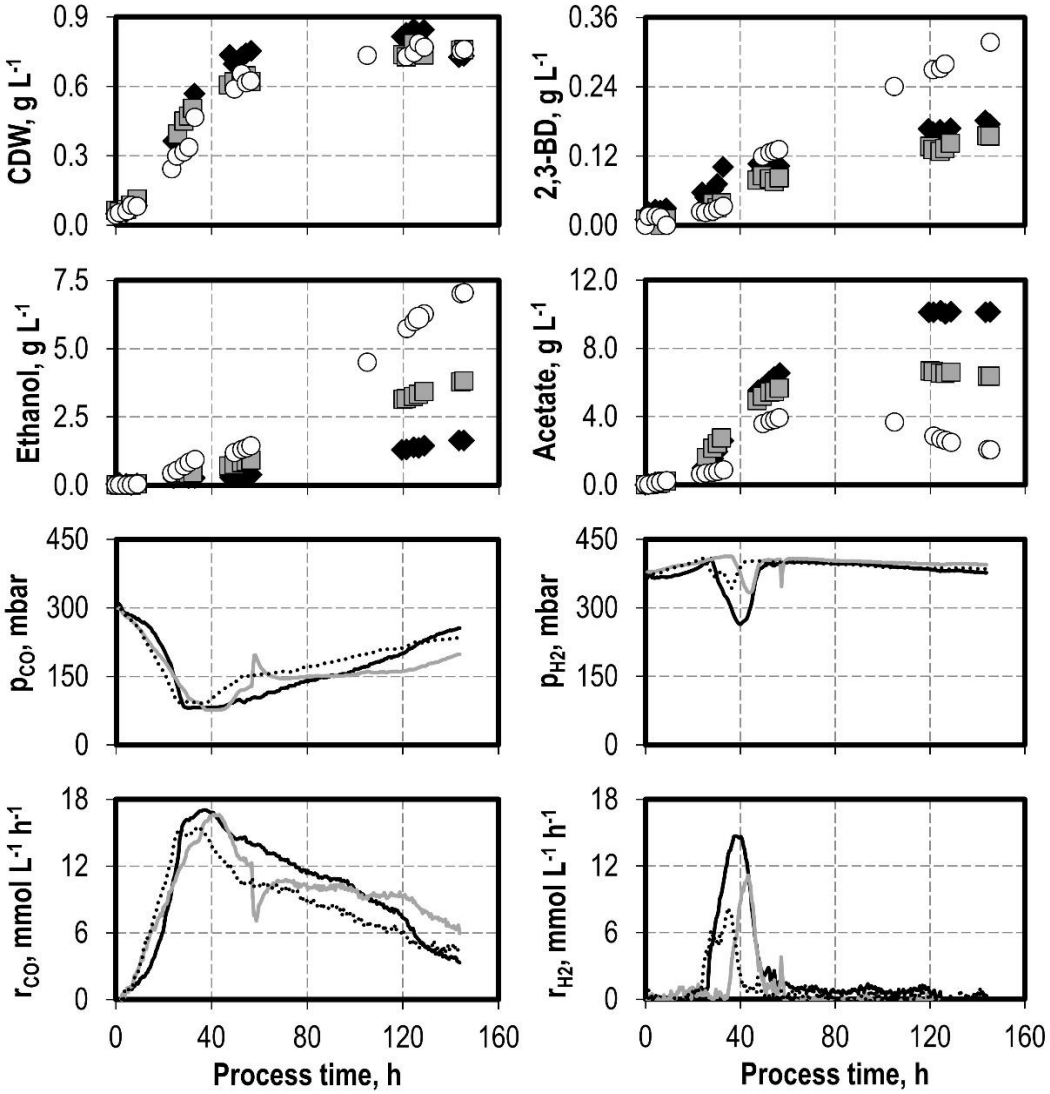

Figure 43 - Cell dry weight (CDW), 2,3-butanediol (2,3-BD), ethanol, and acetate concentrations, CO and H_2 partial pressures in the exhaust (p_{CO}, p_{H2}) and uptake rates (r_{CO}, r_{H2}) of the syngas fermentation with *C. ragsdalei* with gas flow of 1.5 NL h^{-1} with 1:1:1 ($CO:H_2:CO_2$) and a sulfide feed of 0.05 mmol S L^{-1} h^{-1}. Process parameters changed were temperature of 32 °C (black diamonds, black lines), pH 5.0 (white circles, dotted lines) and pH 5.5 (grey squares, grey lines). Processes were conducted, unless otherwise stated, with pH 6.0, at 37 °C, working volume of 1 L, volumetric power input of 3.5 W L^{-1} (800 rpm) and pressure of 1 bar.

Table 18 – Final cell dry weight (CDW), specific growth rate at the exponential growth phase, acetate, ethanol and 2,3-butanediol concentrations, and maximal CO and H_2 uptake rates (r_{CO}, r_{H2}; centered moving average with five values) in the processes with *C. ragsdalei* with changes in process parameters depicted in Figure 43. Errors in the concentrations correspond to the standard deviation of replicates.

Temperature	32	37	37
pH	6.0	5.5	5.0
CDW, g L^{-1}	0.73	0.76	0.76
Specific growth rate, h^{-1}	0.092 ± 0.0031[1]	0.079 ± 0.0034[1]	0.067 ± 0.0026[1]
Acetate, g L^{-1}	10.13	6.37	2.06
Ethanol, g L^{-1}	1.64	3.82	7.05
2,3-butanediol, g L^{-1}	0.17	0.15	0.32
$r_{CO, max}$, mmol L^{-1} h^{-1}	17.01 ± 0.04[2]	15.45 ± 0.12[2]	16.57 ± 0.05[2]
$r_{H2, max}$, mmol L^{-1} h^{-1}	14.66 ± 0.05[2]	7.80 ± 0.32[2]	10.71 ± 0.26[2]

[1]Errors represent the standard error of the linear regression to obtain the specific growth rate.
[2]Values represent the mean of the five uptake rates around the maximum value, and error represent their standard deviation.

Discussion

The alcohol production from the syngas fermentation with a CO-rich syngas could be increased by a sulfide feed, and more substantially by combining it with a lower temperature or with a lower pH, the latter strongly improving the alcohol to acetate ratio. These results were, however, obtained without H_2 consumption. Thus, the same strategies were used in the syngas fermentation of a 1:1:1 ($CO:CO_2:H_2$) syngas with a reduction in the gas flow from 5.0 NL h^{-1} to 1.5 NL h^{-1} to better assess alcohol formation under conditions that force H_2 uptake.

Lowering the gas flow without further changes already strongly influenced process performance, as can be shown by the concentration of the products against that of CDW in the phase of increasing gas uptake, depicted in Figure 44. With the lower gas flow, acetate formation increased relative to the biomass, while that of ethanol decreased. For the case of 2,3-butanediol, no clear tendency can be observed due to scattered data: the scattering relates to the low concentrations, increasing relative measurement errors. Adding the sulfide feed increased even further acetate formation relative to biomass, while not altering alcohol formation within this phase.

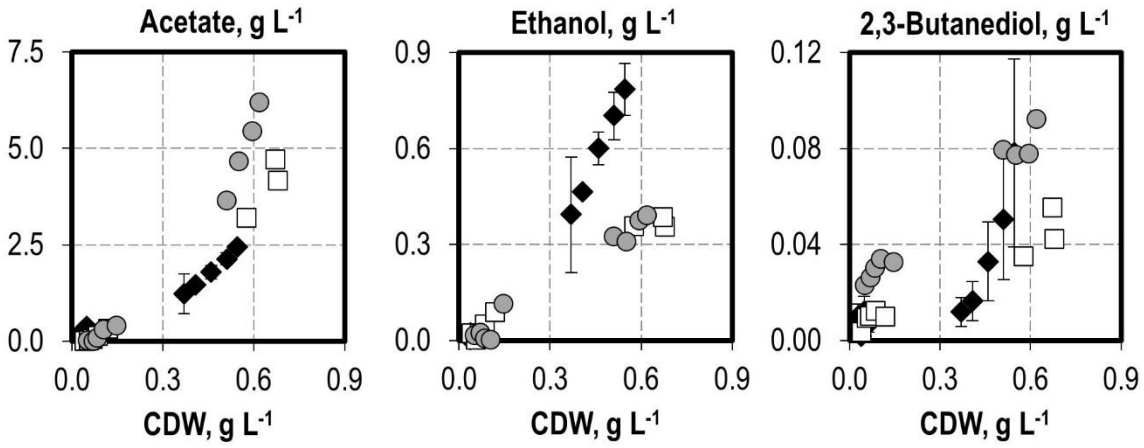

Figure 44 – Product concentration *vs.* the cell dry weight (CDW) for the phase of increasing overall gas uptake rates with *C. ragsdalei* from processes depicted in Figure 42 with an inlet CO partial pressure of 600 mbar (black diamonds), 333 mbar (white squares) and 333 mbar combined with sulfide feed of 0.05 mmol S L^{-1} h^{-1} (grey circles).

Looking closer into alcohol formation in the process with lower gas flow and no sulfide, the concentration of each alcohol, their nonlinear regression and the production rates are shown in Figure 45, along with the H_2 uptake take. To obtain the production rate of ethanol, the process was divided in two overlapping phases: one from the 1st to the 48th process hour, described by equation 4.4, and the other from the 26th hour to the process end, described by equation 4.3. This division was necessary to account for the deviation in the ethanol concentration within the 26th and 53rd process hours. For the production rate of 2,3-butanediol, equation 4.3 was used.

The uptake of H_2 had an immediate impact in the ethanol formation. While measurements of the concentration of ethanol are not available at the start of the H_2 consumption, a clear deviation from the course of the ethanol concentration can be observed within the time in which H_2 was consumed. As the H_2 uptake stopped around the 56th hour, a stronger increase in the ethanol concentration was immediately observed. This is also indicated by the production rate, which locally peaked as the H_2 uptake started, but decreased and remained constant until H_2 consumption stopped, after which it increased again, peaking at 0.93 g L^{-1} d^{-1} at the 74th hour. Thus, the clear driver of ethanol formation was CO. With 2,3-butanediol, no clear distinction in the behaviour of the production rates could be observed as H_2 uptake resumed, from which no conclusion can be drawn. In fact, 2,3-butanediol production resumed as the H_2 uptake had already started.

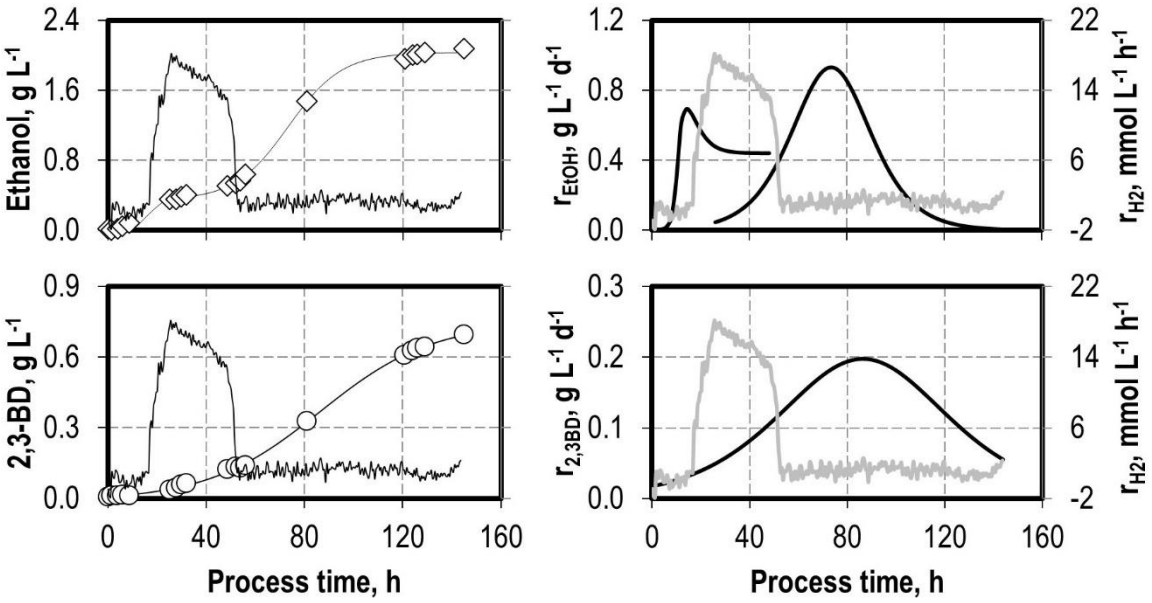

Figure 45 – **Left**: Concentration of ethanol (white diamonds) and 2,3-butanediol (2,3-BD, white circles), nonlinear regression of the ethanol and 2,3-butanediol concentrations (black lines, left); **Right**: H_2 uptake rate (r_{H2}, grey line) and ethanol and 2,3-butanediol production rates (r_{EtOH} and $r_{2,3BD}$, black lines) of the process with *C. ragsdalei* with a gas flow of 1.5 NL h^{-1}, depicted in Figure 42. The residual sum of squares of the nonlinear regressions are presented in Table 23.

By adding the sulfide feed, acetate formation was further promoted in the phase of increased CO and H_2 uptake, as shown in Figure 44, while ethanol formation relative to the CDW remained unchanged and the 2,3-butanediol increased. In this process, the H_2 uptake stopped around the 70th hour, concomitantly to a sharp decline in the CO uptake rate. This preceded a phase in which no measurement of the concentration of products or CDW was conducted, and within which CDW and acetate concentration sharply declined, while the ethanol concentration inversely increased. At the 104 h the CO uptake rate stopped, as well as the acetate and 2,3-butanediol formation, while the concentration of ethanol slightly decreased.

The production rates of ethanol and 2,3-butanediol were calculated for this process using equation 4.3. The production rates, as well as the concentrations and nonlinear regressions for both alcohols and the H_2 uptake rates are shown in Figure 46. Differently than in the process without sulfide, no explicit influence of H_2 could be observed in the ethanol formation. The peak in ethanol formation occurred, nevertheless, once CO was the only consumed gas, corroborating with the analogous process without sulfide. Interestingly, the 2,3-butanediol production rate peaked with the peak in the H_2 uptake rate, differently than in the analogous process without sulfide, but rates were substantially smaller given the strong decrease in 2,3-butanediol formation.

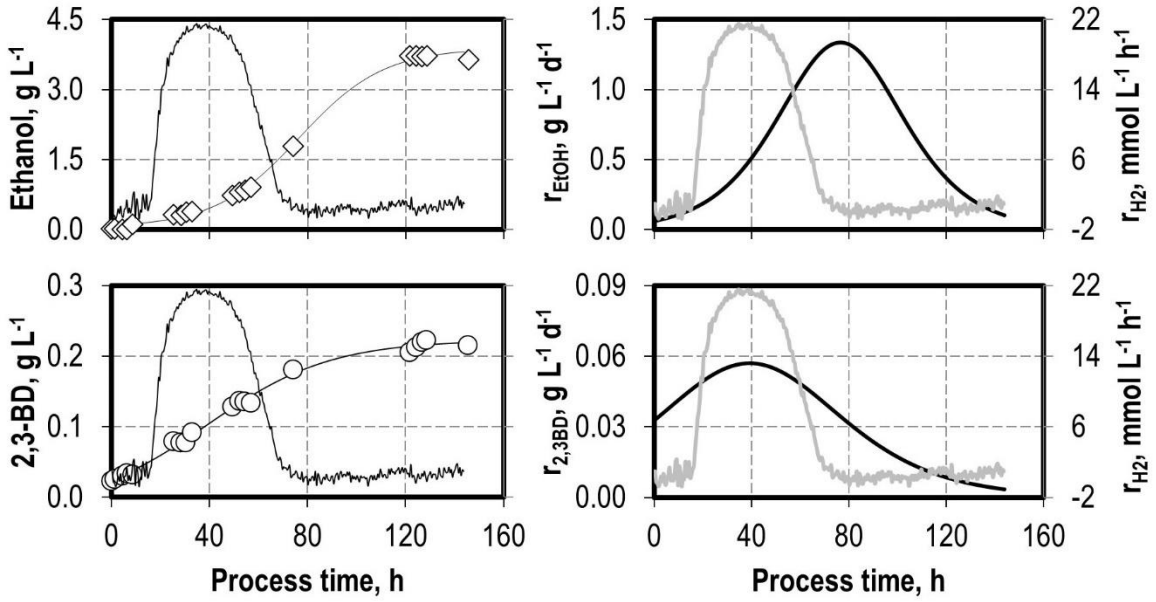

Figure 46 - **Left**: Concentration of ethanol (white diamonds) and 2,3-butanediol (2,3-BD, white circles), nonlinear regression of the ethanol and 2,3-butanediol concentrations (black lines, left); **Right**: H_2 uptake rate (r_{H2}, grey line) and ethanol and 2,3-butanediol production rates (r_{EtOH} and $r_{2,3BD}$, black lines) of the process with *C. ragsdalei* with a gas flow of 1.5 NL h^{-1} and a sulfide feed of 0.05 mmol S L^{-1} h^{-1}, depicted in Figure 42. The residual sum of squares of the nonlinear regressions are presented in Table 23.

The addition of the sulfide feed had mixed effects in the batch process with a lower gas flow and CO inlet partial pressure. It was detrimental to ethanol formation relative to the CDW in the phase of increasing gas uptake rates, but it allowed for a higher maximal CDW and increased the gas uptake, while it enabled the reduction of the acetate to ethanol once the H_2 uptake stopped. While the data is not available to support it, it is likely that this phase of acetate reduction occurred within 70th and 105th hour, period in which no H_2 was consumed and the CO uptake was still positive. In fact, during this time 106.9 mmol CO were consumed, while the concentration of acetate decreased by 53.3 mmol and the concentration of ethanol increased by 42.7 mmol. As the reduction of acetate to ethanol requires two mol of CO (equations 3.2 and 3.8), the CO uptake and acetate consumption measured are well in accordance with the stoichiometry, while the discrepancy in the ethanol concentration might lie in losses due to evaporation. Reducing acetate to ethanol not only deacidifies the cells, but also enables ATP production. The reduction of one mol acetate requires one mol reduced ferredoxin and one mol NAD(P)H. Supplying these redox cofactors with CO requires the production of NADH by the Rnf complex and, if applicable, the electron bifurcation by the transhydrogenase Nfn. Electron bifurcating from ferredoxin to NADH with the Rnf enables the production of ATP by the ATP synthase, which uses the proton motive force generated by the Rnf. If the acetate reduction is strongly favoured, as was the case in this process phase, then

less redox cofactors are available for 2,3-butanediol production, which explains the low 2,3-butanediol production.

This interplay between ethanol and 2,3-butanediol formation can be observed in the data reported by Ricci et al. (2021), in which the 2,3-butanediol production was studied with *C. autoethanogenum* and *C. ljungdahlii* with different media and different gas compositions. In their results, the highest ethanol concentrations were always achieved for both strains with the lowest 2,3-butanediol concentrations. With *C. ljungdahlii*, this was the case with CO_2/H_2 and with pure CO in the gaseous phase.

Lowering the gas flow and CO inlet partial pressures led to an increase in overall activity, since the cells could arrive at similar maximal CO uptake rates as with a gas flow of 5.0 NL h^{-1} plus consumed hydrogen. However, this led to a strongly favoured acetate formation. Implementing a sulfide feed of 0.05 mmol S L^{-1} h^{-1} increased overall activity by increasing the maximal H_2 uptake rate and overall H_2 uptake. It also enabled a higher ethanol formation through a clear reuptake of formed acetate into ethanol once the H_2 uptake stopped, whereby the alcohol to acetate ratio was also increased. To further improve the alcohol to acetate ratio, some of the strategies used in subsection 7.1 were implemented with the lower gas flow and CO inlet partial pressure, to assess if they can further improve alcohol formation.

Decreasing the temperature to 32 °C and the pH to pH 5.5 and pH 5.0 led to higher final CDW concentration (0.73 – 0.76 g L^{-1}), which were in line with the maximal CDW of 0.77 g L^{-1} achieved with the sulfide feed with 37 °C and pH 6.0. These process conditions avoided the decrease in the CDW concentration, which in turn enabled the uptake of CO for the whole process length. Nevertheless, these conditions decreased the maximal activity in comparison to 37 °C and pH 6.0, measured by the combined uptake of CO of H_2, which was 37.02 mmol L^{-1} h^{-1} to 31.67 mmol L^{-1} h^{-1} (32 °C), 23.2 mmol L^{-1} h^{-1} (pH 5.5) and 27.3 mmol L^{-1} h^{-1} (pH 5.0). As CO is the prioritized electron donor in the syngas fermentation with *C. ragsdalei*, this overall decrease was manifested in a decrease in the H_2 uptake rates.

The product formation in each process relative to the CDW concentration for the phase of increasing gas uptake rates is shown in Figure 47. At first glance, all processes underwent similar profiles for acetate formation, while the ethanol formation was strongly divergent between processes. Lowering the temperature stopped ethanol formation at a CDW of 0.36 g L^{-1}, concomitant with the start of the H_2 uptake. Acetate and 2,3-butanediol were further produced at the lower temperature. At pH 5.5, acetate formation was in line with that at a lower temperature, while ethanol and 2,3-butanediol formation increased linearly with the CDW. Further lowering to pH 5.0 led on one hand to a substantially higher ethanol formation within this phase. On the other hand, the acetate and 2,3-butanediol formation underwent a

discontinuity between the CDW concentrations of 0.47 g L^{-1} and 0.57 g L^{-1}, which were measured at 32.92 h and 49.45 h, respectively. H_2 uptake resumed at the 34th hour, so the discontinuity is likely a consequence of the uptake of H_2, which was beneficial not only for acetate, but also for alcohol formation.

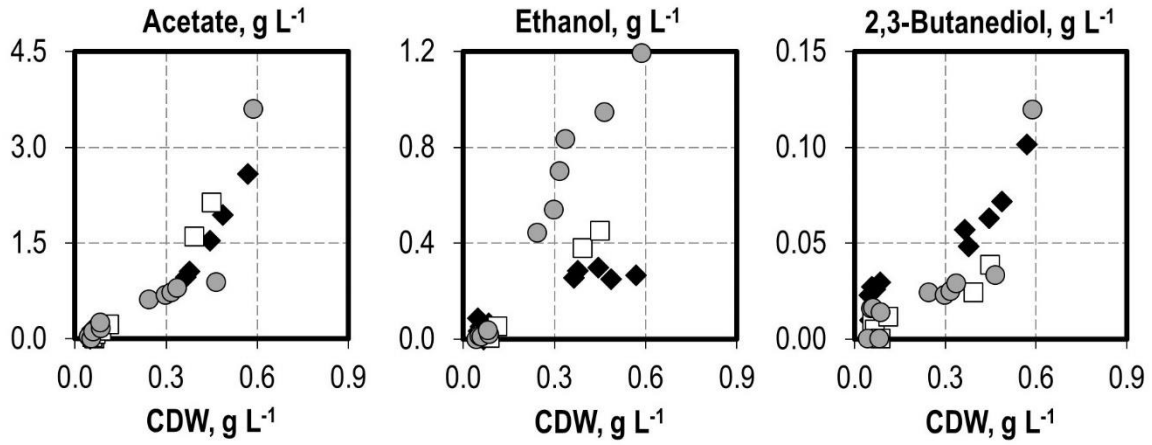

Figure 47 – Product concentration *vs.* the cell dry weight (CDW) for the phase of increasing overall gas uptake rates with *C. ragsdalei* from processes depicted in Figure 43 with temperature 32 °C and pH 6.0 (black diamonds), 37 °C and pH 5.5 (white squares) and 37 °C and pH 5.0 (grey circles).

To further elucidate the dynamics of alcohol formation in these processes and the role of H_2 in them, the concentrations of ethanol and 2,3-butanediol, as well as the nonlinear regression of the concentration against time and the production rate of each alcohol are shown in Figure 48 for a temperature of 32 °C, Figure 49 for pH 5.5 and Figure 50 for the pH 5.0. The equations used for the nonlinear regressions, as well as the residual sum of squares for each are shown in Table 19. For ethanol in the processes with temperature of 32 °C and pH 5.5, it was necessary to separate the data in two intervals, with the nonlinear regression being employed separately in each.

The processes showed a clear flattening of the ethanol concentration during the phase of H_2 uptake, and ethanol formation resumed at higher rates once the H_2 uptake stopped. The peak in the rate of ethanol production lied in all processes within a process time in which only CO was consumed, and as expected from the substantially higher final ethanol concentration, the highest ethanol production rate of 1.98 g L^{-1} d^{-1} was achieved in the process with pH 5.0 at the 102nd process hour. Interestingly, in all processes with the lower gas flow and the sulfide feed, the peak in the 2,3-butanediol production rate occurred well before the peak in the ethanol formation, while without the sulfide feed these occurred closer, and the ethanol peak preceded that of 2,3-butanediol. Since the 2,3-butanediol formation was also overall repressed by the sulfide feed with the lower gas flow, it can be assumed that the sulfide feed removed redox

cofactor from the 2,3-butanediol formation to favour ethanol formation. Further studies would be necessary to better elucidate this interplay.

Table 19 – Equations used for the nonlinear regression of the concentrations of ethanol and 2,3-butanediol and residual sum of squares (RSS) in $g^2\ L^{-2}$ of the processes with *C. ragsdalei* depicted in Figure 43

	Temperature, °C	32	37	37
	pH	6.0	5.5	5.0
Ethanol	Equation	4.3 (0 – 22 h)	4.3	4.4 (0 – 48 h)
		4.3 (23 – 144 h)		4.4 (49 – 144 h)
	RSS	0.017 (0 – 22 h)	0.045	0.032 (0 – 48 h)
		0.006 (23 – 144 h)		0.004 (49 – 144 h)
2,3-Butanediol	Equation	4.3	4.3	4.3
	RSS	0.002	0.001	0.010

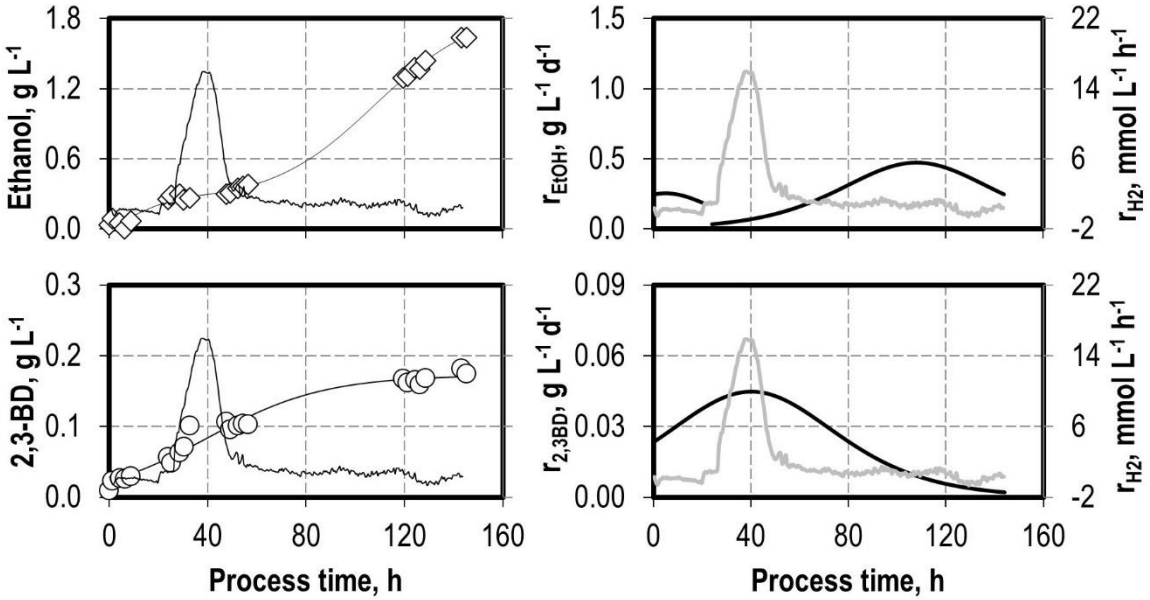

Figure 48 - **Left**: Concentration of ethanol (white diamonds) and 2,3-butanediol (2,3-BD, white circles), nonlinear regression of the ethanol and 2,3-butanediol concentrations (black lines, left); **Right**: H_2 uptake rate (r_{H2}, grey line) and ethanol and 2,3-butanediol production rates (r_{EtOH} and $r_{2,3BD}$, black lines) of the process with *C. ragsdalei* at 32 °C with a gas flow of 1.5 NL h^{-1} and a sulfide feed of 0.05 mmol S L^{-1} h^{-1}, depicted in Figure 43.

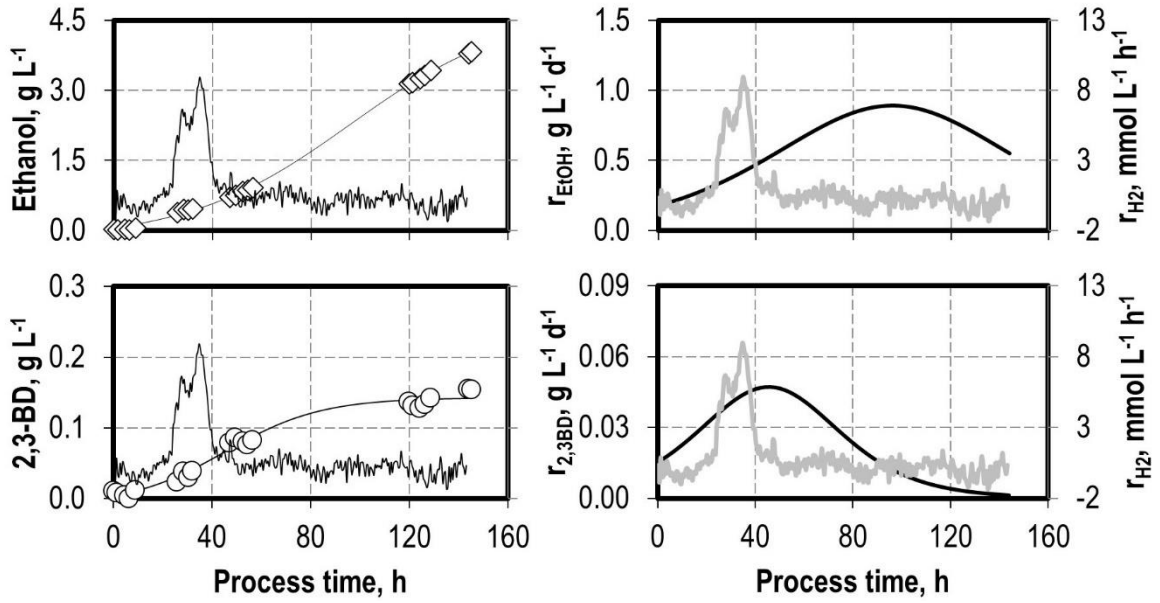

Figure 49 - **Left**: Concentration of ethanol (white diamonds) and 2,3-butanediol (2,3-BD, white circles), nonlinear regression of the ethanol and 2,3-butanediol concentrations (black lines, left); **Right**: H_2 uptake rate (r_{H2}, grey line) and ethanol and 2,3-butanediol production rates (r_{EtOH} and $r_{2,3BD}$, black lines) of the process with *C. ragsdalei* at pH 5.5 with a gas flow of 1.5 NL h^{-1} and a sulfide feed of 0.05 mmol S L^{-1} h^{-1}, depicted in Figure 43

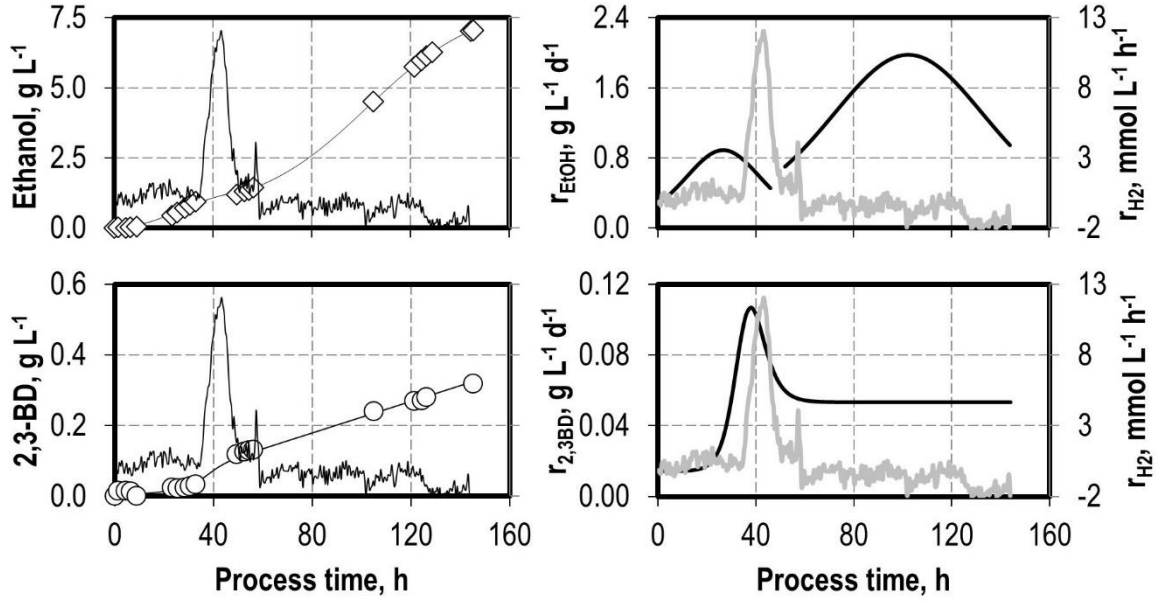

Figure 50 - **Left**: Concentration of ethanol (white diamonds) and 2,3-butanediol (2,3-BD, white circles), nonlinear regression of the ethanol and 2,3-butanediol concentrations (black lines, left); **Right**: H_2 uptake rate (r_{H2}, grey line) and ethanol and 2,3-butanediol production rates (r_{EtOH} and $r_{2,3BD}$, black lines) of the process with *C. ragsdalei* at pH 5.0 with a gas flow of 1.5 NL h^{-1} and a sulfide feed of 0.05 mmol S L^{-1} h^{-1}, depicted in Figure 43.

The ethanol formation in the process with pH 5.0 shows three clear distinct phases. A first phase from process begin to the 33rd hour, in which ethanol was produced with increasing

rates. A second phase from the 33rd to roughly the 55th hour, in which ethanol was produced at lower rates, and which was concomitant to H_2 consumption. A third phase from the 55th process hour to the end of the process, in which most of the ethanol was formed and which coincided with a decline in the acetate concentration. Net acetate consumption likely started at 72 h, which coincides with the process time in which no more base was added by the reactor system to the process to control the pH. By establishing a correlation between the acetate concentration and the activation of the base pump, as shown in Figure 51, the maximal acetate concentration could be estimated to be 4.22 g L^{-1}.

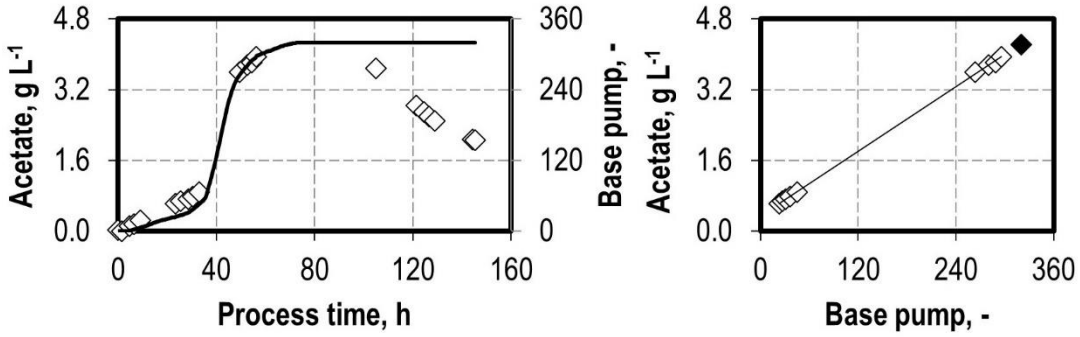

Figure 51 – **Left**: acetate concentration and base pump function; **Right**: correlation between the acetate concentration and the base pump function as the acetate concentration increased, from the process with *C. ragsdalei* with pH 5.0 presented in Figure 43.

Net acetate consumption was only observed in four other processes reported in this dissertation: in the processes with lower pH (subsection 7.1) and the process with lower gas flow and sulfide feed with 37 °C and pH 6.0, reported in this subsection. In the first cases, the acetate concentration decreased shortly after the CO uptake rate peaked, and it coincided with an increasing ethanol production rate. In the latter case, it occurred after the H_2 uptake stopped and more than 40 hours after the total gas uptake rate peaked. Table 20 summarizes the changes in the concentration of acetate and ethanol in these processes, as well as the phase length of the decline in the acetate concentration. These times serve just as a qualitative reference, since in most cases it was not possible to pinpoint at which exact time did the decline in the acetate concentration resume.

In all processes with lower pH presented in Table 20, the increase in ethanol concentration substantially surpassed the stoichiometric conversion of acetate to ethanol 0.78 $g_{Ethanol}$ $g^{-1}_{Acetate}$ (equation 3.15). At pH 6.0, the ratio of ethanol formed *per* acetate consumed was 0.65 $g_{Ethanol}$ $g^{-1}_{Acetate}$, which is lower than the stoichiometric yield. A possible reason for this discrepancy might lie in the evaporation of ethanol. If the ethanol production came only from the reduction of available acetate, then evaporation would play a relatively bigger role in decreasing the ethanol yield from acetate.

Table 20 – Decline in acetate concentration and concomitant increase in ethanol concentration (Δ), ethanol produced per acetate consumed ($\Delta_{Ethanol}\ \Delta_{Acetate}^{-1}$) and phase length of the decrease in acetate concentration for the processes with *C. ragsdalei* with the given process conditions.

pH	Unc.[1]	5.0	5.5	6.0	5.0
Gas flow, NL h^{-1}	5.0	5.0	5.0	1.5	1.5
F_S, mmol S L^{-1} h^{-1}	0	0	0	0.05	0.05
Δ in acetate concentration, g L^{-1}	-0.21	-0.33	-0.53	-2.98	-2.16[2]
Δ in ethanol concentration, g L^{-1}	0.79	0.83	1.28	1.94	4.94[3]
$\Delta_{Ethanol}\ \Delta_{Acetate}^{-1}$, g g^{-1}	3.76	2.52	2.42	0.65	2.29
Phase length, h	14.5	13.9	16.5	47.42	72.0

[1]Uncontrolled
[2]Estimated through the linear relationship between the addition of base for pH control and acetate concentration shown in Figure 51.
[3]Estimated based on the nonlinear regression presented in Figure 50.

Since ethanol is formed through acetate in *C. ljungdahlii* (Richter et al. 2016) and *C. autoethanogenum* (Liew et al. 2017), it is plausible to assume that this is also the case with *C. ragsdalei*, given their similarities (Lee et al. 2019). Therefore, if more ethanol was built than the stoichiometric yield, it means that enough reducing agents were available both for the reduction of available acetate, as well as for the fixation of CO into ethanol. In the case of the processes with lower pH and higher gas flow, this resumed immediately after the peak in the CO uptake rate and close or at the peak in the CDW concentration, which means that there was high CO oxidation concomitant with low biomass formation, thus reducing agents could be effectively and quickly redirected to ethanol production.

In the processes with a lower gas flow, a different dynamic prevailed. For ethanol production, the overall gas uptake needed to have dropped already enough to avoid H_2 uptake, so their capacity for ethanol production relied on how long CO uptake could maintain higher levels to provide the required redox cofactors. In this case, it appears that the lower CO partial pressure was beneficial. Looking into the CO uptake in the processes with gas flow of 5.0 NL h^{-1} and 600 mbar CO at pH 5.0 (Figure 30), the CO uptake sharply decreased after reaching its peak, and remained low for most of the process. This might have been the main hindrance for further ethanol formation. The sulfide feed contributed for a longer period of higher gas uptakes, as shown in section 6 and subsection 7.2, so the lower CO partial pressure and the sulfide feed enabled sufficient CO uptake to occur in the phase of no biomass formation and stopped H_2 uptake, and combined with the driver of a lower pH, enabled the late and substantial ethanol production and net acetate reduction.

8 Summary

Human activity since the industrial era has led to high emissions of greenhouse gases, which were responsible for an increase in the global mean temperature of 0.87 °C, with an increasing trend to 1.5 °C by 2030 – 2052 (Allen M. R., et al., 2018). This temperature increase will meaningfully put natural and human systems out of balance, and thus strong and assertive action is required to reverse this trend (Hoegh-Guldberg, O. et al., 2018). The transport sector is responsible for 0.24 °C of the temperature increase (Dhakal, S. et al., 2022), and one way to decarbonize this sector is by using fuels produced from renewable sources. In this light, using synthesis gas (syngas), a gas mixture containing mainly CO, CO_2 and H_2, from industrial exhaust gasses or derived from the gasification of biogenic residues to produce ethanol through fermentation is a promising technology which has already reached commercial scale (Lanzatech, 2023). This technology has the benefits of requiring mild conditions (temperature, pressure), being flexible regarding the gas composition and capable of using these very low-cost feedstocks (Kennes et al., 2016).

When broadly considering the process of syngas fermentation, identifying an appropriate strain is key. A bacterial group which can grow with the main constituents of syngas is the acetogens. They are obligate anaerobes that use the Wood-Ljungdahl pathway (WLP) to produce acetyl-CoA from two molecules of CO_2 (Ragsdale and Pierce, 2008), whereby CO and H_2 can serve as electron donors. Several acetogens of the genus *Clostridium* are of research interest, because of their capacity to produce alongside acetate diverse alcohols such as ethanol, 2,3-butanediol, butanol and hexanol (Lee et al., 2019). *Clostridium ragsdalei* is an acetogen which naturally produces acetate, ethanol and 2.3-butanediol and is closely related to the well-studied *Clostridium ljungdahlii* (Lee et al., 2019). Even though *C. ragsdalei* has been shown to produce higher alcohol to acetate ratios than other strains from the same clade (Bengelsdorf et al., 2016), it has been substantially less studied than other strains such as *C. ljungdahlii*. Therefore, *C. ragsdalei* was chosen as the subject of study within this work. The first aim of this work was to compare the syngas fermentation with *C. ragsdalei* with that with well-studied acetogen *C. ljungdahlii* under the ideal conditions of pH 6.0 and 37 °C (Tanner et al., 1993; Huhnke et al., 2008). As several published strain-comparisons were conducted in anaerobic flasks (Bengelsdorf et al. 2016; Cotter et al., 2009b; Ricci et al, 2021), the comparison conducted here was performed in a more relevant reactor setup of a continuously gassed stirred-tank reactor in batch mode.

With a syngas of the composition 3:1:1 ($CO:CO_2:H_2$) at atmospheric pressure in a fully controlled and continuously gassed batch process, *C. ragsdalei* showed a higher activity than

C. ljungdahlii, with a fivefold higher specific growth rate (0.10 ± 0.006 h^{-1}) and a 22.7% increase in the maximal CO uptake rate. *C. ragsdalei* mainly produced acetate, with an alcohol to acetate ratio of 0.41 $g_{alcohol}$ $g^{-1}_{acetate}$, while *C. ljungdahlii* shifted carbon mainly to alcohol, with an alcohol to acetate ratio of 2.28 $g_{alcohol}$ $g^{-1}_{acetate}$. To investigate if *C. ljungdahlii* was inhibited by the CO in the syngas, inlet CO partial pressures of 200 mbar and 100 mbar were implemented. The specific growth rate of *C. ljungdahlii* increased roughly twofold with 200 mbar CO (0.047 ± 0.009 h^{-1}) and threefold with 100 mbar CO (0.066 ± 0.002 h^{-1}), indicating a clear CO inhibition with *C. ljungdahlii*. CO inhibition has been observed in other *clostridial* strains (Doll, 2018; Mayer et al., 2018), and it most likely works by inhibiting the hydrogenase of the formate dehydrogenase/electron bifurcating hydrogenase complex (HytA-E/FDH). The role of the hydrogenase in the CO_2 reduction to formate with CO as electron donor is, however, unclear (Wang et al., 2013). In this regard, *C. ragsdalei* is the most adequate of both strains for the fermentation of a CO-rich syngas, although improvement in the alcohol production is necessary.

Syngas fermenting acetogens can use CO and H_2 as electron donors. However, in the batch processes with *C. ljungdahlii* and *C. ragsdalei* with a CO-rich syngas (600 mbar CO), no H_2 was consumed, despite its presence. Once the inlet CO partial pressure was reduced to 100 mbar with *C. ljungdahlii*, H_2 uptake occurred with a maximal rate of 22.14 ± 0.342 mmol L^{-1} h^{-1}. A closer look was taken into the condition which supported H_2 uptake in the presence of CO in processes with *C. ragsdalei,* with a gas flow rate of 10 NL h^{-1}, working volume of 1 L, a gas composition of 5% (v/v) CO, 47.5% (v/v) CO_2 and 47.5% (v/v) H_2, and volumetric power inputs of 3.5 W L^{-1} and 11.7 W L^{-1}. H_2 uptake resumed as the CO partial pressure in the exhaust decreased to 47.3 ± 1.5 mbar. Extending it to further process conditions with both strains rendered a threshold CO partial pressure of 47.1 ± 4 mbar, under which H_2 uptake resumes. It could be demonstrated that this threshold was not due to gas-liquid mass transfer limitation, which indicated that the inhibition of the hydrogenase of the HytA-E/FDH by CO was overcome at such low CO partial pressures. This hydrogenase has high activity and has been shown to be the most abundant protein in the proteome of *C. autoethanogenum* (Wang et al., 2013) and *C. ljungdahlii* (Richter et al., 2016), which explains why the maximal H_2 uptake rate of *C. ljungdahlii* was higher than the maximal CO uptake of *C. ragsdalei* in the fermentation of a CO-rich syngas.

One of the promising aspects of the syngas fermentation is the prospect of combining the gasification of biogenic residues with syngas fermentation. However, this syngas contains impurities, depending on the feedstock and gasification conditions (Broer et al., 2015; Broer and Brown, 2016). Evaluating the impact of these different impurities on the process is essential to design adequate gas purification and conditioning steps. One aim of this work was

to assess the effect of the three possible impurities NH_3, H_2S and NO_3^- on the syngas fermentation and compare the tolerance of the strains *C. ljungdahlii* and *C. ragsdalei* to these impurities. By individually investigating the influence of these defined impurities and identifying inhibiting concentrations, a more rational approach would be possible to design a syngas cleanup strategy. Overall, all impurities studied decreased the cell activity of both strains, except for nitrate with *C. ljungdahlii*, which led to similar CDW and acetate concentrations, and 0.1 g L^{-1} H_2S with *C. ragsdalei*, which led to a substantial increase in the final CDW concentration, maximal CO uptake rate and total alcohol concentration. Under the assumption of a continuously gassed batch process over 60 h with complete dissolution of the impurities, *C. ljungdahlii* would tolerate a syngas containing 236 ppm NO_x (assuming the complete conversion to nitrate) and *C. ragsdalei* would tolerate a syngas containing 108 ppm H_2S without a gas cleanup step. Meanwhile, NH_3 for both strains, NO_x for *C. ragsdalei* and H_2S for *C. ljungdahlii* would need to be removed from the syngas, considering the concentrations ranges studied.

The addition of 0.1 g L^{-1} H_2S with *C. ragsdalei* led to an overall improvement in the syngas fermentation. To better understand this discrepancy, the concentration of cysteine in the medium was measured in the syngas fermentation with *C. ragsdalei* and *C. ljungdahlii*. This has been the first time that these measurements were performed in the syngas fermentation with these or closely related strains, and it was possible to show that more than 90% of the cysteine was depleted within the first 50 h of the processes. The H_2S in the exhaust was quantified in the process with *C. ragsdalei*, and it was clear that the H_2S loss rate reached its maximal value (0.18 mmol L^{-1} h^{-1}) shortly after the peak in the estimated depletion rate of cysteine (0.146 mmol L^{-1} h^{-1}). This indicates that the H_2S was produced from the cysteine depletion. Overall, 74% of the sulfur put into the system as cysteine was quantified as lost through the exhaust as H_2S, which is a very strong indication that sulfide limitation might play a role in the syngas fermentation. This loss of sulfide, lastly, elucidates why increasing the concentration cysteine, the main source sulfide, did not alter process outcomes substantially in previously published results (Abubackar et al., 2012; Infantes et al., 2020).

To curb this sulfide limitation, sulfide was supplied throughout batch processes with *C. ragsdalei* as a continuous feed of $Na_2S{\cdot}9H_2O$ at rates of 0.10 mmol S L^{-1} h^{-1} and 0.05 mmol S L^{-1} h^{-1}. Both cases substantially changed the process outcomes. The higher sulfide rate decreased the specific growth rate by 38% (0.062 ± 0.003 h^{-1}), while the maximal CO uptake rate remained roughly unchanged and the alcohol to acetate ratio increased twofold to 0.81 $g_{alcohol}$ $g^{-1}_{acetate}$. The lower sulfide rate strongly increased overall activity, with the maximal CDW concentration and CO uptake rate increasing 45% (0.74 g L^{-1}) and 83% (28.03 ± 0.50 mmol L^{-1} h^{-1}), respectively. Furthermore, the alcohol to acetate ratio increased

to 1.78 $g_{alcohol}$ $g^{-1}_{acetate}$. It could be shown that the benefits of the lower sulfide feed lied partially in curbing the sulfide limitation, thereby enabling higher cell dry weight (CDW) concentrations and thus higher final concentration of products. Furthermore, the sulfide feed also fomented alcohol formation in detriment of acetate production both in the growth as well as in the stationary and death phases. As the CO uptake rates increased *per* CDW concentration, the most efficient allocation of abundant redox cofactors was the two-step reduction of acetate to ethanol, which still enables the production of ATP (Allaart et al, 2023; Richter et al., 2016). The sulfide feed of 0.05 mmol S L^{-1} h^{-1} was also implemented with *C. ljungdahlii*, increasing roughly twofold both the final CDW concentration (1.46 g L^{-1}) and the H_2 uptake rate (40.66 ± 0.302 mmol L^{-1} h^{-1}).

Favouring the formation of alcohol over that of acetate in the syngas fermentation is challenging, since the formation of acetate offers a higher ATP yield per mol electron donor than that of ethanol or 2,3-butanediol (Richter et al 2016, Schuchmann and Müller, 2014). This was reflected in the syngas fermentation with *C. ragsdalei* of a CO-rich syngas (600 mbar CO) under ideal conditions (pH 6.0 and 37 °C), which led to a favoured acetate formation, even though CO as electron donor should favour the formation of more reduced products (Hurst and Lewis, 2010). Therefore, one aim of this work was to improve alcohol production through a systematic comparison of the effect of key parameters in the outcomes of batch processes with *C. ragsdalei* in a continuously gassed stirred-tank reactor. This approach was initially undertaken by individually changing the pH and process temperatures, and subsequently combining the improved conditions. Lowering the temperature to 32 °C increased the final CDW concentration, the overall CO uptake and the final alcohol concentration (5.34 g L^{-1} ethanol and 1.35 g L^{-1} 2,3-butanediol) without increasing the maximal CO uptake rate. The alcohol formation relative to that of CDW diverged only once the growth rate slowed, indicating that the higher alcohol formation did not occur through a metabolic shift during the growth phase. Lowering the pH to pH 5.5 led to the highest alcohol to acetate ratio (2.86 $g_{alcohol}$ $g^{-1}_{acetate}$) of the pH levels investigated, as well as the highest final ethanol concentration (3.95 g L^{-1}). In turn, it could be shown that the 2,3-butanediol concentration decreased with decreasing pH. Combining pH 5.5 and 32 °C failed to combine the benefits of each individual parameter change.

On a next step, the improved pH 5.5 and temperature 32 °C were individually and simultaneously combined with the sulfide feed of 0.05 mmol S L^{-1} h^{-1}. The implementation of the sulfide feed had a clear beneficial effect in the alcohol to acetate ratio, maximal CO uptake rate, and final ethanol and 2,3-butanediol concentrations in all combinations of pH and temperatures, as can be seen in Figure 52. It increased the final CDW concentration at pH 6.0, while it decreased the specific growth rate in all processes. With the combination of the sulfide

feed, 32 °C and pH 6.0, the highest CDW concentration (1.18 g L^{-1}), maximal CO uptake rate (34.9 ± 0.14 mmol L^{-1} h^{-1}), ethanol (7.67 g L^{-1}) and 2,3-butanediol (1.76 g L^{-1}) concentrations of this work with *C. ragsdalei* were achieved, while the combination of the sulfide feed, 32 °C and pH 5.5 led to the highest alcohol to acetate ratio (17.58 $g_{alcohol}$ $g^{-1}_{acetate}$) of this work, related to ethanol and 2,3-butanediol concentrations of 6.0 g L^{-1} and 1.03 g L^{-1}, respectively.

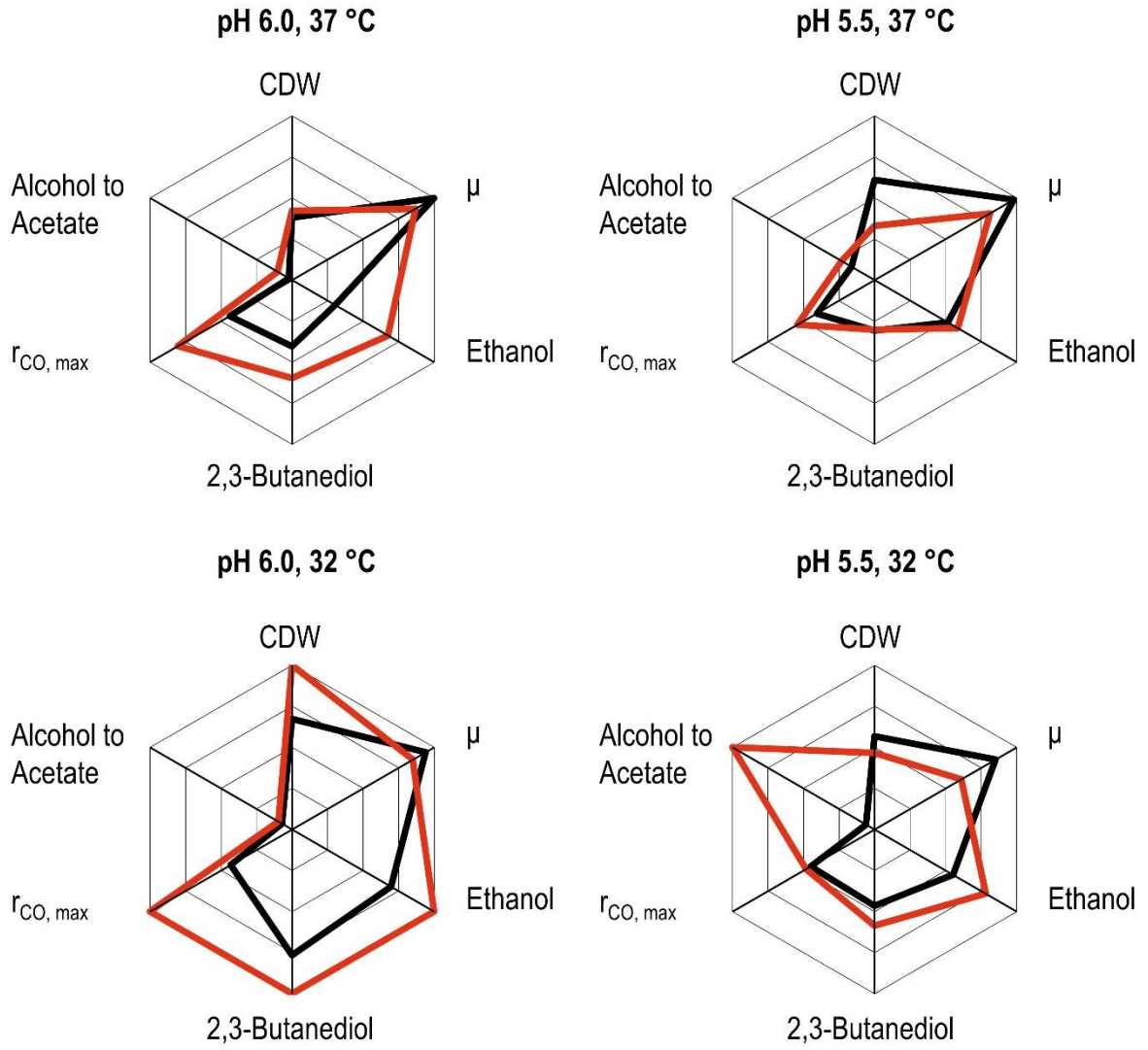

Figure 52 – Comparison of the cell dry weight (CDW) concentration, specific growth rate (μ), final ethanol and 2,3-butanediol concentrations, maximal CO uptake rate ($r_{CO, max}$) and alcohol to acetate ratio of the batch processes with *C. ragsdalei* at pH 6.0 and pH 5.5, temperatures of 32 °C and 37 °C and with a sulfide feed of 0.05 mmol S L^{-1} h^{-1} (red lines) and without a sulfide feed (black lines). Other general process conditions were: working volume of 1 L, volumetric power input of 3.5 W L^{-1} (800 rpm), gas flow of 5.0 NL h^{-1} with 3:1:1 ($CO:H_2:CO_2$) and pressure of 1 bar. Values of the variables were normalized to the range of 0.0 – 1.0 relative to the maximal value for all processes.

High alcohol formation could be achieved with *C. ragsdalei* with a CO-rich syngas by lowering the process temperature, pH and implementing an adequate sulfide feed. However, to achieve

higher carbon conversions, the fixation of CO_2 with H_2 is necessary, since the use of CO as electron donor generates CO_2. To improve alcohol formation with concomitant CO and H_2 uptake, the lower pH levels of pH 5.5 and pH 5.0, the temperature of 32 °C and the sulfide feed of 0.05 mmol S L^{-1} h^{-1} were implemented with a gas flow of 1.5 NL h^{-1} (working volume of 1 L) and a gas composition of 1:1:1 ($CO:CO_2:H_2$) at 1 bar. Analog to the fermentation of the CO-rich syngas, the sulfide feed increased the alcohol to acetate ratio and the maximal gas uptake rate. However, differently than with the CO-rich syngas, the lower temperature and the pH 5.5 were insufficient to strongly promote alcohol formation. This was achieved at pH 5.0, at which the final ethanol concentration increased 3.4-fold (7.05 g L^{-1}) and the alcohol to acetate ratio 14.4-fold (3.58 $g_{alcohol}$ $g^{-1}_{acetate}$). The ethanol formation was only fomented once the H_2 uptake stopped, which resulted in a phase of acid accumulation and another of net acetate consumption, a feature seldom observed in the processes within this work.

C. ragsdalei was shown to have the ability to substantially convert syngas into alcohol under adequate conditions. In comparison to the well-studied strain *C. ljungdahlii*, *C. ragsdalei* had both higher specific growth rates and maximal CO uptake rate in batch processes in a continuously gassed stirred-tank reactor with a CO-rich syngas at pH 6.0 and 37 °C, while it favoured the production of acetate over that of alcohols. This reflects one the challenges of the syngas fermentation, which is to favour alcohol formation over that of acetate, even though the formation of acetate yields more ATP from the electron donors CO and H_2 than that of ethanol or 2,3-butanediol. It could be successfully demonstrated that implementing a sulfide feed of 0.05 mmol $Na_2S{\cdot}9H_2O$ L^{-1} h^{-1} at 32 °C at both pH 6.0 and pH 5.5 could substantially improve process performance in several metrics, as can be seen in Figure 52. Furthermore, in comparison to the highest values for *C. ragsdalei* in previously published results, these processes led to strong increases in the ethanol space-time yield (54.8 $mg_{ethanol}$ L^{-1} d^{-1}, 80% increase in comparison to results from Devarapalli et al., 2016) and the alcohol to acetate ratio (17.58 $g_{alcohol}$ $g^{-1}_{acetate}$, 3,3-fold increase in comparison to results from Kundyiana et al., 2010).

9 Outlook

This work investigated the syngas batch fermentation with *Clostridium ragsdalei* under different conditions, to assess its performance for alcohol production and its tolerance to the syngas major constituents and impurities. Continuous processes offer, in comparison to batch processes, higher space-time yields and on an industrial scale lower costs of capital and labour. Therefore, assessing the performance of *C. ragsdalei* in continuous processes would be the next natural step to further explore this less studied strain. This would allow for processes in which nutrients are continuously fed into the reaction system, thus curbing nutrient limitations. Furthermore, conducting continuous processes with a submerged membrane reactor with cell retention would enable a decoupling of the biomass and product formation with *C. ragsdalei*, which could lead to higher productivities.

One important aim of the syngas fermentation is a high conversion of carbon, which necessarily requires the uptake of H_2 in the presence of CO. This work showed a clear threshold CO partial pressure, under which H_2 resumes, and this threshold is most likely given by the inhibition of the hydrogenase HytA. Investigating if this threshold is also dependent on the H_2 partial pressure would shed further light into whether the HytA inhibition is the main factor impeding H_2 uptake at higher CO partial pressures.

Inhibition concentrations for ammonia, nitrate and hydrogen sulfide could be identified for *C. ljungdahlii* and *C. ragsdalei* with processes in which the concentration of the defined impurities was given at the process start, prior to inoculation. However, in a continuously gassed process with real syngas, the impurities would accumulate over the process, rather than be present at the process start. Thus, investigating the effect of defined impurities through the continuous feed of each impurity could show if the cells are able to adapt, which could eventually also have an effect in the product distribution of the syngas fermentation.

Implementing a sulfide feed of 0.05 mmol S L^{-1} h^{-1} led to clear improvements in the syngas fermentation with both strains. Fine adjustments to the feed rate might lead to an improved alcohol production. Furthermore, replacing the cysteine totally or partially by the sulfide feed would have the benefit of removing a costly constituent of the medium, increasing economic feasibility. Not only the sulfide feed, but also pH and temperature could be fine adjusted to find the ideal parameters for alcohol production.

Lastly, further understanding the mechanism with which sulfide influences the syngas fermentation might lead to substantial improvements in the field. This work indicated that the CODH throughput increased by the higher CO uptake rates relative to the cell dry weight, but

confirmation is required. Furthermore, measuring the ratios of the redox cofactors NAD/NADH and NADP/NADPH with and without the sulfide feed might give more clues about the mechanisms with which sulfide influences the process.

10 Bibliography

Abubackar, H. N.; Fernández-Naveira, Á.; Veiga, M. C.; Kennes, C. (2016): Impact of cyclic pH shifts on carbon monoxide fermentation to ethanol by *Clostridium autoethanogenum*. In Fuel 178, pp. 56–62. DOI: 10.1016/j.fuel.2016.03.048.

Abubackar, H. N.; Veiga, M. C.; Kennes, C. (2012): Biological conversion of carbon monoxide to ethanol: effect of pH, gas pressure, reducing agent and yeast extract. In Bioresource Technology 114, pp. 518–522. DOI: 10.1016/j.biortech.2012.03.027.

Ahmed, A.; Lewis, R. S. (2007): Fermentation of biomass-generated synthesis gas: effects of nitric oxide. In Biotechnology and Bioengineering 97 (5), pp. 1080–1086. DOI: 10.1002/bit.21305.

Aitken, A.R.; Learmonth, M. (2009): Estimation of Disulfide Bonds Using Ellman's Reagent. In John M. Walker (Ed.): The Protein Protocols Handbook, vol. 82. Totowa, NJ: Humana Press (Springer Protocols Handbooks), pp. 1053–1055.

Aklujkar, M.; Leang, C.; Shrestha, P. M.; Shrestha, M.; Lovley, D. R. (2017): Transcriptomic profiles of *Clostridium ljungdahlii* during lithotrophic growth with syngas or H_2 and CO_2 compared to organotrophic growth with fructose. In Scientific reports 7 (1), p. 13135. DOI: 10.1038/s41598-017-12712-w.

Allaart, M.T., Diender, M., Sousa, D.Z. & Kleerebezem, R. (2023) Overflow metabolism at the thermodynamic limit of life: How carboxydotrophic acetogens mitigate carbon monoxide toxicity. Microbial Biotechnology, 00, 1– 9. Available from: https://doi.org/10.1111/1751-7915.14212

Allen, M.R., O.P. Dube, W. Solecki, F. Aragón-Durand, W. Cramer, S. Humphreys, M. Kainuma, J. Kala, N. Mahowald, Y. Mulugetta, R. Perez, M.Wairiu, and K. Zickfeld, 2018: Framing and Context. In: Global Warming of 1.5°C. An IPCC Special Report on the impacts of global warming of 1.5°C above pre-industrial levels and related global greenhouse gas emission pathways, in the context of strengthening the global response to the threat of climate change, sustainable development, and efforts to eradicate poverty [Masson-Delmotte, V., P. Zhai, H.-O. Pörtner, D. Roberts, J. Skea, P.R. Shukla, A. Pirani, W. Moufouma-Okia, C. Péan, R. Pidcock, S. Connors, J.B.R. Matthews, Y. Chen, X. Zhou, M.I. Gomis, E. Lonnoy, T. Maycock, M. Tignor, and T. Waterfield (eds.)]. Cambridge University Press, Cambridge, UK and New York, NY, USA, pp. 49-92. https://doi.org/10.1017/9781009157940.003.

Arslan, K.; Bayar, B.; Nalakath Abubackar, H.; Veiga, M. C.; Kennes, C. (2019): Solventogenesis in *Clostridium aceticum* producing high concentrations of ethanol from syngas. In Bioresource technology 292, p. 121941. DOI: 10.1016/j.biortech.2019.121941.

Barik, S.; Prieto, S.; Harrison, S. B.; Clausen, E. C.; Gaddy, J. L. (1988): Biological production of alcohols from coal through indirect liquefaction. In Applied Biochemistry and Biotechnology 18 (1), pp. 363–378. DOI: 10.1007/BF02930840.

Barton L. L., Fauque G. D.. (2009): Biochemistry, physiology and biotechnology of sulfate-reducing bacteria. Adv Appl Microbiol.;68:41-98. doi: 10.1016/S0065-2164(09)01202-7.

Bengelsdorf, F. R.; Poehlein, A.; Linder, S.; Erz, C.; Hummel, T.; Hoffmeister, S.; Daniel, R.; Dürre, P. (2016): Industrial Acetogenic Biocatalysts: A Comparative Metabolic and Genomic Analysis. In Frontiers in microbiology 7, p. 1036. DOI: 10.3389/fmicb.2016.01036.

Broer, K. M.; Brown, R. C. (2016): Effect of Equivalence Ratio on Partitioning of Nitrogen during Biomass Gasification. In Energy Fuels 30 (1), pp. 407–413. DOI: 10.1021/acs.energyfuels.5b02197.

Broer, K. M.; Woolcock, P. J.; Johnston, P. A.; Brown, R. C. (2015): Steam/oxygen gasification system for the production of clean syngas from switchgrass. In Fuel 140 (6), pp. 282–292. DOI: 10.1016/j.fuel.2014.09.078.

Cline, Joel D. (1969): Spectrophotometric determination of hydrogen sulfide in natural waters. In Limnology and Oceanography 14 (3), pp. 454–458. DOI: 10.4319/lo.1969.14.3.0454.

Cotter, J. L., Chinn, M. S., & Grunden, A. M. (2009a). Ethanol and acetate production by *Clostridium ljungdahlii* and *Clostridium autoethanogenum* using resting cells. Bioprocess and Biosystems Engineering, 32(3), 369–380. https://doi.org/10.1007/s00449-008-0256-y

Cotter, J. L.; Chinn, M. S.; Grunden, A. M. (2009b): Influence of process parameters on growth of *Clostridium ljungdahlii* and *Clostridium autoethanogenum* on synthesis gas. In Enzyme and Microbial Technology 44 (5), pp. 281–288. DOI: 10.1016/j.enzmictec.2008.11.002.

Dhakal, S., J.C. Minx, F.L. Toth, A. Abdel-Aziz, M.J. Figueroa Meza, K. Hubacek, I.G.C. Jonckheere, Yong-Gun Kim, G.F. Nemet, S. Pachauri, X.C. Tan, T. Wiedmann, (2022): Emissions Trends and Drivers. In IPCC, 2022: Climate Change 2022: Mitigation of Climate Change. Contribution of Working Group III to the Sixth Assessment Report of the Intergovernmental Panel on Climate Change [P.R. Shukla, J. Skea, R. Slade, A. Al Khourdajie, R. van Diemen, D. McCollum, M. Pathak, S. Some, P. Vyas, R. Fradera, M. Belkacemi, A. Hasija, G. Lisboa, S. Luz, J. Malley, (eds.)]. Cambridge University Press, Cambridge, UK and New York, NY, USA. doi: 10.1017/9781009157926.004

Datar, R. P.; Shenkman, R. M.; Cateni, B. G.; Huhnke, R. L.; Lewis, Randy S. (2004): Fermentation of biomass-generated producer gas to ethanol. In Biotechnology and Bioengineering 86 (5), pp. 587–594. DOI: 10.1002/bit.20071.

Devarapalli, M., Atiyeh, H. K., Phillips, J. R., Lewis, R. S., & Huhnke, R. L. (2016). Ethanol production during semi-continuous syngas fermentation in a trickle bed reactor using *Clostridium ragsdalei*. Bioresource Technology, 209, 56–65. https://doi.org/10.1016/j.biortech.2016.02.086

Doll, K. (2018). Reaktionstechnische Untersuchungen zur autotrophen Herstellung von Alkoholen mit *Clostridium carboxidivorans*. Dissertation. Munich: Technische Universität München. https://mediatum.ub.tum.de/?id=1438916

Doll, K.; Rückel, A.; Kämpf, P.; Wende, M.; Weuster-Botz, D. (2018): Two stirred-tank bioreactors in series enable continuous production of alcohols from carbon monoxide with *Clostridium carboxidivorans*. In Bioprocess and Biosystems Engineering 41 (10), pp. 1403–1416. DOI: 10.1007/s00449-018-1969-1.

Emerson, D. F.; Woolston, B. M.; Liu, N.; Donnelly, M.; Currie, D. H.; Stephanopoulos, G. (2019): Enhancing hydrogen-dependent growth of and carbon dioxide fixation by *Clostridium ljungdahlii* through nitrate supplementation. In Biotechnology and Bioengineering 116 (2), pp. 294–306. DOI: 10.1002/bit.26847.

Fowles, M.; Carlsson, M. (2021): Steam Reforming of Hydrocarbons for Synthesis Gas Production. In Topics in Catalysis 64 (17-20), pp. 856–875. DOI: 10.1007/s11244-021-01496-z.

García-Robledo, E., Corzo, A., & Papaspyrou, S. (2014). A fast and direct spectrophotometric method for the sequential determination of nitrate and nitrite at low concentrations in small volumes. In Marine Chemistry, 162, 30–36. https://doi.org/10.1016/j.marchem.2014.03.002.

Grethlein, A. J.; Jain, M. K. (1992): Bioprocessing of coal-derived synthesis gases by anaerobic bacteria. In Trends in Biotechnology 10, pp. 418–423. DOI: 10.1016/0167-7799(92)90290-C.

Gu H, Yang Y, Wang M, Chen S, Wang H, Li S, Ma Y, Wang J (2017) Novel cysteine desulfidase CdsB involved in releasing cysteine repression of toxin synthesis in *Clostridium difficile*. In Frontiers in Cellular and Infection Microbiology 7. https://doi.org/10.3389/fcimb.2017.00531

Haryanto, A.; Fernando, S. D.; Pordesimo, L. O.; Adhikari, S. (2009): Upgrading of syngas derived from biomass gasification: A thermodynamic analysis. In Biomass and Bioenergy, Volume 33, Issue 5, pp 882-889, https://doi.org/10.1016/j.biombioe.2009.01.010.

Hermann, M.; Teleki, A.; Weitz, S.; Niess, A.; Freund, A.; Bengelsdorf, F.R.; Takors, R. (2020): Electron availability in CO_2, CO and H_2 mixtures constrains flux distribution, energy management and product formation in *Clostridium ljungdahlii*. In Microbial Biotechnology 13 (6), pp. 1831–1846. DOI: 10.1111/1751-7915.13625.

Hoegh-Guldberg, O., D. Jacob, M. Taylor, M. Bindi, S. Brown, I. Camilloni, A. Diedhiou, R. Djalante, K.L. Ebi, F. Engelbrecht, J.Guiot, Y. Hijioka, S. Mehrotra, A. Payne, S.I. Seneviratne, A. Thomas, R. Warren, and G. Zhou, 2018: Impacts of 1.5 ºC Global Warming on Natural and Human Systems. In: Global Warming of 1.5 °C. An IPCC Special Report on the impacts of global warming of 1.5 °C above pre-industrial levels and related global greenhouse gas emission pathways, in the context of strengthening the global response to the threat of climate change, sustainable development, and efforts to eradicate poverty [Masson-Delmotte, V., P. Zhai, H.-O. Pörtner, D. Roberts, J. Skea, P.R. Shukla, A. Pirani, W. Moufouma-Okia, C. Péan, R. Pidcock, S.Connors, J.B.R. Matthews, Y. Chen, X. Zhou, M.I. Gomis, E. Lonnoy, T.Maycock, M.Tignor, and T. Waterfield (eds.)]. Cambridge University Press, Cambridge, UK and New York, NY, USA, pp. 175-312. https://doi.org/10.1017/9781009157940.005.

Hu, P.; Bowen, S. H.; Lewis, R. S. (2011): A thermodynamic analysis of electron production during syngas fermentation. In Bioresource Technology 102 (17), pp. 8071–8076. DOI: 10.1016/j.biortech.2011.05.080.

Hu, P.; Jacobsen, L. T.; Horton, J. G.; Lewis, R. S. (2010): Sulfide assessment in bioreactors with gas replacement. In Biochemical Engineering Journal 49 (3), pp. 429–434. DOI: 10.1016/j.bej.2010.02.006.

Huhnke R. L.; Lewis R.S.; Tanner R.S.: Isolation and characterization of novel clostridial species. Patent no. US 7,704, 723 B2.

Hurst, K. M.; Lewis, R. S. (2010): Carbon monoxide partial pressure effects on the metabolic process of syngas fermentation. In Biochemical Engineering Journal 48 (2), pp. 159–165. DOI: 10.1016/j.bej.2009.09.004.

IEA (2022a), Biofuels, IEA, Paris https://www.iea.org/reports/biofuels, License: CC BY 4.0

IEA (2022b), Renewables 2022, IEA, Paris https://www.iea.org/reports/renewables-2022, License: CC BY 4.0

Infantes, A.; Kugel, M.; Neumann, A. (2020): Effect of Cysteine, Yeast Extract, pH Regulation and Gas Flow on Acetate and Ethanol Formation and Growth Profiles of *Clostridium ljungdahlii* Syngas Fermentation.

Jack, J., Lo, J., Maness, P.-C., & Ren, Z. J. (2019). Directing *Clostridium ljungdahlii* fermentation products via hydrogen to carbon monoxide ratio in syngas. Biomass & Bioenergy, 124, 95–101. https://doi.org/10.1016/j.biombioe.2019.03.011

Kabil O, Banerjee R. (2010): Redox biochemistry of hydrogen sulfide. In Journal of Biological Chemistry. 285(29):21903-7. DOI:10.1074/jbc.R110.128363.

Kennes, D.; Abubackar, H. N.; Diaz, M.; Veiga, M. C; Kennes, C. (2016). Bioethanol production from biomass: carbohydrate vs syngas fermentation. Journal of Chemical Technology & Biotechnology, 91(2), 304–317. doi:10.1002/jctb.4842

Kerby, R.; Zeikus, J. G. (1983): Growth of *Clostridium thermoaceticum* on H_2/CO_2 or CO as energy source. In Current Microbiology 8 (1), pp. 27–30. DOI: 10.1007/BF01567310.

Köpke, M., Held, C., Hujer, S., Liesegang, H., Wiezer, A., Wollherr, A., Ehrenreich, A., Liebl, W., Gottschalk, G., & Dürre, P. (2010). *Clostridium ljungdahlii* represents a microbial production platform based on syngas. Proceedings of the National Academy of Sciences of the United States of America, 107(29), 13087–13092. https://doi.org/10.1073/pnas.1004716107

Köpke, M.; Mihalcea, C.; Liew, F.; Tizard, J. H.; Ali, M. S.; Conolly, J. J. et al. (2011): 2,3-butanediol production by acetogenic bacteria, an alternative route to chemical synthesis, using industrial waste gas. In Applied and environmental microbiology 77 (15), pp. 5467–5475. DOI: 10.1128/AEM.00355-11.

Kundiyana, D. K., Huhnke, R. L., & Wilkins, M. R. (2010). Syngas fermentation in a 100-L pilot scale fermentor: design and process considerations. Journal of Bioscience and Bioengineering, 109(5), 492–498. https://doi.org/10.1016/j.jbiosc.2009.10.022

Kundiyana D. K., Wilkins M. R., Maddipati P., Huhnke R. L. (2011) Effect of temperature, pH and buffer presence on ethanol production from synthesis gas by "*Clostridium ragsdalei*". In Bioresource Technology 102:5794–5799. https://doi.org/10.1016/j.biortech.2011.02.032

LanzaTech. (n.d.). Lanzatech.com. Retrieved March 16, 2023, from https://lanzatech.com/

Lee, J.; Lee, J. W.; Chae, C. G.; Kwon, S. J.; Kim, Y. J.; Lee, J.; Lee, H. S. (2019): Domestication of the novel alcohologenic acetogen Clostridium sp. AWRP: from isolation to

characterization for syngas fermentation. In Biotechnology for Biofuels 12, p. 228. DOI: 10.1186/s13068-019-1570-0.

Liakakou, E. T.; Infantes, A.; Neumann, A.; Vreugdenhil, B. J. (2021): Connecting gasification with syngas fermentation: Comparison of the performance of lignin and beech wood. In Fuel 290 (1), p. 120054. DOI: 10.1016/j.fuel.2020.120054.

Lide, D. R. (2008): CRC handbook of chemistry and physics. A ready-reference book of chemical and physical data. 88th ed. /editor-in-chief, David R. Lide. Boca Raton, Fla., London: CRC. https://doi.org/10.1021/ja077011d

Liew, F., Henstra, A. M., Köpke, M., Winzer, K., Simpson, S. D., & Minton, N. P. (2017). Metabolic engineering of *Clostridium autoethanogenum* for selective alcohol production. Metabolic Engineering, 40, 104–114. https://doi.org/10.1016/j.ymben.2017.01.007

Liu Z. Y., Jia D. C., Zhang K. D., Zhu H. F., Zhang Q., Jiang W. H., Gu Y., Li F. L.. (2020). Ethanol metabolism dynamics in *Clostridium ljungdahlii* grown on carbon monoxide. In Applied and Environmental Microbiology 86(14). https://doi.org/10.1128/AEM.00730-20.

Maddox, I. S.; Steiner, E.; Hirsch, S.; Wessner, S.; Gutierrez, N. A.; Gapes, J. R.; Schuster, K. C. (2000): The cause of "acid-crash" and "acidogenic fermentations" during the batch acetone-butanol-ethanol (ABE-) fermentation process. In Journal of Molecular Microbiology and Biotechnology 2 (1), pp. 95–100.

Mayer, A.; Schädler, T.; Trunz, S.; Stelzer, T.; Weuster-Botz, D. (2018): Carbon monoxide conversion with *Clostridium aceticum*. In Biotechnology and Bioengineering 115 (11), pp. 2740–2750. DOI: 10.1002/bit.26808.

Metcalf & Eddy Inc.; Tchobanoglous, G.; Burton, F. L.; Tsuchihashi, R.; & Stensel, H. D. (2014). Wastewater engineering: Treatment and resource recovery (5th ed.). McGraw-Hill Education.

Ntagia, E.; Chatzigiannidou, I.; Williamson, A. J.; Arends, J. B. A.; Rabaey, K. (2020): Homoacetogenesis and microbial community composition are shaped by pH and total sulfide concentration. In Microbial Biotechnology 13 (4), pp. 1026–1038. DOI: 10.1111/1751-7915.13546.

O'Flaherty, V.; Mahony, T.; O'Kennedy, R.; Colleran, E. (1998): Effect of pH on growth kinetics and sulphide toxicity thresholds of a range of methanogenic, syntrophic and sulphate-reducing bacteria. In Process Biochemistry 33 (5), pp. 555–569. DOI: 10.1016/S0032-9592(98)00018-1.

Oswald, F.; Zwick, M.; Omar, O.; Hotz, E. N.; Neumann, A. (2018): Growth and Product Formation of *Clostridium ljungdahlii* in Presence of Cyanide. In Frontiers in Microbiology 9, p. 1213. DOI: 10.3389/fmicb.2018.01213.

Phillips, J. R.; Huhnke, R. L.; Atiyeh, H. K. (2017): Syngas Fermentation: A Microbial Conversion Process of Gaseous Substrates to Various Products. In Fermentation 3 (2), p. 28. DOI: 10.3390/fermentation3020028.

Phillips, J. R.; Clausen, E. C.; Gaddy, J. L. (1994): Synthesis gas as substrate for the biological production of fuels and chemicals. In Applied Biochemistry and Biotechnology 45-46 (1), pp. 145–157. DOI: 10.1007/BF02941794.

Ragsdale, S. W. (2007): Nickel and the carbon cycle. In Journal of inorganic biochemistry 101 (11-12), pp. 1657–1666. DOI: 10.1016/j.jinorgbio.2007.07.014.

Ragsdale, S. W. (2008a): Enzymology of the Wood-Ljungdahl pathway of acetogenesis. In Annals of the New York Academy of Sciences 1125, pp. 129–136. DOI: 10.1196/annals.1419.015.

Ragsdale, S. W.; Pierce, E. (2008b): Acetogenesis and the Wood-Ljungdahl pathway of $CO_{(2)}$ fixation. In Biochimica et Biophysica Acta 1784 (12), pp. 1873–1898. DOI: 10.1016/j.bbapap.2008.08.012.

Ramachandriya, K. D.; Wilkins, M. R.; Patil, K. N. (2013): Influence of switchgrass generated producer gas pre-adaptation on growth and product distribution of *Clostridium ragsdalei*. In Biotechnology and Bioprocessing Engineering 18 (6), pp. 1201–1209. DOI: 10.1007/s12257-013-0384-3.

Ramió-Pujol, S.; Ganigué, R.; Bañeras, L.; Colprim, J. (2015): Incubation at 25 °C prevents acid crash and enhances alcohol production in *Clostridium carboxidivorans* P7. In Bioresource Technology 192, pp. 296–303. DOI: 10.1016/j.biortech.2015.05.077.

Ricci, L.; Agostino, V.; Fino, D.; Re, A. (2021): Screening of Gas Substrate and Medium Effects on 2,3-Butanediol Production with *C. ljungdahlii* and *C. autoethanogenum* Aided by Improved Autotrophic Cultivation Technique. In Fermentation 7 (4), p. 264. DOI: 10.3390/fermentation7040264.

Richter, H.; Molitor, B.; Wei, H.; Chen, W.; Aristilde, L.; Angenent, L. T. (2016): Ethanol production in syngas-fermenting *Clostridium ljungdahlii* is controlled by thermodynamics rather than by enzyme expression. In Energy & Environmental Science 9 (7), pp. 2392–2399. DOI: 10.1039/c6ee01108j.

Richter, H.; Martin, M.; Angenent, L. (2013): A two-stage continuous fermentation system for conversion of syngas into ethanol. In Energies 6 (8), pp. 3987–4000. DOI: 10.3390/en6083987.

Rückel, A.; Hannemann, J.; Maierhofer, C.; Fuchs, A.; Weuster-Botz, D. (2021): Studies on syngas fermentation with *Clostridium carboxidivorans* in stirred-tank reactors with defined gas impurities. In Frontiers in Microbiology 12, p. 655390. DOI: 10.3389/fmicb.2021.655390.

Rückel, A.; Oppelt, A.; Leuter, P.; Johne, P.; Fendt, S.; Weuster-Botz, D. (2022): Conversion of syngas from entrained flow gasification of biogenic residues with *Clostridium carboxidivorans* and Clostridium *autoethanogenum*. In Fermentation 8 (9), p. 465. DOI: 10.3390/fermentation8090465.

Saxena, J.; Tanner, R. S. (2011): Effect of trace metals on ethanol production from synthesis gas by the ethanologenic acetogen, *Clostridium ragsdalei*. In Journal of industrial microbiology & biotechnology 38 (4), pp. 513–521. DOI: 10.1007/s10295-010-0794-6.

Saxena, J.; Tanner, R. S. (2012): Optimization of a corn steep medium for production of ethanol from synthesis gas fermentation by *Clostridium ragsdalei*. In World journal of microbiology & biotechnology 28 (4), pp. 1553–1561. DOI: 10.1007/s11274-011-0959-0.

Schuchmann, K.; Müller, V. (2014): Autotrophy at the thermodynamic limit of life: a model for energy conservation in acetogenic bacteria. In Nature Reviews. Microbiology 12 (12), pp. 809–821. DOI: 10.1038/nrmicro3365.

Schuchmann, K.; Müller, V. (2016): Energetics and Application of Heterotrophy in Acetogenic Bacteria. In Applied and Environmental Microbiology 82 (14), pp. 4056–4069. DOI: 10.1128/AEM.00882-16.

Sharma, B.; Larroche, C.; Dussap, C. (2020): Comprehensive assessment of 2G bioethanol production. In Bioresource Technology 313, p. 123630. DOI: 10.1016/j.biortech.2020.123630.

Shen, S.; Gu, Y.; Chai, C.; Jiang, W.; Zhuang, Y.; Wang, Y. (2017): Enhanced alcohol titre and ratio in carbon monoxide-rich off-gas fermentation of *Clostridium carboxidivorans* through combination of trace metals optimization with variable-temperature cultivation. In Bioresource technology 239, pp. 236–243. DOI: 10.1016/j.biortech.2017.04.099.

Shen, S.; Wang, G.; Zhang, M.; Tang, Y.; Gu, Y.; Jiang, W.; Wang, Y.; Zhuang, Y. (2020): Effect of temperature and surfactant on biomass growth and higher-alcohol production during syngas fermentation by *Clostridium carboxidivorans* P7. In Bioresources and Bioprocessing. 7 (1), p. 702. DOI: 10.1186/s40643-020-00344-4.

Sun, X.; Atiyeh, H. K.; Huhnke, R. L.; Tanner, R. S. (2019): Syngas fermentation process development for production of biofuels and chemicals: A review. In Bioresource Technology Reports 7 (4), p. 100279. DOI: 10.1016/j.biteb.2019.100279.

Takors, R.; Weuster-Botz, D. (2018): Prozessmodelle. In Horst Chmiel, Ralf Takors, Dirk Weuster-Botz (Eds.): Bioprozesstechnik, vol. 3. Berlin, Heidelberg: Springer Berlin Heidelberg, pp. 71–105.

Tanner, R. S.; Miller, L. M.; Yang, D. (1993): *Clostridium ljungdahlii* sp. nov., an acetogenic species in clostridial rRNA homology group I. In International journal of systematic bacteriology 43 (2), pp. 232–236. DOI: 10.1099/00207713-43-2-232.

Tse, T. J.; Wiens, D. J.; Reaney, M. J. T. (2021): Production of Bioethanol – A Review of Factors Affecting Ethanol Yield. In Fermentation 7 (4), p. 268. DOI: 10.3390/fermentation7040268.

Valgepea, K; Lemgruber, R. S. P.; Meaghan, K.; Palfreyman, R. W.; Abdalla, T.; Heijstra, B. D.; Behrendorff, J. B.; Tappel,R; Köpke, M.; Simpson, S. D.; Nielsen,L. K.; Marcellin, E. (2017) Maintenance of ATP Homeostasis Triggers Metabolic Shifts in Gas-Fermenting Acetogens. In Cell Systems 4, 505-515. http://dx.doi.org/10.1016/j.cels.2017.04.008

Wang, S.; Zhang, Y.; Dong, H.; Mao, S.; Zhu, Y.; Wang, R.; Luan, G.; Li, Y. (2011): Formic acid triggers the "Acid Crash" of acetone-butanol-ethanol fermentation by *Clostridium acetobutylicum*. In Applied and environmental microbiology 77 (5), pp. 1674–1680. DOI: 10.1128/AEM.01835-10.

Wang, S.; Huang, H.; Kahnt, J.; Mueller, A. P.; Köpke, M.; Thauer, R. K. (2013): NADP-specific electron-bifurcating FeFe-hydrogenase in a functional complex with formate dehydrogenase in *Clostridium autoethanogenum* grown on CO. In Journal of Bacteriology 195 (19), pp. 4373–4386. DOI: 10.1128/JB.00678-13.

Weuster-Botz, D.; Takors, R. (2018): Wachstumskinetik. In Horst Chmiel, Ralf Takors, Dirk Weuster-Botz (Eds.): Bioprozesstechnik, vol. 40. Berlin, Heidelberg: Springer Berlin Heidelberg, pp. 45–70.

Wiechmann, A., Müller, V. (2019). Synthesis of Acetyl-CoA from Carbon Dioxide in Acetogenic Bacteria. In: Geiger, O. (eds) Biogenesis of Fatty Acids, Lipids and Membranes. Handbook of Hydrocarbon and Lipid Microbiology. Springer, Cham. https://doi.org/10.1007/978-3-319-50430-8_4

Xu, D.; Lewis, R.S. (2012) Syngas fermentation to biofuels: Effects of ammonia impurity in raw syngas on hydrogenase activity. In Biomass Bioenergy, 45, 303–310. https://doi.org/10.1016/j.biombioe.2012.06.022

Yang, Y., Cao, W., Shen, F., Liu, Z., Qin, L., Liang, X., & Wan, Y. (2023). L-Cys-Assisted Conversion of H_2/CO_2 to Biochemicals Using Clostridium ljungdahlii. Applied Biochemistry and Biotechnology, 195(2), 844–860. https://doi.org/10.1007/s12010-022-04174-2

Yoo, C. G., Meng, X., Pu, Y., & Ragauskas, A. J. (2020). The critical role of lignin in lignocellulosic biomass conversion and recent pretreatment strategies: A comprehensive review. Bioresource Technology, 301(122784), 122784. https://doi.org/10.1016/j.biortech.2020.122784

Younesi, H.; Najafpour, G.; Mohamed, A. R. (2005): Ethanol and acetate production from synthesis gas via fermentation processes using anaerobic bacterium, *Clostridium ljungdahlii*. In Biochemical Engineering Journal 27 (2), pp. 110–119. DOI: 10.1016/j.bej.2005.08.015.

List of Abbreviations

ACS	Acetyl-CoA synthase
ALDH	Aldehyde dehydrogenase
AOR	Aldehyde:ferredoxin oxidoreductase
ASR	Anaerobic sulfite reductase
ATP	Adenosine triphosphate
BDH	2,3-butanediol dehydrogenase
C. ljungdahlii	*Clostridium ljungdahlii*
C. ragsdalei	*Clostridium ragsdalei*
CaADH	NADPH dependent primary-secondary alcohol dehydrogenase
CDW	Cell dry weight
CFeSP	Corrinoid iron-sulfur protein
CH_2-THF	Methylene-tetrahydrofolate
CH_3-THF	Methyl-tetrahydrofolate
CODH	Carbon monoxide dehydrogenase
FBN	Fuel bound nitrogen
Fd	Ferredoxin
FDH	Formate dehydrogenase
HCO-THF	Formyl-tetrahydrofolate
HytA-E	Hydrogenase, subunits A - E
NAD, NADH	Nicotinamide adenine dinucleotide
NADP, NADPH	Nicotinamide adenine dinucleotide phosphate
Nfn	Electron-bifurcating transhydrogenase
PFOR	Pyruvate:ferredoxin oxidoreductase
PMF	Proton motive force
Rnf	Membrane integral ferredoxin-NAD oxidoreductase enzyme complex
RP	Redox Potential
RSS	Residual sum of squares
THF	Tetrahydrofolate
WLP	Wood-Ljungdahll pathway

List of Symbols

c_X	Cell concentration, cell dry weight concentration, g L^{-1}
r_i	Production rate component *i*, g L^{-1} h^{-1}
G_i	Conversion factor of component i
v_i	Molar fraction of component i
$c_{in,i}$	Concentration of component *i* in feed, g L^{-1}
c_i	Concentration of component *i*, g L^{-1}
c	Concentration, g L^{-1}
[ ]	Concentration, M
a_i	Empirical coefficients
n	Empirical factor, -
c_i^*	Equilibrium concentration of *i* on the interface, mol L^1
R	Gas constant, kJ K^{-1} mol^{-1}
F	Gas volume flow, NL h^{-1}
k_p	Growth independent product formation rate, g L^{-1} h^{-1}
H_i	Henry constant of i, kPa L mol^{-1}
K_I	Inhibition constant, g L^{-1}
m_i	Mass of component *i* in the reactor volume, g
μ_{max}	Maximal specific growth rate, h^{-1}
q_i'	Molar flow density of *i*, mol m^2 s^-
α	OD-CDW concentration factor, g L^{-1}
OD	Optical density at 600 nm
F_{out}	Outlet volume flow, L h^{-1}
$K_{l,i}$	Overall transport coefficient, m s^{-1}
$p_{i,s}$	Partial pressure of *i* on the interface, kPa
c_p	Product concentration, g L^{-1}
r_p	Product formation rate, g L^{-1} h^{-1}
$Y_{Xp,\mu}$	(Biomass related) product yield, g g^{-1}
V	Reactor volume, L
$K_{s,i}$	Saturation constant of substrate *i*, g L^{-1}
μ	Specific growth rate, h^{-1}
q_p	Specific product formation rate, h^{-1}

$\Delta G^{0}_{T,i}$	Standard Gibbs free energy of the reaction corrected for temperature and pH, kJ mol^{-1}
υ_i	Stoichiometric coefficient of species *i*
$c_{s,i}$	Substrate *i* concentration, g L^{-1}
T	Temperature, K
t	Time, h
$\Delta G'_T$	Transformed Gibbs free energy of the reaction, kJ mol^{-1}
k_g, k_l	Transport coefficient of the gas (g) and liquid (l) phases, m s^{-1}
F_{in}	Volume flow of feed, L h^{-1}
a	Volumetric surface area, m^2 m^{-3}

Appendix

Media Composition

Table 21 – Detailed composition of the cultivation medium according to Doll et al. (2018)

Component	Concentration	Unit
	Mineral Solution	
NH_4Cl	100	g L^{-1}
NaCl	80	g L^{-1}
KCl	10	g L^{-1}
KH_2PO_4	10	g L^{-1}
	Magnesium Solution	
$MgSO_4 \cdot 7H_2O$	20,47	g L^{-1}
	Calcium Solution	
$CaCl_2 \cdot 2H_2O$	2,65	g L^{-1}
	Trace Elements Solution	
Nitrilotriacetic Acid	2,00	g L^{-1}
$MnSO_4 \cdot H_2O$	1,12	g L^{-1}
$NH_4Fe(SO_4)_2 \cdot 6H_2O$	1,10	g L^{-1}
$CoCl_2 \cdot 6H_2O$	0,37	g L^{-1}
$ZnSO_4 \cdot 7H_2O$	0,36	g L^{-1}
$CuCl_2 \cdot 2H_2O$	25,0	mg L^{-1}
$NiCl_2 \cdot 6H_2O$	37,0	mg L^{-1}
$Na_2MoO_4 \cdot 2H_2O$	23,0	mg L^{-1}
Na_2SeO_4	20,0	mg L^{-1}
$Na_2WO_4 \cdot 2H_2O$	22,0	mg L^{-1}
	Vitamin Solution	
Pyridoxine hydrochloride	12,0	mg L^{-1}
Thiamine hydrochloride	6,00	mg L^{-1}
Riboflavine	5,00	mg L^{-1}
Ca-Pantothenate	5,00	mg L^{-1}
Lipoic acid	5,00	mg L^{-1}
4-Aminobenzoic acid	5,00	mg L^{-1}
Nicotinic acid (Niacin)	5,00	mg L^{-1}
Vitamine B12	5,00	mg L^{-1}

D-Biotin	2,00	mg L^{-1}
Folic acid	2,00	mg L^{-1}
2-Mercaptoethansulfonic acid	23,0	mg L^{-1}
	Cysteine Solution	
Cysteine-HCl	50	g L^{-1}

Table 22 – Composition of the phosphate saline buffer (PBS), pH 7,4.

Component	Concentration	Unit
Na_2HPO_4	1,44	g L^{-1}
KH_2PO_4	0,20	g L^{-1}
KCl	0,20	g L^{-1}
NaCl	8,00	g L^{-1}

Equipment and Chemicals

Equipment	Producer
Anaerobic Chamber	Coy Laboratory Products Inc., Grass Lake, USA
Autoclave	Systec VX-150, H ± P 500 EC-Z
Centrifuge (floor-standing)	Rotixa 50 RS, Hettich Centrifuge
Centrifuge (table-top)	Mikro 20, Hettich Centrifuge
Drying Oven	Series E 28 L, Binder
Heating Mantle (Wise Therm WHM 12015)	Witeg Labortechnik GmbH
Mass Flow Controller	WMR 4000, Westphal Mess-und Regeltechnik GmbH
Mass Flow Meter	Wagner Mess- und Regeltechnik GmbH
Micro Gas Chromatograph	490 Micro GC System, Agilent Technologies
Shaking Incubator	Wise-Cube WIS-20, Witeg Labortechnik GmbH
Single-use Syringes	Becton Dickinson
Spectrophotometer	Genesys 10S UV-Vis, Thermo Scientific
Sterile Cannulas	B. Braun

Residual Sum of Squares

Table 23 – Residual sum of squares, RSS $(g\ L^{-1})^2$, of the nonlinear regression of the cell dry weight (CDW) and product concentrations of the process from which production rates were presented, differentiated by the gas flow (F_g), pH, temperature and sulfide feed rate (F_s)

				RSS, $(g\ L^{-1})^2$			
F_g	pH	Temperature	F_s, mmol $L^{-1}\ h^{-1}$	CDW	Acetate	Ethanol	2,3-BD[1]
5.0	6.0	37	0			0.002	0.064
5.0	6.0	37	0.05			0.023	0.010
5.0	6.0	32	0			0.116	0.001
5.0	6.0	32	0.05	0.004	0.372	0.073	0.061
5.0	5.5	37	0			0.056	0.009
5.0	5.5	37	0.05			0.024	0.001
5.0	5.5	32	0			0.127	0.000
5.0	5.5	32	0.05			0.154	0.008
1.5	6	37	0			0.001[2]	0.001
						0.008[3]	
1.5	6	37	0.05			0.095	0.001

[1]2,3-butanediol
[2]Regression for the process interval of 0 – 48 h
[3]Regression for the process interval of 26 – 144 h